CHARACTERIZATION OF THE PHOTOSENSITIVE RESPONSE IN POLYSILANE-BASED ORGANIC/INORGANIC HYBRID MATERIALS

By

Haripin Chandra

A Dissertation Submitted to the Faculty of the

DEPARTMENT OF MATERIALS SCIENCE AND ENGINEERING

In Partial Fulfillment of the Requirements
For the Degree of
DOCTOR OF PHILOSOPHY

In the Graduate College

THE UNIVERSITY OF ARIZONA

2007

THE UNIVERSITY OF ARIZONA
GRADUATE COLLEGE

As members of the Dissertation Committee, we certify that we have read the dissertation

prepared by Haripin Chandra

entitled Characterization of the photosensitive response in polysilane-based organic/inorganic hybrid materials

and recommend that it be accepted as fulfilling the dissertation requirement for the

Degree of Doctor of Philosophy

_____ Date: 11/29/07
Dr. Barrett G. Potter

_____ Date: 11/29/07
Dr. Pierre Lucas

_____ Date: 11/29/07
Dr. Kelly S. Potter

_____ Date: 11/29/07
Dr. Pierre A. Deymier

Final approval and acceptance of this dissertation is contingent upon the candidate's submission of the final copies of the dissertation to the Graduate College.

I hereby certify that I have read this dissertation prepared under my direction and recommend that it be accepted as fulfilling the dissertation requirement.

_____ Date: 11/29/07
Dissertation Director: Dr. Barrett G. Potter

STATEMENT BY AUTHOR

This dissertation has been submitted in partial fulfillment of requirements for an advanced degree at The University of Arizona and is deposited in the University Library to be made available to borrowers under rules of the library.

SIGNED: *Haripin Chandra*

ACKNOWLEDGEMENT

I would like to thank my advisors, Dr. B.G. Potter Jr., and Dr. Kelly Simmons-Potter, for their guidance, patience and supports which make it possible to complete this work. I have become a better person and more mature professionally with their guidance. I am really grateful for their support and friendship.

I would also express my thanks to the rest of my committee members, Dr. Pierre A. Deymier and Dr. Pierre Lucas of the Department of Materials Science and Engineering. I am thankful for additional advice on completing this work. I have learned a great deal from them.

I would also thank Dr. Gregory M. Jamison and Dr. Joseph W. Thomes Jr., from the Sandia National Laboratory for their support and supplying materials used in this work. Dave Musgraves, a graduate student in Dr. Potter's group, deserves special thanks for helping me in Gaussian calculations. I would also like to acknowledge Katarzyna (Kasia) Sieluzycka, Veronica Augustyn and Scott Cooper, who helped a lot in obtaining thermal annealing data.

I would especially thank my family: my parents, Tjen Tek Fa and Tjen Helen and my siblings, Zein Viccar Tjen and Wina Tjen for their support emotionally when I was down. I would also thank Diana 'Momo' Yahya, a very special someone, for her support, sacrifice and understanding.

Financial support from Sandia National Laboratory and State of Arizona TRIF Optics Initiative are gratefully acknowledged.

DEDICATION

To a very special someone, Diana ‘Momo’ Yahya.

TABLE OF CONTENTS

TABLE OF CONTENTS (continued)

TABLE OF CONTENTS (continued)

LIST OF FIGURES

LIST OF FIGURES (continued)

LIST OF FIGURES (continued)

LIST OF FIGURES (continued)

LIST OF FIGURES (continued)

LIST OF FIGURES (continued)

LIST OF TABLES

ABSTRACT

The motivation for the current work stems from a unique application, i.e. the photopatterning of optical functionality in a photosensitive material immediately prior to use. In this case, optical devices such as diffraction gratings and optical interconnects are produced in thin films using integrated photonic sources under relatively uncontrolled environmental conditions. The compatibility of the material photoexcitation mechanism with wavelength and fluence levels available from compact solid-state optical sources and the need to understand the impact of local atmospheric composition and temperature on the photosensitive material response are therefore of primary concern.

The primary goal of the current study was to investigate photoexcitation mechanisms and photoinduced optical and structural changes in promising candidate material systems for this application: polysilane and polygermane-based molecular hybrid polymers. The work pursued the development of a fundamental understanding of the key photophysical and photostructural responses of thin films composed of both pure, linear-chain polysilanes and of a Ge-Si copolymer. The effects of molecular modifications to the polymers, including polymer backbone catenate structure and side-group identity, on the optical and photosensitive behavior observed in these systems are examined. Through such effort, an understanding of how such structural characteristics influence key photosensitive properties, i.e. the excitation wavelength and the resulting photoinduced optical property changes, was attained.

A related objective in the present work was to characterize the thermal stability of these hybrid polymers, specifically in terms of the effect of thermal treatment on as-deposited and photomodified materials. In this case, an evaluation of the similarities and differences in structural modification in response to both thermal and optical fields was pursued.

The primary mechanism associated with the photoinduced phenomena observed in both polysilane and polygermane involves backbone chain scissioning and the formation of silane-radicals upon absorption of near-UV ($\lambda \approx 300$ to 400 nm) photons, resonant with the lowest energy, $\sigma - \sigma^*$ (HOMO-LUMO) transition of the Group IVA backbone. The final photoproducts obtained result from a mixture of different competing processes which occur subsequent to this initial photoscissioning. In aerobic atmospheric environments, the radicals formed capture oxygen and form oxide linkages forming the dominant photoproducts. On the other hand, under anaerobic conditions, photooxidation is suppressed while hydride passivation of the radical dominates the response. The oxidized product, resulting from irradiation under the aerobic environment, exhibited higher refractive index changes than irradiation under anaerobic conditions. Photoexcitation using higher energy photons (typically $\lambda \approx 230$ to 300 nm) are resonant with side-group transitions associated with π-conjugated states of the cyclic moieties. Under these conditions, the excitation accesses both these organic side-groups as well as the Group IVA backbone structure. Such excitation conditions resulted in a larger photoinduced structural modification in the irradiated polymer, as observed both in terms of its electronic structure as well as the resulting refractive index change.

Thermally induced structural modification to the backbone and side-group moieties were found to be qualitatively similar those produced under optical irradiation. For example, the primary structural changes were again associated with backbone chain scissioning. Photoinduced structural modifications through resonant optical excitation of the material, however, tended to be more focused on the specific structural moieties accessed.

1. INTRODUCTION

Photosensitivity refers to a stable, refractive index modification upon optical illumination. From a technological standpoint, the ability to manipulate refractive index in such photosensitive materials allows the generation of refractive index patterns within the material. Optical functionality arising from these photopatterned structures, such as Bragg gratings in fibers [1], optical sensor systems [2] and planar waveguides [3], can be readily integrated within photonic systems using a single-step direct-write procedure without the need for multi-step, photolithographic processing and etching [4].

The motivation of the present study is derived from a unique application of photosensitive materials: write-as-needed photopatterning. This refers to the photopatterning of refractive index structure, and associated optical function, immediately prior to use. In this application, optical devices such as diffraction gratings and optical interconnects are produced in the thin film material under relatively uncontrolled conditions within the application environment. The optical system for this application would thus include a compact solid-state optical source, a pattern generator and a photosensitive thin film. Compatibility of the photosensitive materials used with commonly available solid-state optical sources (with tens of mW output at λ = 230 nm – 450 nm) and with the photoprocessing environment (atmospheric composition, temperature) is of primary concern in this case. High refractive index changes are desirable especially for waveguide interconnects in write-as-needed applications. A high refractive index contrast between the core and clad regions (i.e. exposed and unexposed

regions) of waveguide enables more tightly confined guided wave optical field profiles over a greater wavelength range, thus impacting the development of high areal density integrated photonic systems for frequency multiplexing [5]. Other design considerations include the anticipated operating wavelength for the refractive index structure. In the present context, operational wavelengths ranging from the visible to near-IR (1.06, 1.3, 1.5 μm) are targeted.

There are a number of different photosensitive material systems, ranging from inorganic materials, including oxide (silicate-based, germanosilicate-based) and non-oxide (chalcogenide) glasses, to organics such as conjugated polymers and anthracene based materials. Photosensitivity in germanosilicate and silicate based glass are closely associated with the presence of oxygen-deficient Ge and/or Si defect centers [4,6-7]. Typical refractive index changes of $\sim 10^{-4}$ can be obtained using relatively high irradiation fluences (~ kJ / cm^2) at wavelengths ranging from 193 nm – 248 nm [4,6-7]. These refractive index changes in germanosilicate and silicate based glass can be enhanced to $\sim 10^{-2}$ by employing several different processing strategies, including hydrogen loading at elevated temperature [8] and writing with high-energy photons (<248 nm) and at high pulse energies [9]. The inorganic silicate-based glass is not an effective candidate for our application, however as integrable, solid state sources operating at <248 nm are typically not readily available at the fluences necessary

Chalcogenide photosensitivity is associated with the excitation of non-bonding lone-pair electrons in the chalcogen atoms [10-11]. Photoinduced refractive index changes in the chalcogenide system can reach ~0.04 under relatively low fluences (30

J/cm^2) using 365 nm and 400 nm photon sources as observed in the As_2Se_3 system [10]. The deposition of chalcogenide thin films typically requires either evaporation or sputtering. Either method, however, can produce inhomogeneities in film stoichiometry which can, in turn, produce local variation in the photosensitive response. [11-12]. Moreover, chalcogenide glass exhibits high transparency in the mid- IR, outside the targeted operational wavelengths of interest in the current study.

The present work focuses on inorganic-organic molecular hybrid photosensitive material systems based on linear chains of Group IVA inorganic polymers functionalized with organic side groups. These materials, i.e. polysilanes and polygermanes, exhibit unique electronic and optical properties that make them well-suited for write-as-needed applications. Although inorganic glasses, such as silicate and germanosilicate glass, have stability advantages over inorganic/organic hybrid polymers the latter offers advantages in photosensitivity and materials processing. Group IVA inorganic linear chain polymers can attain refractive index changes of up to 0.14 with relatively low optical fluence (< 5 J/cm^2) [13-15]. Furthermore, through molecular engineering of the backbone and side-group moieties present, the optical response of these materials can be modified to offer different "writing" wavelengths and optimized compatibility with photon sources. From a processing perspective, the solid polymer dissolves in common solvents such as tetrahydrofuran (THF), toluene, and hexane which allow facile solution deposition of thin films via spin-coating at relatively low temperature (<100 C).

2. OBJECTIVES

As mentioned previously, the motivation of present work arose from a unique application: write-as-needed rapid photopatterning of refractive index structures under nonlaboratory environments. The primary goal of the current study is to develop a fundamental understanding of the photophysical/photostructural response of photosensitive inorganic/organic hybrid polysilane and polygermane materials that are under investigation as important candidates for this intended application. The study seeks to understand the effects of polymer backbone catenate structure and side-group identity on the optical and photosensitive behavior observed in these systems. Such effort provides better understanding of how such structural characteristics influence key photosensitive properties, e.g. excitation wavelength sensitivity and the resulting photoinduced optical constant (n and k) changes. Moreover, the effect of local atmospheric environment on the photostructural modifications produced and the associated photoinduced refractive index change is of central interest in the context of the write-as-needed application.

A related objective in the present work is the characterization of the thermal stability of these hybrid polymers, specifically in terms of the effect of thermal treatment on as-deposited and photomodified material optical behavior. Since device function will be dependent upon a stable, photoinduced refractive index contrast between UV-irradiated and “blank” regions, an understanding of how thermal history can affect the originally produced index contrast is important in the evaluation of deployment

environment options for these device structures. By comparing the effect of thermal treatment on structural and optical properties changes between pre-exposed and photomodified regions, insight into the relative thermal stability of photowritten devices will be obtained. Fundamentally, such studies will also provide the means to establish an understanding of similarities and differences in structural modification in response to both thermal and optical fields.

3. BACKGROUND

3.1 Historical Background

A typical Group IVA-based inorganic polymer is a linear-chain polysilylene which consists of silicon backbone functionalized with organic side-groups, as shown in Figure 3.1. The polysilane family includes both a 3-D network-type Si topology (polysilyne) as well as more linear Si chains (polysilylene). In this work, the terms polysilane and polysilylene are used interchangeably to describe polymers with a linear chain Si structure unless otherwise noted.

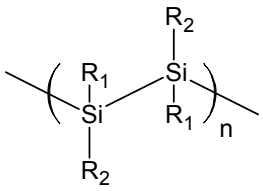

Figure 3.1. Chemical structure of linear chain polysilane (polysilylene).

Polysilane has first synthesized by Kipping in 1920 using condensation of chlorosilane monomer with sodium metal, but the polysilane product could not be extracted from the solution [16]. In the 1970s, Yajima, *et al.*, [17] were able to polymerize polydimethylsilane which was subsequently used as a precursor to develop silicon carbide fibers. In early 80's, poly(dimethyl)silane was prepared from highly purified monomer. However, the resulting polymer was only slightly soluble in organic solvents at elevated temperature [18]. The same group also developed soluble, high

molecular weight polysilane block copolymer (5,000-10,000 MW) with adequate film forming properties for property measurement [19]. West and co-workers prepared poly[(methyl)(phenyl)-co-(methyl)]silane, which dissolved easily in common organic solvents, up to 1,000,000 MW, shortly afterward in 1981 [20]. The first soluble homopolymer polysilane was poly[(methyl)(phenyl)silane]. This polymer was synthesized from methylphenyldichlorosilane in the presence of a sodium catalyst [21]. Since then, polysilane based materials has been extensively investigated, yielding more than 1300 journal publications to date. The unique electronic, optical and chemical properties of this material system have been the focus of extensive study in the context of applications involving such phenomena as photodegradation (photoresist materials) [22], low-dimensionality semiconductor behavior [23], optical activity [24] and photoinduced refractive index change [14,25-27].

Other Group IVA inorganic linear chain polymers, such as germane and stannane-based systems, are less fully investigated compared to their silane counterpart. This is largely due to difficulties in high yield polymerization of the associated monomers as germane and stannane polymers tend to form cyclic and acyclic catenates resulting in low molecular weight structures [28]. The first soluble, high molecular weight organogermane homopolymer and Ge-Si copolymer was developed in the mid 1980s by Trefonas and West [29] while soluble, high molecular weight organostannane material was not synthesized until 1995 [30]. Again, due to difficulties in the synthesis of polygermane and germane-silane linear chain copolymer, the development of applications based on these systems was slower than that observed in polysilanes. One

example of an application utilizing polygermane materials and germane-silane copolymers is based on their strong photoconductivity [31].

3.2 Polymer Synthesis

One of the most viable synthesis routes for high molecular weight, linear polysilane is the Wurtz coupling method, depicted in the scheme of Figure 3.2 [32]. This method employs condensation of dichlorosilane at elevated temperature in an inert solvent such as toluene or xylene using a dispersed alkali metal as a catalyst. Sodium is typically used as the catalytic agent in Wurtz coupling. Lithium metal tends to result in the formation of cyclic oligomers [33] while potassium metal can lead to the degradation of high molecular weight species [34]. Polymerization of poly[(methyl)(phenyl)silane], which is used in current study, has been produced with yields up to 55% via Wurtz coupling using sodium catalyst [35].

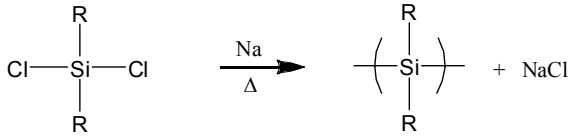

Figure 3.2. Polysilane synthesis: Wurtz coupling method.

Another synthesis route available for the production of linear polysilane materials is the use of a dehydrogenative coupling method, also known as σ-bond metathesis, as first described by Aitken and Harrod [36-39]. In this method complex Zr or Ti compound catalysts are used to polymerize $R^1R^2SiH_2$ compound in the general form of Cp_2MX (Cp = η-C_5H_5, M = Zr or Ti, X = H_2, acid or alkyl as shown in Figure 3.3. This method can efficiently polymerize the silane monomer with up to 99% monomer conversion rates observed [39]

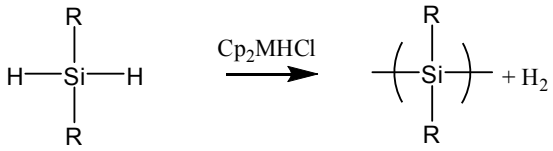

Figure 3.3. Polysilane synthesis: Dehydrogenative coupling method [39].

Polysilane can also be produced using an electroreductive coupling method [40]. In this case, the electroreduction of chlorosilane is carried out with Mg rod electrodes in an undivided electrochemical cell under ultrasonic frequencies of 47 MHz. Other metals, such as Cu, Pt, Ni and Zn can also be used although not as effectively as Mg. The electroreductive method produces high molecular weight polysilane with 20-40% yield; however it also produces ~2% of a siloxane byproduct [40].

Polygermane and Ge-Si linear chain copolymer are synthesized using methods analogous to polysilane polymerization, including the Wurtz coupling method [29,41] and the electroreductive coupling method [42]. The Wurtz coupling method employs

condensation of dichlorogermane and dichlorogermane-dichlorosilane mixtures with a sodium catalyst at elevated temperature to produce associated polygermane and Ge-Si copolymers, respectively. However, this method typically has a low yield resulting from the formation of a bimodal distribution of polymeric molecular weights [29]. The method, applied to the synthesis of polygermane and Ge-Si copolymer, provides a yield of ~20% compared with polysilanes exhibiting 40-50% yields [29]. The electroreductive coupling method has advantages over the Wurtz coupling approach for the production of polygermane and Ge-Si copolymers in terms of the molecular weight distribution of the resulting polymer. Past efforts have resulted in a monomodal MW distribution, and an improved yield of up to 35% [42].

3.3. Molecular Structure and Electronic Structure

3.3.1 Electron delocalization

Gilman *et al.,* was the first group to have observed the unique UV absorption associated with Si-Si bonding [43-44] in linear chain oligosilanes. In this case, they observed that $(Si(CH_3)_2)_n$ and $(SiH_2)_n$ (n = 2-8) absorbed at 190 nm – 215 nm which is a much longer wavelength (lower energy) than hydrocarbon absorption (150nm - 190nm). The absorbed wavelength is red-shifted with longer chain length which suggested electron delocalization along the Si chain structure. Early theory suggested that the photon absorption in polysilane based system was caused by transition between the Highest Occupied Molecular Orbital (HOMO) of $\sigma_{Si\text{-}Si}$ and the 3d $\pi_{Si\text{-}Si}$ orbitals along the

backbone chains. However, later investigations using molecular orbital calculation concluded d-orbitals have no significant role in either the HOMO or lower energy occupied orbitals [32, 45-46].

The characteristic electron delocalization associated with the conjugated molecular bond states of the Si-chain can be explained qualitatively in terms of overlapping sp^3 orbitals using the Sandorfy C model [32, 47]. The Sandorfy C model, as the name suggested, was initially developed for alkanes and estimates the interaction energy (resonance integral) between two silicon atoms while using periodic boundary conditions to represent the polymerized system [48]. In this model, contributions to the energetic of molecular states arising from Si-Si bonding are divided into two primary factors, delineated by atomic orbital interactions along the backbone chain. Here, the "vicinal" contribution describes the interaction arising from sp^3 hybrid orbitals of adjacent Si atoms directly participating in interatomic bonding, i.e. those pointing at their Si neighbors. The "geminal" contribution describes sp^3 interactions between orbitals associated with common Si-atoms (see Figure 3.4).

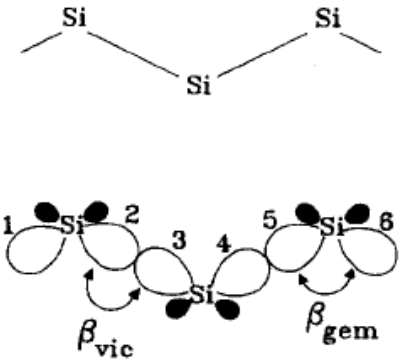

Figure 3.4. σ-bond planar topology of interacting Si $3sp^3$ orbitals in linear chain polysilane illustrating the different contributions to the observed, delocalized molecular orbital states associated with the Si-Si backbone. $\beta_{vicinal}$ (β_{vic}) is interaction energy between two sp^3 of adjacent Si participating in σ-bond. $\beta_{geminal}$ (β_{gem}) is interaction energy between two sp^3 on the same Si atoms [48].

The resonance integral, $\beta_{vicinal}$. describes the interaction energy contribution from sp^3 orbitals of adjacent silicon atoms responsible for Si-Si σ-bonds. An analysis of the resonance integral indicates the formation of a strongly bonding σ_{SiSi} localized bond orbital and strongly antibonding σ^*_{SiSi} orbital (see Figure 3.5). A weaker resonance integral, $\beta_{geminal}$, associated with the interaction between two sp^3 orbital on the same silicon atom serves to remove the degeneracy associated with the states arising from the vicinal interaction. In terms of the spatial distribution of the molecular orbital states associated with the Si-Si backbone, the Sandorfy model indicates that the $\beta_{geminal}$ also serves to couple the more localized σ_{SiSi} and σ^*_{SiSi} orbitals arising from the Si-Si pair interaction to form delocalized σ_{SiSi} and σ^*_{SiSi} orbitals which provide the basis for electron delocalization along Si-chains [47]. Figure 3.5 shows molecular orbital diagram of

different vicinal and geminal interaction energies and the corresponding location of orbital nodes along the backbone chains for the states involved. As the number of Si atoms participating in the backbone increases, additional orbital states from these Si atoms eventually results in the formation of bands associated with the σ and σ* orbital states arising from the vicinal interaction. Similarly, longer Si chains also contribute additional states to the energy levels arising from the geminal interaction. The overall effect is to produce delocalized band states associated with both the HOMO and LUMO levels. Optical absorption transitions between these HOMO and LUMO bands are responsible for the lowest energy absorption peaks observed in the polysilane systems of the current study. It is important to note that, in addition to chain length, changes in the Si-Si bond topology along the backbone chain will necessarily influence the energetic and spatial characteristics of orbital states associated with the Si-Si moiety.

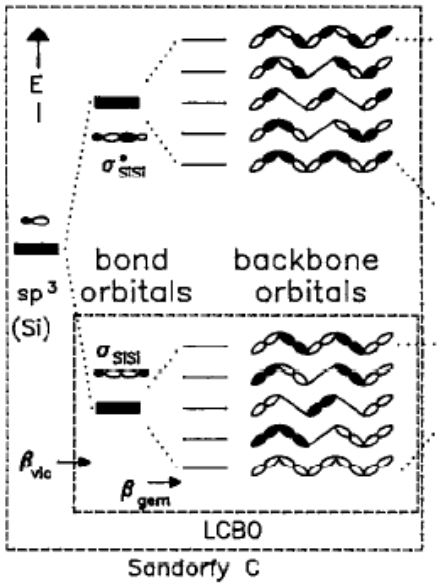

Figure 3.5. Schematic of the construction of σ orbitals of a long all-*trans* polysilane [48].

3.3.2. Effect of backbone constituents on electronic structure

Different backbone constituents affect the electronic energy level structure of the resulting polymers, producing concurrent modifications in the electronic absorption spectra. Saturated carbon backbone chains with no π-bonds for example, do not exhibit electron delocalization along the σ-bonds and exhibit absorption transitions associated with HOMO-LUMO transition at 150 nm – 190 nm [43-44]. Other group IVA backbone species, like the polysilane discussed in the previous section, provide electron delocalization producing absorption associated with σ bonds conjugation at longer wavelengths (>300 nm). Heavier backbone constituents tend to exhibit longer

wavelength absorption features associated with the backbone, for example n-butyl-silane [50], n-butyl-germane [35] and n-butyl-stannane [51], exhibit absorption features at 314 nm, 333 nm, and 365 nm, respectively. The difference in absorbed photon wavelength is related to the direct band-gap of these polymers and is supported by band density calculations indicating that polysilane (SiH_2) has a slightly higher band-gap than polygermane (GeH_2), (3.89 eV vs. 3.31 eV). These computations were performed using a first principles local density functional (LDF) method [52]. The same group also reported that the band-gap of the Si-Ge copolymer, independent of either a block or disordered structure, only depended on the ratio of silane and germane component in the backbone [52].

Given the effect of delocalization on electron transition energy, the polymer molecular weight influences the maximum wavelength (lowest energy) of the lowest energy absorption transition (corresponding to the HOMO-LUMO transition ($\sigma - \sigma^*$)) [32,52-53]. The effect can be qualitatively associated with 1-D confinement of the electron. Discontinuities in the backbone structure, associated with either physical truncation of the chain or modification of bond conformation, define the spatial extent of the electron motion. In this case, the absorbed photon wavelength is red-shifted with increasing chain length with consistent backbone conformation. Polysilanes containing aryl side-groups such as poly[(methyl)(phenyl)silane] exhibit a lowest energy absorption band shift from 200 nm to 340 nm corresponding to a chain length increase from 50 repeat units to 2000 repeat units. The effect saturates at 360 nm [53-54]. Polysilanes containing alkyl side-groups also exhibit a consistent trend, as illustrated in Figure 3.6.

The absorption wavelength maxima in this case shift from 200 nm to 300 nm with increasing backbone chain length [32, 55].

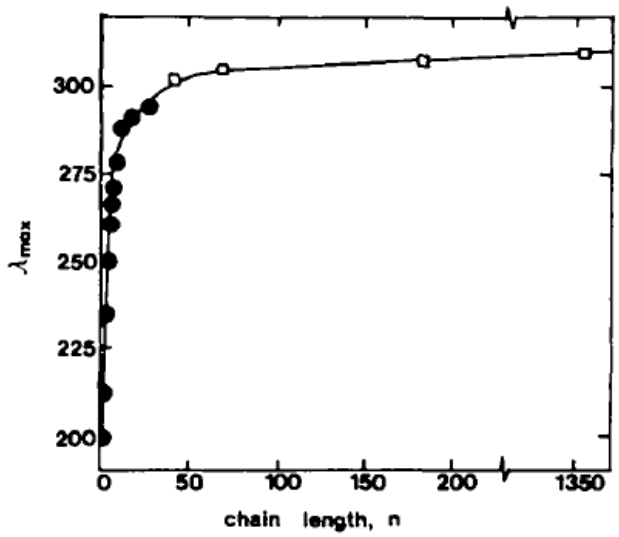

Figure 3.6. Absorption wavelength maxima of polyalkylsilane. Dark circle - $Me(Me_2Si)_nMe$. White square - $[(n\text{-dodecyl})(Me)Si)]_n$ [55]

As mentioned above, the effect of chain length on the HOMO-LUMO transition energy can be qualitatively elucidated using the example of a 1-D potential well. The delocalized σ-orbitals of the Si-backbone can be interpreted as a 1-D potential 'box' in which the electrons are free to move. The spatial extent of that motion is defined by finite potential barriers corresponding to the end of a chain or a point of discontinuity in bond conformation. The problem can be solved analytically for the case of an infinite potential well. Here, the electron energy inside this well is

$$E_n = \frac{\hbar^2 \pi^2}{2mL^2} n^2 \tag{3.1}$$

where $\hbar$ is reduced Planck constant, m is mass of electron and L is chain length.

Longer catenates also provide a higher molar extinction coefficient per Si-Si bond participating in the structure than shorter chain lengths. Gilman *et al.*, observed molar absorptivity increases with increasing Si chain length in $(Si(CH_3)_2)_n$ (n = 2-8) solution [44]. However, the Trefonas group was the first to recognize the correlation between chain length and molar extinction coefficients in polyalkylsilane as shown in Figure 3.7. In this case, the molar extinction coefficient increases with the number of Si repeat units and reaches a limiting value at 40-50 repeat units [55].

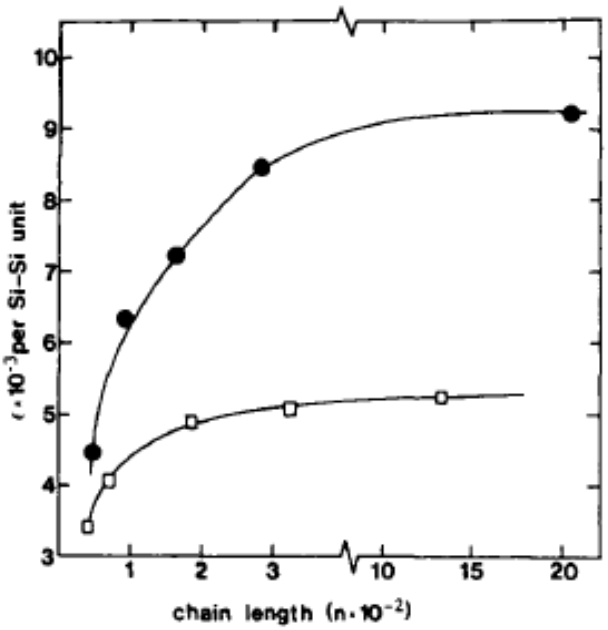

Figure 3.7. Molar extinction coefficient correlation with Si chain repeat units. Dark circle - $Me(Me_2Si)_nMe$. White square - $[(n\text{-dodecyl})(Me)Si)]_n$ [55]

3.3.3. Effect of side-groups and conformation on electronic structure

Polysilane polymers have many stable backbone conformations, including helical, *trans* or *gauche* type arrangements. The conformations are dictated by the sterics of the different organic side-groups attached to backbone. The *gauche* conformation forms a 60° dihedral angle between adjacent silicon atoms while the *trans* conformation has180° dihedral angle as illustrated in Figure 3.8. [48].

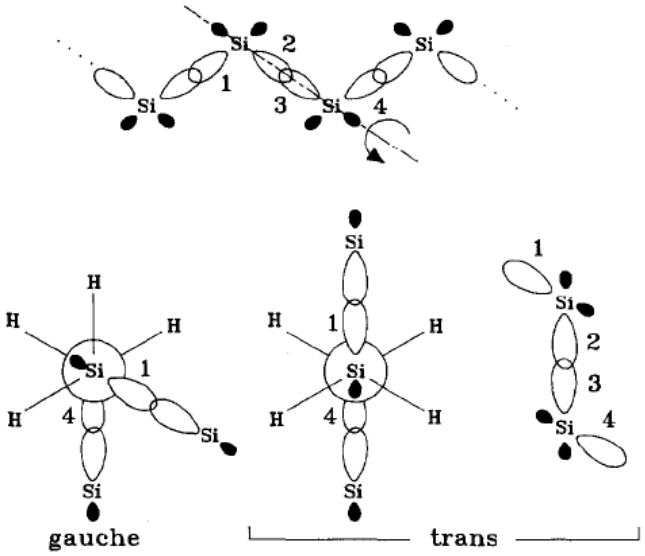

Figure 3.8. Relative orientation of sp^3 orbital in *gauche* and *trans* arrangement in oligosilane [48].

Since these conformations will influence the energetic of the delocalized σ and σ^* orbitals, different conformations in polysilane are observable through variation in the corresponding absorption energy of the HOMO-LUMO transition in these materials. Polysilanes with an alkyl side group, such as poly(di-n-hexyl)silane exhibit both helical and *trans* conformations that absorb at 317 nm and 354 nm, respectively [56-57]. In the context of the present study, poly[(methyl)(phenyl)silane] exhibits both *trans* and *gauche* arrangement at room temperature producing distinct σ-σ^* transitions at 3.63 eV (342 nm) and 3.73 eV (333 nm), respectively [58-63].

Chain conformation is strongly affected by different organic side-groups attached to backbone chains. For example, when two bulky side groups are attached to a backbone chain, such as in a poly(diarylsilane), these bulky side groups often force the

backbone to form an all-*trans* structure [64-65]. Zeigler *et al.*, investigated polysilanes with different side groups and found an approximate linear correlation between the position of absorption maximum and the sum of side-group substituents radii attached to backbone [62-63]. Long alkyl side-groups such as in poly(di-n-hexylsilylene) also affect backbone conformation by favoring interchain interaction to allow crystallization. Here, close packed chain structures are formed which force the backbone to have a *trans* planar structure [66-67]. These phenomena are mainly observed in solution where silicon chains are free to move.

In addition to steric related affects on backbone conformation, side group electronic structure can also influence the nature of the backbone lowest excited state through orbital admixing [59, 62, 68-70]. Aryl side-group such as phenyl and anisyl (methoxy-benzene) (Figure 3.9) provide orbital admixing between delocalized σ orbital from the backbone and π orbital from the side-group in the Highest Occupied Molecular Orbital (HOMO) [62]. Alkyl side-group-containing polysilanes, however, have all electrons of the backbone participating in σ-bonding and do not exhibit this phenomenon. Other evidence of orbital admixing is observed when the aryl group is buffered from the chain by insulating carbon atoms; the absorption spectra resemble those of simple alkyl substituents [55]. The first transition ($\sigma - \sigma^*$) in aryl-containing polysilane, such as in poly[(methyl)(phenyl)silane], is 2.5 eV - 5 eV (25-30 nm) lower in energy (longer wavelength) than polysilane with alkyl side-groups [59, 62, 69-72]. Additional aryl groups added to existing aryl-silane components such as in poly(diphenyl)silane have only a limited effect on the first transition energy [68,71]. A similar phenomenon of

orbital admixing between aryl side-group and delocalized backbone chains is also observed in polygermane and Ge-Si copolymers [68].

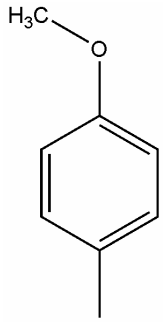

Figure 3.9. Diagram of anisyl (methoxy-benzene) side-group constituent.

In addition to backbone transition energy red-shifting, orbital admixing in PMPS also provides for an additional transition from a $\sigma - \pi$-admixed HOMO state to a π^* state, arising from the aryl group, which exists at a lower energy than $\pi - \pi^*$ transition in benzene (4.39 eV to 4.90 eV) as illustrated in Figure 3.10 [59]. The energy of the phenyl related transitions (labeled S_1, S_2 and S_3 in Figure 3.10) are between 4.39 eV to 7 eV while the energy of alkyl-side-group-related transitions (not shown in the diagram) are typically above 9 eV [59].

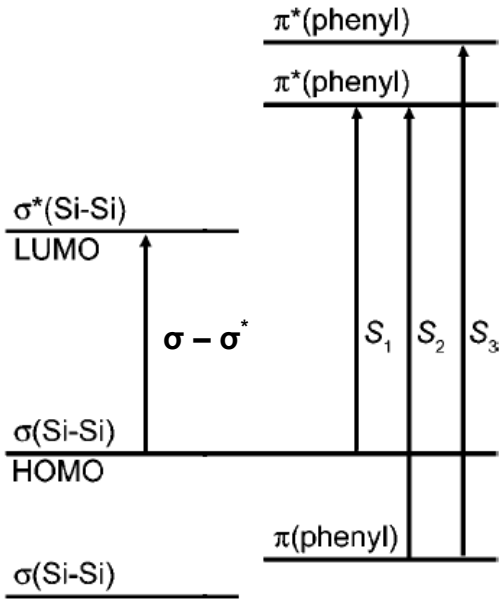

Figure 3.10. Band energy of poly[(methyl)(phenyl)silane] [59].

3.4. Photoinduced modifications in polysilane based materials

The primary photochemical decomposition mechanism in polysilane systems is a photoinduced backbone scissioning to produce silyl radicals [32, 53, 72-73]. Kumada *et al.*, studied different cyclic and linear polysilane derivatives in the presence of tri-alkyl silane trapping reagents and concluded that monomers of silylene and silyl radicals are concurrently produced as intermediates, subsequent to the initial photoscissioning

process. Although most of the intermediate silyl radicals subsequently form final photomodification products, the radicals are still observable in vibrational spectra after UV exposure which was confirmed with Density Functional Theory calculation [74-75].

Photolysis of the backbone chains occurs preferentially at longer segments which have lower bonding energies than shorter ones [76]. As Si-Si bonds are broken under UV-irradiation, the lowest energy absorption, corresponded to the $\sigma - \sigma^*$ transition, shifts to higher energy and exhibits a reduced absorption strength [77-81]. This effect is illustrated in Figure 3.11. Again, the blue shift observed with chain scissioning can be qualitatively interpreted as 1-D confinement of carriers along the conjugation length of the chains whose average length is reduced with UV fluence.

The photoinduced silyl radicals can follow different reaction paths after they are formed. One such pathway is their recombination with other silyl radical to form lower molecular weight polysilane chains, thus contributing to the blue-shift in UV absorption spectra. This structural product has been confirmed using Gel Permeation Chromatography (GPC) techniques [79-81]. Silyl radicals can also recombine with oxygen and water from surrounding environment to form siloxane bridging structures [82-84].

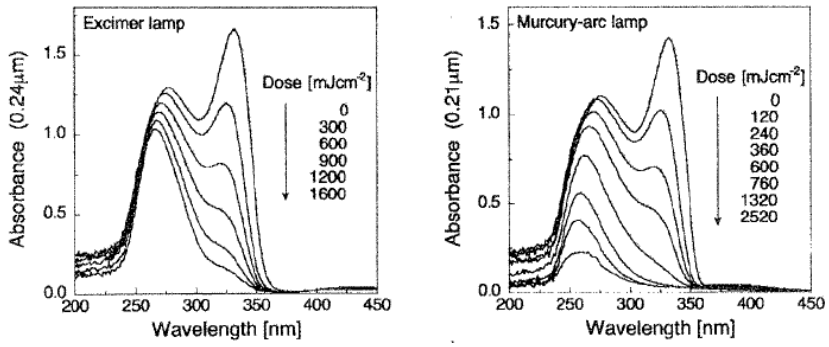

Figure 3.11. Absorption spectra of poly[(methyl)(phenyl)silane] irradiated with excimer lamp (308 nm) and mercury-arc lamp (185, 254 and 313 nm) [78].

Photoinduced structural modifications primarily involve backbone scissioning with photon energy irradiation higher than $\sigma - \sigma^*$ transition energy, the lowest energy transition. However, side-group related photoinduced modification is typically only with higher energy photon irradiation, i.e. resonant with side-groups moieties. The photoexposure results in the disruption of these side-group substituents while also producing modifications to the backbone structure. For example, UV irradiation with energy of 5.10 eV (248 nm) in poly[(methyl)(phenyl)silane] disrupts π orbitals of phenyl group and causes ring opening reactions to yield dialdehydes structures in response to this photoinduced structural modification [85]. Other possible mechanisms involve complete removal of phenyl groups from the chain [86].

The alkyl group, in contrast, has a higher transition energy (> 9 eV) compared to transitions involving the phenyl group. As a result, photoirradiation with photon energy below 9 eV (138 nm) will have limited direct impact on alkyl moieties .

Electronic structure differences arising from photostructural modifications necessarily result in changes in the material absorption spectrum which produce modifications in the material refractive index, through the Kramer-Kronig relation [86]. The effect of photoexposure on refractive index in polysilanes has been confirmed experimentally [25-26,78]. Nagayama *et al.*, investigated photoinduced refractive index changes in polysilane containing different side-groups (both alkyl and aryl groups) using an excimer lamp (308 nm) and a mercury-arc lamp (185, 254 and 313 nm) as excitation sources [78]. The maximum refractive index changes produced in polysilanes with alkyl only side-groups were found to range from -0.05 to -0.08 while systems containing aryl side-groups have higher refractive index changes, typically between -0.11 to -0.14. High photoinduced refractive index changes attained in system containing aryl groups are associated with $\sigma - \pi$ conjugation. Irradiation with high energy photons (λ = 185 nm and 254 nm) disrupt both backbone chains and side-groups in aryl-polysilanes while in contrast, the photon energy only disrupt backbone chains in polysilane with alkyl side-group [78]. There were no refractive index studies for polygermane and Ge-Si copolymers prior to the current study.

3.5. Thermal induced modifications in polysilane based materials

Thermal properties of polysilanes were initially studied when using the material as a precursor for SiC [17] and SiO_2 [87]. In both photoinduced and thermal induced modifications, initial structural disruptions involved backbone scissioning and the formation of silyl radicals before modification to the side-groups were observed. This is consistent with higher Si-C bond strength (~90 kcal/mol) and C-C bond strength (~85 kcal/mol) compare to Si-Si bond strength (~80 kcal/mol) and Si-H bond strength (~79 kcal/mol) [88]. The silyl radicals produced could react with side-groups and form a cross-linked network structure as well as participating in back-biting processes, in which a radical formed at the end of the chain recombined with the one at the opposite end to form cyclic oligomers [91-92]. Under aerobic environments, oxygen will be incorporated in these radicals and produced siloxane bridge structures [89-90].

The backbone scissioning of polysilane Si-Si bonds starts at 150 C, observed using DSC (Differential Scanning Calorimetry) and GPC (Gel Permeation Chromatography) [89-90]. Pan *et al.*, studied thermal decomposition of poly[(methyl)(phenyl)silane] (PMPS) in thin films by a pyrolisis method [91-92]. In this study, PMPS was heated and evolved gases were measured by mass spectrometry. They detected Si monomer radical formation at 270 C – 477 C. At higher temperatures, i.e. 280 C – 480 C, organic groups, such as phenyl and methyl in PMPS, detached from backbone catenates [91-92].

4. EXPERIMENTAL PROCEDURES

4.1. Materials

All Group IVA-based inorganic polymers used in the current studies were synthesized at Sandia National Laboratories by Dr. G.M. Jamison. The polysilane based materials used in the present studies were poly[(methyl)(phenyl)]silylene (PMPS), poly[bis-(ethylphenyl)]silylene (PBEPS). A copolymer system involving both silane and germane backbone substituents, i.e. bis-(ethylphenyl)silane-co-[(hexyl)(phenyl)]germane (Ge-Si copolymer) was also examined. Figure 7.1 provides the repeating units for these polymer materials.

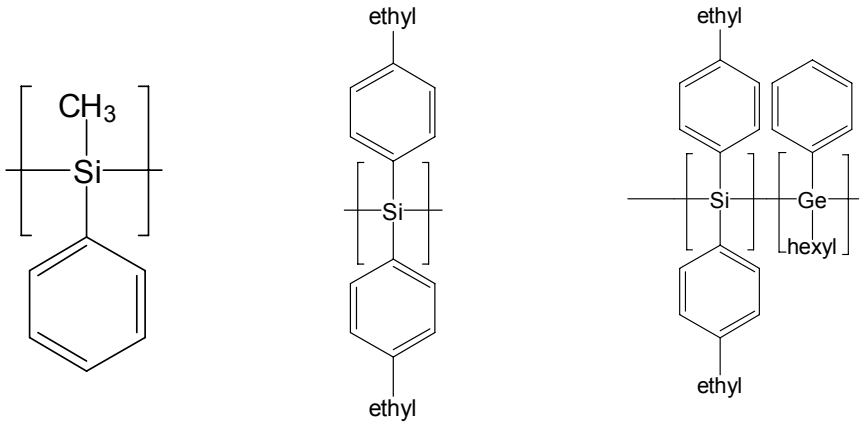

Figure 4.1. Repeat unit structure of (a) poly[(methyl)(phenyl)silylene], (b) poly[bis-(ethylphenyl)silylene], (c) bis-(ethylphenyl)silane-co-[(hexyl)(phenyl)]germane.

Both PBEPS and PMPS materials consist of silicon backbone chains with different side-groups. The PBEPS contains ethyl-phenyl components on both sides of the silicon backbone while the PMPS structure consists of methyl and phenyl side-groups on alternate sides of the central backbone chain. In the copolymer, the silicon repeat unit is identical to that of the PBEPS structure, i.e. bis-(ethylphenyl) side-groups attached to silane components, however, 5 mol% of these silane units are replaced with the (hexyl)(phenyl)germane unit. Such a controlled introduction of alternative side group and backbone moieties offers the opportunity examine the impact of molecular design on the ensuing photosensitive and thermal response of these materials.

All materials were polymerized using a Wurtz-coupling method with commercially available monomers which were distilled under vacuum prior to use [25]. Dichloro(methylphenyl)silane monomer was polymerized in this manner to form PMPS, whereas PBEPS was polymerized from bis-(4-ethylphenyl)dichlorosilane monomer. The monomers were polymerized in the presence of a metallic sodium catalyst in anhydrous toluene at 120°C. The resulting solution mixture was quenched with isopropyl alcohol to remove excess sodium. An equal amount of water was then added to remove any NaCl byproduct and any solution resulting from an isopropyl or methyl alcohol quench. The weight-average molecular weight of PMPS after polymerization and subsequent fractionation (to isolate higher molecular weight materials), was found to be ~42,000 respectively via gel permeation chromatography (GPC) analysis (polystyrene standard), while Ge-Si copolymer and PBEPS molecular weight was found to be 4850 [94]. The PMPS structure were confirmed by multinuclear (^{1}H, ^{13}C, ^{29}Si) NMR analysis. Proton

NMR also was used to confirm PBEPS and Ge-Si copolymer structures, including the relative Ge:Si fraction present in the backbone.

The bis-(ethylphenyl)silane-co-[(hexyl)(phenyl)]germane copolymer was synthesized from bis-(4-ethylphenyl)dichlorosilane and (n-hexyl)(phenyl)-dichlorogermane monomers with 95:5 silane:germane molar ratio. The monomer mixture was dropped slowly into a stirred 4.4-fold excess of sodium in toluene to maintain a gentle reflux. The excess sodium metal was quenched with methanol until gas evolution ceased and separated from the polymer solution using saturated sodium bicarbonate. The solution was filtered with Celite (dry filtrate with anhydrous $MgSO_4$). After toluene evaporated, the viscous white solid was dissolved into more toluene and filtered with 0.45 μm Teflon filter into methanol solution. The suspension was filtered to produce Ge-Si copolymer powder. All polymer powder was stored in vials covered with aluminum foil to prevent light exposure [94].

Thin films of polysilane (PBEPS and PMPS) and Ge-Si copolymer were deposited from solution using spin coating techniques. PMPS powder was dissolved in toluene. PBEPS and Ge-Si copolymers, in contrast to PMPS, were dissolved in tetrahydrofuran (THF) for increased solubility. Typical spin conditions involved a spin speed of 2500 rpm for 30 seconds with the solution squeezed through a 0.45 – 1 μm polytetrafluoroethylene (PTFE) syringe filter. The deposited films were then annealed on a hot plate for 30 minutes to remove any excess solvent after deposition. All sample preparations and thin film depositions were performed in a glove box under dry argon and low light conditions.

Different solution concentrations were used to control thin film thickness for compatibility with different spectroscopy studies requirements. Typical PMPS and Ge-Si samples, which were used for UV-visible and ellipsometric investigations, were deposited from a solution of 6.25% weight polymer in an appropriate solvent onto silica substrates. The thickness of these PMPS thin films samples was ~350 +/- 5 nm while Ge-Si copolymer films were ~350 +/- 15 nm. Thinner polymer films were required for vacuum-UV spectroscopy as electronic absorption in the vacuum UV region was generally about 2-3 times higher than in the visible-near UV wavelength band. In this case a 0.5 wt % solution was used to produce 100 – 150 nm thick polymer films on MgF_2 substrates.

In contrast, transmission Fourier Transform Infrared Spectroscopy (FTIR) required thicker films. In this case, solution concentration was increased to 12.5% to produce 1.5 – 2.0 μm thick films of PMPS and Ge-Si copolymer thin films on KCl substrates. All PBEPS thin films were deposited from 4.39% weight polymer/THF solution. The PBEPS thin film was spun coat onto SiO_2 and KCl substrates for UV absorption and FTIR analysis respectively to produce 280 nm ± 5 nm thick films. The thickness data for all films were obtained using stylus profilometry and confirmed by ellipsometer measurement over a 1 cm^2 area. The stylus profilometer used was a Veeco Model 6M with a 12.5 μm-radius diamond stylus tip providing a spatial resolution of 0.533 μm and a vertical resolution of 1 nm.

4.2. Optical exposure and thermal treatment

4.2.1 Optical exposure

The photoinduced response of the polymer films, including modifications in electronic structure, vibrational structure, and refractive index were monitored as a function of cumulative incident fluence, excitation wavelength and local environment condition using various spectroscopy techniques. The as-deposited PMPS, PBEPS and Ge-Si copolymer behavior, such as refractive index and optical absorption spectra, were compared to those obtained after UV exposure. The UV sources used for optical exposure were a pulsed nitrogen laser (λ = 337.1 nm, E_{inc} = 3.68 eV, pulsed intensity = 0.19 mJ / cm^2 / pulse, pulse length = 800 ps, rep. rate = 5 Hz) and a KrF excimer laser (λ = 248 nm, E_{inc} = 5.10 eV, pulsed intensity ranging from 1.2 to 8 mJ / cm^2 / pulse, pulse length = 20 ns, rep. rate = 5 Hz). Different pulse intensities were used in the excimer laser (1.2 – 8 mJ/cm^2/pulse) in order to evaluate the damage threshold of the PMPS films, an important issue for rapid photowriting in the target application. In addition to these optical-bench photon sources, compact solid-state UV light emitting diodes (LED) with continuous wave (cw) output (λ = 370.0 nm, E_{inc} = 0.287 mW/cm^2) was used as excitation sources for the PBEPS and Ge-Si copolymer photosensitive study. LED's were selected in order to match the output wavelength with known absorption features in these materials. These compact optical sources were also consistent with those anticipated for the on-the-fly writing application.

All UV irradiations were performed in a stainless steel controlled atmosphere chamber equipped with silica windows for optical access. The photoresponses of

polysilane (PMPS and PBEPS) and Ge-Si copolymer under aerobic (dry air, oxygen) and anaerobic (forming gas (5%/95% H_2/N_2), nitrogen) local environments were compared. Prior to optical exposure, the chamber was purged for 5-10 minutes using the appropriate gas at an elevated flow rate, which allowed at least 7-8 chamber volume replacements. During optical exposure, a flow rate of approximately 10 ml / min was maintained through an in-line desiccant filter. A schematic of a picture of controlled environmental chamber and the optical setup are shown in Figures 4.2 and 4.3, respectively. Photosensitivity studies typically involved iterative cycles of UV exposure and spectroscopic evaluation to monitor changes in the absorption spectra or refractive index.

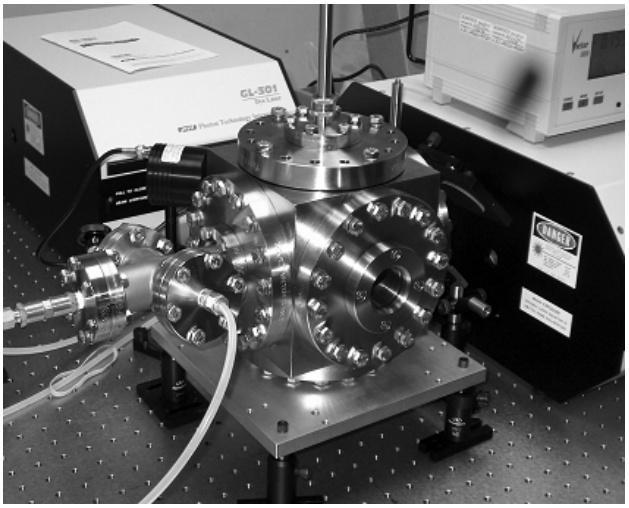

Figure 4.2. Controlled environmental chamber used for UV-irradiation of molecular hybrid thin films.

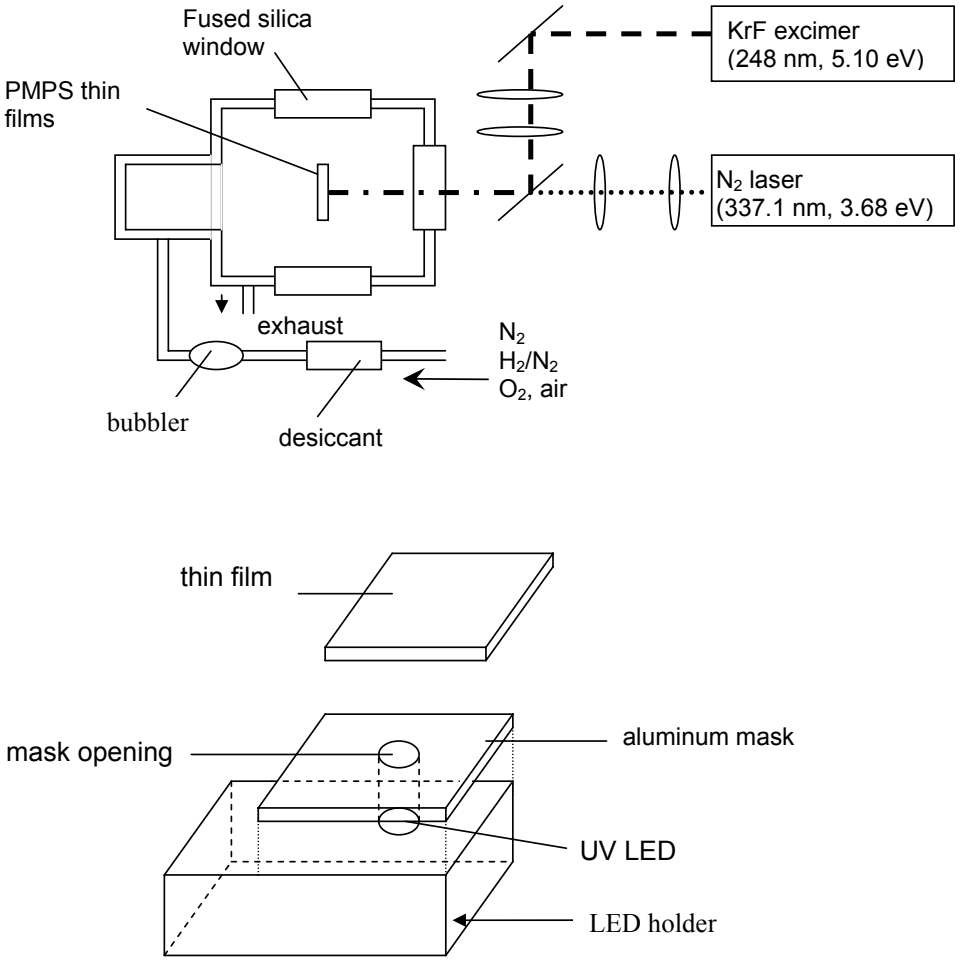

Figure 4.3. (Top) Optical setup for PMPS thin films irradiated with nitrogen or excimer lasers. (Bottom) A detail view of the masking geometry used for irradiation of PBEPS and Ge-Si copolymer materials using LED optical sources. The entire assembly, including LED, stainless steel mask, and sample, were placed inside the stainless steel chamber of Figure 4.2 and shown in the schematic (Top).

4.2.2 Thermal Treatment

The thermal response of as-deposited and UV-irradiated materials were examined in terms of their electronic structure, molecular structure, and refractive index. These characteristics were monitored as a function of different heat treatment schedules using UV-vis and FTIR absorption spectroscopies and ellipsometry. As-deposited and UV-irradiated PMPS samples were obtained on the same substrate. By masked exposure with an aluminum sheet to produce the "as-deposited" sample . The other half of the same substrate was irradiated with the 3.68 eV nitrogen laser beam until no further UV absorption spectral changes were observed (typically at fluence levels of 3.3 J/cm^2). Different sets of PMPS samples were UV-irradiated under either air or nitrogen in order to investigate the effect of local atmospheric environment used during the initial photowriting on the subsequent response of the material to heat treatment. A thermal study of PMPS subjected to high-photon energy UV exposure (5.10 eV) from the KrF excimer source was not pursued as the absorption bands of interest in near-UV and visible region of these samples had been completely bleached prior to thermal treatment.

In the heat treatment process, PMPS thin films samples were placed on a silica boat and placed inside pre-heated, controlled atmosphere tube furnace. A flowing nitrogen (about 10 ml/min) environment was used during all thermal processing. In addition to the process control thermocouple used for tube furnace system, an additional thermocouple was placed just above silica boat to confirm the local temperature near the sample as illustrated in Figure 4.4 (top). After each heat treatment, the thin film sample was moved to the end of the furnace tube for cooling outside the heating zone under an

excess flow of nitrogen (Figure 4.4 – bottom). The cool down step after heating was designed to reduce oxidation of the hot PMPS thin films upon their removal from the process tube into the lab environment. Similar to the photoresponse studies, thermally induced modifications of the PMPS materials were also monitored using UV-visible spectroscopy, FTIR and ellipsometry techniques.

In the first thermal study, two sets of PMPS thin films, irradiated under different local environments (nitrogen and air), were subjected to sequential isochronal thermal anneals in the tube furnace. Treatment temperatures ranged from 60 C - 260 C at 5-10 C increments. Sample were held at temperature for 10 minutes. The thermal treatment process involved iterative spectroscopic measurement and heat treatment of the same sample throughout the heat treatment schedule.

The second part of this study involved isothermal heat treatment at 120C, 160C, 190C and 200C. At each heat treatment temperature, structural changes in two different sets of PMPS films irradiated under different local atmospheres (nitrogen and air) were compared as a function of heat treatment time. Again, typical processing involved iterative analysis of the samples (via FTIR and UV-vis spectroscopy) at the set temperature.

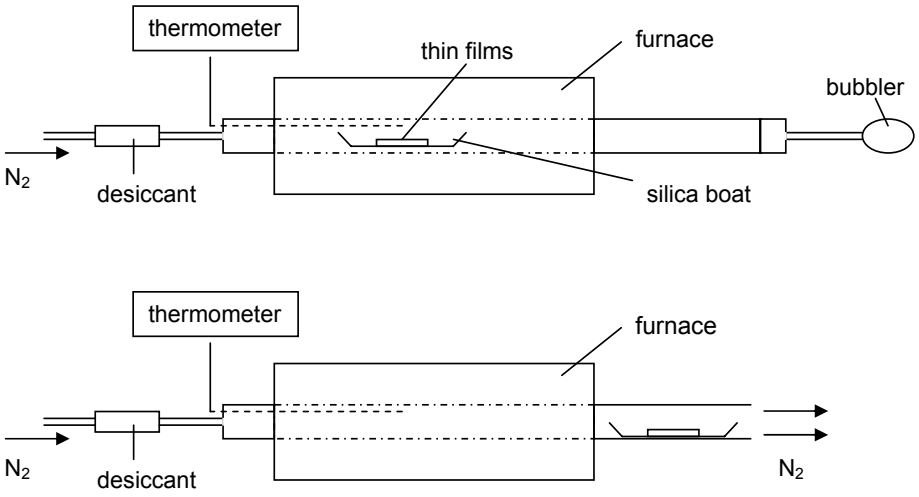

Figure 4.4. Schematic of thermal treatment; (top) during thermal treatment, (bottom) after heat treatment.

4.3. Materials properties characterization

4.3.1. Electronic structure

Photoinduced modification of electronic structure of PMPS and Ge-Si copolymer was observed with a combination of UV-visible (0-6 eV) and VUV (5-11 eV) spectroscopies while PBEPS films were only observed in the UV-visible energy range. The VUV spectra were collected over the energy (wavelength) range 5-11 eV (115 – 250 nm) with 0.1 nm resolution using an Acton Model VM-504 single-beam spectrometer. The spectrometer utilized a deuterium light source and thermoelectrically stabilized photomultiplier detector. The optical beam path was evacuated to ~3.0 x 10^{-6} - 1.0 x 10^{-5} Torr during data collection. A Perkin Elmer Lambda 950 double-beam UV-visible spectrometer was used to monitor the visible to near-UV region. Spectra were collected with a spectral bandpass of 1 nm. All VUV and near-UV absorption data were collected at room temperature. Multiple consecutive scans of materials absorption spectra in both VUV and near-UV confirmed that spectroscopic measurement involving low intensity UV light did not alter the absorption properties of the thin films.

Ellipsometry measurement used a He-Ne photon source (λ = 632.8 nm) to measure thin film refractive index (n) and thickness (t). Multiple measurement of refractive index is performed over an approximately 1 cm^2 area of the as-deposited thin films or ~0.5 cm^2 of the UV-irradiated area. Experimental error in the ellipsometer measurement was found to be approximately +/- 0.005, arising from both instrumental error and typical sample inhomogeneities. In addition to experimental measurement, calculation of Δn and Δt based on UV-visible and vacuum-UV absorption spectra are

performed using the Kramers-Kronig method [95]. The accuracy of the calculated $\Delta n_{632.8}$ value is ~5% based on uncertainty in film thickness measurements (via stylus profilometry) and sample-to-sample variation.

4.3.2. Molecular structure

Photoinduced molecular structural modification of PMPS, PBEPS and Ge-Si copolymer was monitored using Fourier Transform Infrared Spectroscopy (FTIR) (Bruker Tensor 27) from 400 cm^{-1} to 4000 cm^{-1}. In this measurement, KCl substrates were used because of their wide optical window at low wavenumber (down to ~420 cm^{-1}) and low cost. Typical measurements used a nitrogen purge for 5-10 minutes to reduce spectral interference from atmospheric water vibrations at around 1600 cm^{-1}. The resolution of the FTIR spectra is 4 cm^{-1} and the spectra reported represent a signal average of 128 scans.

4.3.3. Molecular modeling and quantum calculation

These experimental vibrational studies were augmented by Density Functional Theory (DFT) calculations of Si-based oligomers anticipated to represent some of the medium range structure of these materials both before and after photon and thermal exposure. A normal mode analysis of energy minimized structures allowed for correlation with experimental FTIR results. While insufficient for a full analysis of the high molecular weight polymeric systems under study, this approach did enable confirmation of vibrational band assignment in the as-synthesized polymer films and the

structural nature of photoproducts, e.g. the results of chain scissioning and oxidation. Density Functional Theory (DFT) calculations were performed using commercially available software, Gaussian 03 by Gaussian Inc [96]. The computation employed Becke's Three Parameter Hybrid Method using the Lee Yang and Parr Correlation (B3YLP) [97]. The basis set used for both the geometrical optimization (through energy minimization) and the subsequent normal mode frequency calculation was 6-31G*. The calculated frequencies were scaled by a factor of 0.9613, which was derived empirically to provide a match between experimental data and the calculated frequencies.

Oligomers examined via DFT (and their associated polymeric system) include (methyl)(phenyl)pentasilane (PMPS as-synthesized), (methyl)(phenyl)pentasiloxane (PMPS, irradiated), (methyl)(phenyl)pentagermane (copolymer, as-synthesized), (methyl)(phenyl)pentagermano-oxide (copolymer, irradiated), (bisphenyl)butasilane (bi-phenyl, as synthesized) and (hexyl)(phenyl)pentagermane (copolymer, as-synthesized).

While it is anticipated that energy minimization and normal mode analyses with larger clusters would be more consistent with the materials systems examined experimentally, limited computational resources precluded more involved computations on larger systems. For example, the relatively short chain oligomers used in the present calculations prevented a realistic analysis of the Ge-Si copolymer since a model with longer backbone chain would be required to accurately represent both the 5 mol% Ge content and the statistical variation of Ge position along the backbone. This problem was addressed by dividing actual molecules used in experiment into smaller systems to fit the

computational limitations. The calculation results from these smaller systems were gain insight into the behavior exhibited in experiment.

4.4. Photopatterning

Patterned UV exposure was used to produce Bragg gratings on 1 μm thick PMPS thin films using a UV-grade fused silica zero-order-suppressed phase mask (Lasiris Inc). The phase mask used has a period of 0.543 μm with first-order diffraction efficiencies of 32.5%. The setup of grating photowriting is illustrated in Figure 4.5. The typical setup included dual planar convex lenses (f = 75 mm) to collimate the incident UV-beam. In this demonstration, the gratings were produced with a KrF excimer laser (λ = 248 nm, E_{inc} = 5.10 eV, pulsed intensity = 3.5 mJ / cm^2 / pulse, pulse length = 20 ns, rep. rate = 5 Hz) with total fluence of 7-8 J/cm^2.

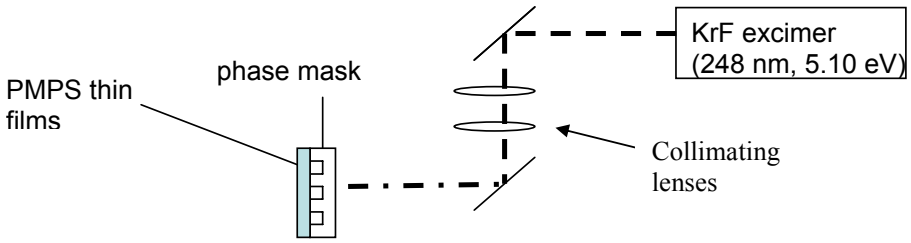

Figure 4.5. Schematic of Bragg-grating photowriting experiment.

The efficiency of the photoinduced gratings produced in the PMPS films was measured using a He-Ne laser (632.8 nm). Both first order and zeroth order diffraction signal detection was accomplished using a lock-in amplifier arrangement that employed a mechanical chopper in the beam path (repetition rate = 35 Hz). A Si photodiode served as the detector. The grating efficiency was calculated by normalizing the first order diffraction signal with zeroth-order signal.

5. RESULTS AND ANALYSIS

5.1. Electronic structure and optical properties of as-deposited materials

As described in the background section, modifications of side group and backbone chemistry are anticipated to influence the transition energetic of the HOMO-LUMO (σ-σ*) transition in polysilylene through modification of both backbone bond conformation and inherent changes in the nature of the conjugated electronic states involved. Different organic side-groups and backbone constituents affect materials electronic structure, particularly the lowest energy (the longest wavelength) absorption band arising from the σ-σ^* transition associated with the backbone chains.

Figure 5.1 contains absorption spectra collected in the near-UV region for poly[(methyl)(phenyl)silane] (PMPS), poly[(bis-ethylphenyl)]silane (PBEPS) and Ge-Si copolymer systems of the present study. The spectra reflect the variation in electronic structure expected with different organic side groups and different backbone constituents.

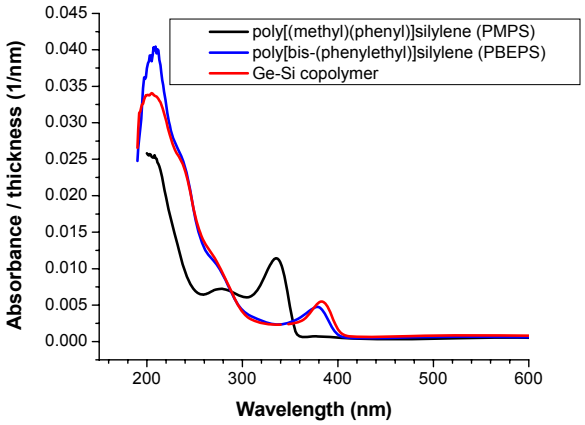

Figure 5.1. Representative of near-UV spectra of as-deposited PMPS, PBEPS and Ge-Si copolymer.

Poly[(methyl)(phenyl)silane] (PMPS) exhibits the σ-σ^* transition at 337.1 nm (3.68 eV). Replacing the organic side groups of PMPS with the ethyl-substituted phenyl groups on either side of the silicon chains in PBEPS forces the backbone into an all-*trans* conformation which the corresponding transition to lower energy - 378 nm (3.28 eV) [64,65]. In the Ge-Si copolymer, the 5 mol % Ge for Si replacement in the backbone produced an additional red-shift of the lowest energy absorption transition to 385 nm (3.22 eV). A reduction in backbone σ-σ^* (HOMO-LUMO) transition energy is anticipated based on computational results involving trans-polygermane in which an all-polygermane-based chain structure is anticipated to exhibit a HOMO-LUMO transition as much as 0.5 eV lower than the analogous polysilane (dependent on conformation) [52,98].

Phifer *et al.*, [59] have investigated the electronic structure of PMPS from the visible to VUV energy regions, and provided a structural interpretation of the spectral features observed (see further discussion below). In this context, near-UV and vacuum-UV (VUV) spectra for each exposure condition were combined and fitted with Gaussian peak components associated with the optical transitions identified in Ref [59] in order to more clearly quantify the changes in PMPS spectral behavior observed. From an initial guess of peak positions, peak heights, and widths, an automated nonlinear least squares routine was utilized to minimize the residual difference between the experimental spectrum and the fitted curve. In all cases, peak width, height and position were allowed to vary during the fitting process. Uncertainties in peak area and position arising from variations in initial parameter values was found to be ~1% resulting in an uncertainty in the total peak area changes computed over the entire spectra range to be < 2%. Representative experimental and fitted spectra for as-deposited PMPS from near-UV to vacuum-UV regions are presented in Figure 5.2.

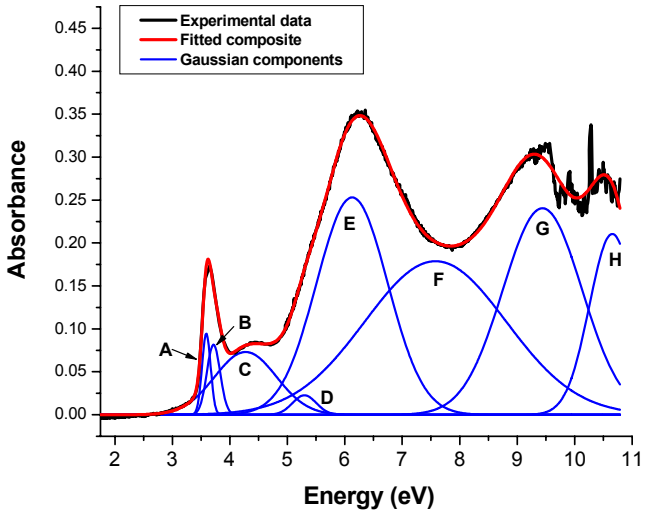

Figure 5.2. Representative peak fitting results for as-deposited PMPS absorption spectra (see text for discussion of fitting procedure and uncertainty estimates). Dotted lines denote the experimental spectrum while bolded curves are the fitted peaks [99].

Absorbance peaks of PMPS in the vacuum-UV regions (>5.5 eV) are primarily associated with both phenyl and methyl side groups transitions. These peaks are larger in magnitude compared to those associated with σ-bond conjugation in the Si backbone. The VUV absorption spectra above 11 eV contain sharp features due to incomplete normalization of deuterium light output within this low spectral irradiance region of the lamp spectrum. Fitted Gaussian components in Figure 5.2 are labeled alphabetically. Backbone related absorption resonances are centered at 3.68 eV (A), 3.73 eV (B) and 7.6 eV (F). Phenyl group transitions are centered at 4.36 eV (C), 5.29 eV (D) and 6.1 eV (E).

Other resonance peaks, both centered at 9.4 eV (G) and 10.7 (H), are associated with the methyl group.

Ge-Si copolymer absorption spectra in both near-UV and vacuum-UV regions are combined and fitted with Gaussian components using the same methodology as that used for the PMPS absorption spectra. The representative spectra of as-deposited Ge-Si copolymer and Gaussian components are provided in Figure 5.3. There are no references available on germane-based vacuum-UV spectra, thus, the Gaussian components used to fit the experimental data were derived from insights obtained from the PMPS absorption bands identification. The peak-fitting process and peak assignments in Ge-Si absorption spectra were based on PMPS as they both contain phenyl group and are anticipated to be dominated by resonances associated with the silane backbone. Therefore, as described previously, the lowest energy peak in the absorption spectra, 3.8 eV (A) is due to σ-σ^* transition of backbone. An absorption peak corresponding to the higher order backbone transition is centered at 7.2 eV (E). Three different Gaussian components were used to represent phenyl-group transitions at 5.2 eV (B), 5.8 eV (C) and 6.1 eV (D). The ethyl and hexyl group transitions are expected to have the highest energy, 9.1 eV (F). A more comprehensive discussion of these peak assignments will be presented in a later section.

The typical refractive index of as-deposited PMPS is approximately 1.699 +/- 0.005 as measured by ellipsometry at λ = 632.8 nm. As anticipated, both the Ge-Si copolymer and PBEPS have similar as-deposited refractive indices, i.e. 1.565 +/- 0.009 and 1.563 +/- 0.004, respectively. A broader range of uncertainty in refractive index for

of the Ge-Si copolymer reflects the film non-uniformity characteristic of the Ge-Si copolymer films when compared to that typically observed in PBEPS or PMPS.

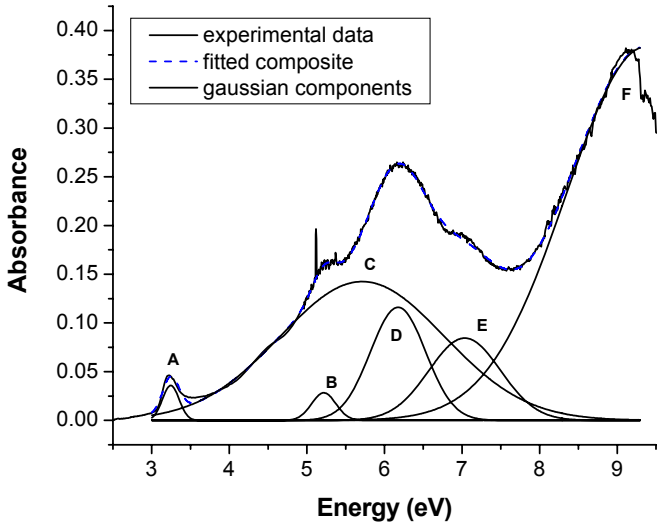

Figure 5.3. Representative peak fitting results for Ge-Si absorption spectra (see text for discussion of fitting procedure). Dotted lines denote the experimental spectrum while bolded curves are the fitted peaks.

5.2. Structural properties of as-deposited materials

5.2.1. Poly[(methyl)(phenyl)silane] (PMPS)

Vibrational spectra collected from as-deposited PMPS thin films between 400 cm^{-1} to near 3500 cm^{-1} are provided in Figure 5.4. The figures contain both experimental results and the spectra predicted from a normal mode vibrational frequency analysis of the optimized (phenyl)(methyl)pentasilane structure obtained via DFT. Computed normal mode frequencies have been scaled as discussed in the Experimental section. .

The experimental FTIR data show reasonable agreement with the DFT calculation. However, in some cases, the DFT calculated spectra contain additional bands which do not exist in experiment. For example, two extra resonances observed in the normal mode analysis (Figure 5.4) at 870 cm^{-1} and 2100 cm^{-1} are associated with Si-H used to terminate the oligomeric structure used in the computation. The Si-H vibrational resonances are typically not observed in the experimental results from the as-deposited PMPS due to the much lower relative Si-H content in the high MW polymer compared to the model oligomer. This (methyl)(phenyl)silane oligomer only contained of five repeat units each capped with terminating hydrides. Therefore, Si-H bonds contribution in the calculated system is significant as shown in Figure 5.4.

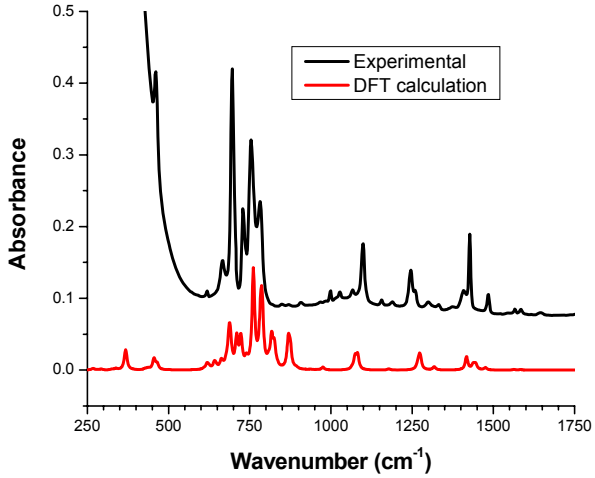

(a)

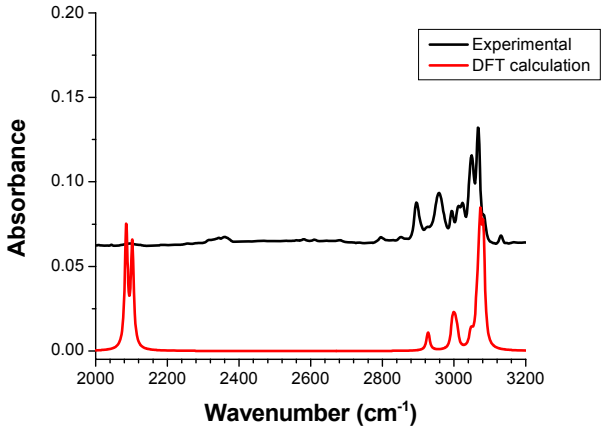

(b)

Figure 5.4. Vibrational spectra of as-deposited PMPS (black line) and a computed spectrum (red line) obtained from the DFT normal mode analysis of a model oligomeric cluster (a) 250-1750 cm^{-1}. (b) 2000-3250 cm^{-1}.

Overall, however, the good agreement observed between computation and experiment enables insight into the structural basis for the peaks observed. For example a vibrational band at ~450 cm^{-1} has been associated with the Si-Si stretching vibration, and it is found to exist in both the DFT and the experimental spectra. A more detailed discussion regarding the DFT calculation and the experimental results is presented in the next section.

All vibrational spectra observed contain a large absorption band at near 400 cm^{-1} which is the limit of optical window for the KCl substrate. In PMPS (Figure 5.4), a peak corresponding to the Si backbone chain asymmetric stretch is observed experimentally at 450-480 cm^{-1} [74,100-101]. The peak is superimposed upon the sharply increasing absorption edge arising from the from KCl substrate. Another band associated with the backbone structure is observed at 1000-1100 cm^{-1}. This relatively weak and broad absorption band is caused by Si-O-Si stretching vibrations [100], hence, it does not exist in the DFT calculation of the pentasilane structure.

Side-group-related resonances such as Si-methyl are located at 730 cm^{-1}, 755 cm^{-1} and 1240-1290 cm^{-1}. The vibrational bands at 730 cm^{-1} and 755 cm^{-1} are associated with Si-C stretching and rocking vibrations, respectively [100, 102] while the band at 1240-1290 cm^{-1} is associated with the CH_3 deformation vibration [102]. A strong Si-phenyl stretching vibration is located at 1100 cm^{-1} [56,102]. The phenyl group has several vibrational bands. For example C-C stretching vibrations are located at 1405 cm^{-1} and 1480 cm^{-1} while the phenyl rocking vibrational band is located at 980 cm^{-1}. More C-H vibrational bands, associated with methyl and phenyl groups, are found overlapping in

the 2750-3300 cm^{-1} range. A summary of vibrational band assignments in as-deposited PMPS is available in Table 1.

Table 1. Summary of vibrational resonance energies and their assignments in as-deposited PMPS thin films.

Frequencies (cm^{-1})	**Peaks identification**	**Corresponding structure**	**Ref.**
450 cm^{-1}	Si-Si stretching vib.	backbone	[74,100-101]
665 cm^{-1}	C-C out of plane vib.	phenyl	[100]
695 cm^{-1}	C-H out of plane vib.	phenyl	[100]
730 cm^{-1}	Si-C stretching vib.	backbone-phenyl	[100]
755 cm^{-1}	Si-C rocking vib	backbone-phenyl	[100, 102]
785 cm^{-1}	C-H in plane vibration	phenyl	[100]
997 cm^{-1}	C-C rocking vib	phenyl	[103]
1030 cm^{-1}	=C-H in plane deformation	phenyl	[100]
1068 cm^{-1}	=C-H in plane deformation	phenyl	[100]
1100 cm^{-1}	Si-phenyl stretch	backbone-phenyl	[56-102]
1000-1100 cm^{-1}	Si-O-Si – stretch	backbone	[100]
1240-1260 cm^{-1}	$-CH_3$ sym. deformation vib.	Si-methyl	[100]
1405 cm^{-1}	C-C stretching (sym)	phenyl	[102-103]
1470 cm^{-1}	C-C stretching (asym)	phenyl	[100,102-103]
1425 cm^{-1}	$-CH_3$ bending vib.	Si-methyl	[100]

5.2.2. Poly[bis-(ethylphenyl)silane] (PBEPS) and Ge-Si copolymer

Figure 5.5 provides an overview of vibrational absorption bands observed in the Ge-Si copolymer and PBEPS in the wavenumber range 400-3500 cm^{-1}. As mentioned earlier, absorption below 500 cm^{-1} is limited by the KCl substrates used. The spectra collected from the Ge-Si copolymer and PBEPS are similar in appearance (with different absorption magnitude). This is analogous to the similar electronic absorption behavior observed for both materials in the UV-visible region (Figure 5.1).

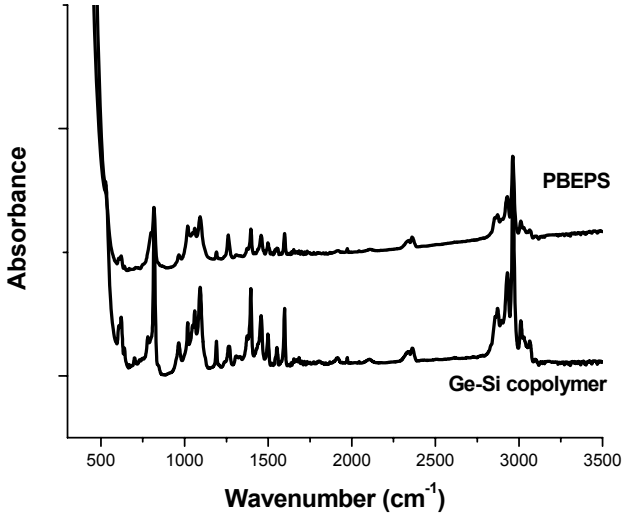

Figure 5.5. Representative vibrational spectra obtained experimentally for Ge-Si copolymer and PBEPS) in the region 400 cm^{-1} to 3500 cm^{-1}.

Figure 5.6 depicts the IR absorption spectra of PBEPS and Ge-Si copolymer in the 400 – 900 cm^{-1} range, which contains absorption bands associated with backbone-

sidegroup vibrational modes. The presence of (hexyl)(phenyl)germane substituents produces additional absorption bands in the IR absorbance spectrum due to the hexyl group that is exclusively attached to germane. An absorption peak associated with the C-C stretch, located approximately at 510 cm^{-1} , nearly coincides with the 520 cm^{-1} band (ethyl-phenyl vibration) [100]. A -CH_2- rocking vibrational band from the hexyl group is observed at 700 cm^{-1} only in the Ge-Si copolymer absorption spectra [100].

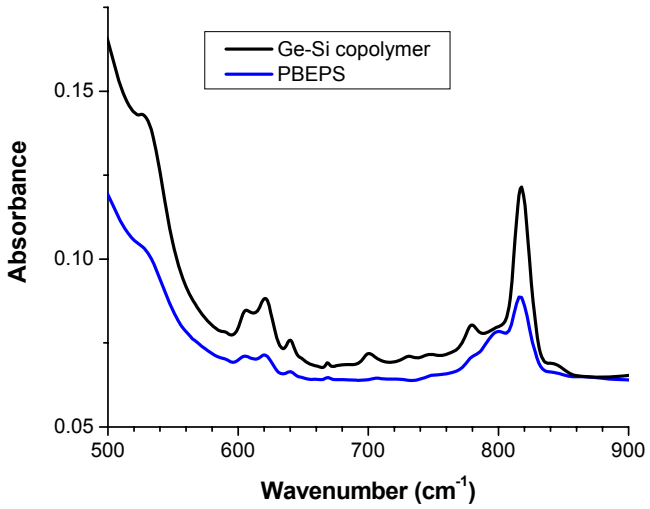

Figure 5.6. Vibrational spectra of as-deposited PBEPS and Ge-Si copolymer thin films in the region of 500 cm^{-1} and 900 cm^{-1}.

Other than the specific absorption bands mentioned above, both PBEPS and Ge-Si copolymer IR absorption spectra have common absorption bands arising from the bis-(ethylphenyl)silane moieties. For example, a vibrational peak at 520 cm^{-1} corresponds to

the =C-C-C in-plane bending vibration of the ethyl-phenyl components [100]. The Si-biphenyl (Si-Ph_2) in-plane bending mode is associated with absorption at 600-640 cm^{-1} [100,104-105]. Other phenyl-related vibration bands are also consistent with PMPS materials, which include a phenyl side-group. For example, peaks were observed corresponding to the Si-phenyl stretching vibrations at 1090 cm^{-1}, a C-C ring rocking vibration at 965 cm^{-1} and a phenyl C-H stretching vibration at 3030-3080 cm^{-1}. A complete summary of PBEPS and Ge-Si copolymer peak identifications is provided in Table 2.

Table 2. Summary of vibrational resonance energies and their assignments in as-deposited Ge-Si copolymer.

Frequencies (cm^{-1})	**Peaks identification**	**Corresponding structure**	**Ref.**
Bis(ethylphenyl)silane			
520 cm^{-1}	=C-C-C in plane in ethyl-phenyl	Ethyl-phenyl	[100]
600-640 cm^{-1}	ring in plane bending in $R_2SiPhenyl_2$	phenyl	[100]
830 cm^{-1}	C-H in plane vibration	phenyl	[100]
965 cm^{-1}	C-C rocking vibration	phenyl	[100]
1030 cm^{-1}	=C-H in plane deformation	phenyl	[100]
1060 cm^{-1}	=C-H in plane deformation	phenyl	[100]
1100 cm^{-1}	Si-phenyl	phenyl	[100]
(hexylphenyl)germane			
510 cm^{-1}	C-C-C-C stretch	hexyl	[100]
700 cm^{-1}	-(CH2)n- n > 3 stretch	hexyl	[100, 104-105]

5.3. UV-INDUCED RESPONSE: Electronic spectroscopy (VUV and UV-vis absorption)

5.3.1. Poly[(methyl)(phenyl)silane] (PMPS)

Figure 5.7 contains representative of UV-visible absorption spectra for PMPS films subjected to 337.1 nm (3.68 eV) (Figure 5.7a) and 248 nm (5.10 eV) (Figure 5.7b) optical exposures as well as spectral behavior modifications after these two different energy photon exposures. The relative impact of incident cumulative fluence on the spectral behavior of the absorption is significantly dependent upon the photon energy used. Lower photon energy exposure ($h\upsilon$ = 3.68 eV) produced a marked decrease in the lowest energy absorption peak as well as a shift in this band to higher energy. This peak is associated with the lowest energy σ-σ^* transition of the Si backbone chains. Conversely, exposure with 5.10 eV photons produced more widespread absorption bleaching with significant reduction in absorption strength extending up to 5.5 eV. The lowest energy absorption band in this case exhibits a smaller blue shift after 5.10 eV irradiation compared to that observed under 3.68 eV irradiation. The 5.1 eV irradiation energy is resonant with the π-π^* electronic transition of the phenyl group. The effect of exposure energy is observed not only in the near-UV but also in the vacuum-UV (VUV) spectral region.

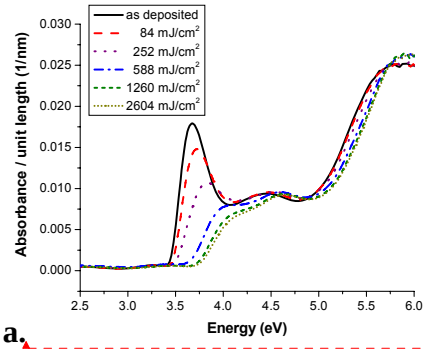

a.

Formatted: Font: 14 pt, Bold

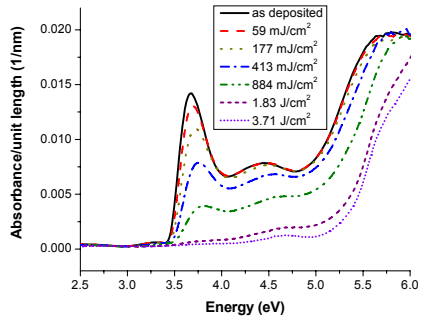

b.

Formatted: Font: 14 pt, Bold

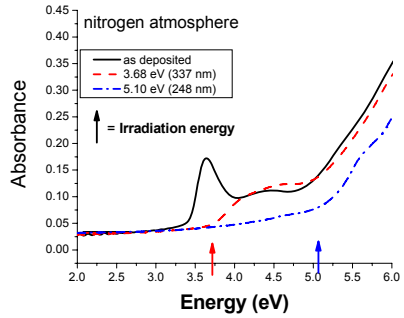

c.

Formatted: Font: 14 pt, Bold

Figure 5.7. Optical absorption spectra for PMPS thin films as a function of cumulative UV-fluence under an air atmosphere. (a) 3.68 eV incident photon energy, (b) 5.10 eV incident photon energy and (c) spectral modification comparison with different irradiation wavelength [13,99].

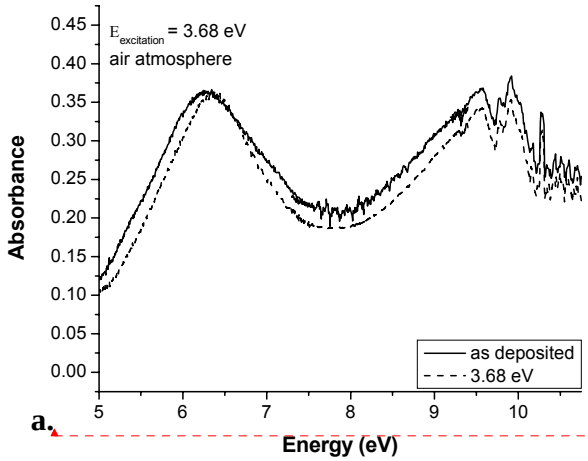

Formatted: Font: 14 pt, Bold

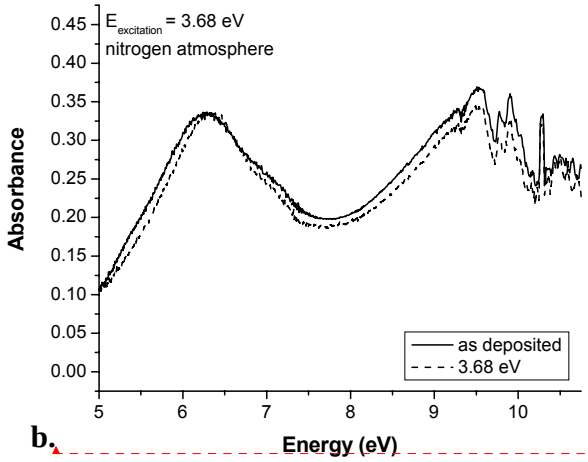

Formatted: Font: 14 pt, Bold

Figure 5.8. UV-induced absorption spectral changes in the vacuum-UV energy region after irradiation with 3.68 eV nitrogen laser under different local environment. (a) in air. (b) in nitrogen [99].

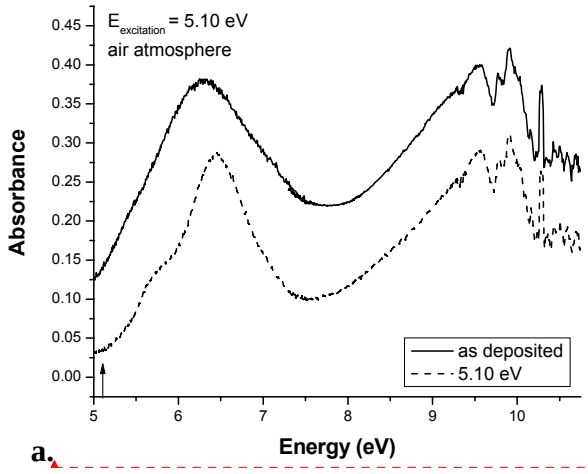

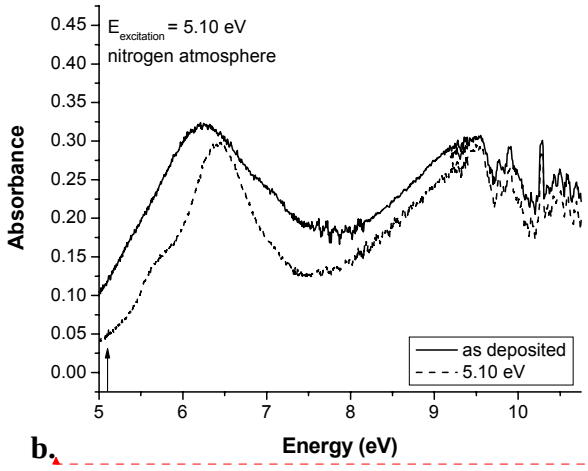

Formatted: Font: 14 pt, Bold

Formatted: Font: 14 pt, Bold

Figure 5.9. UV-induced absorption spectral changes in the vacuum-UV energy region after irradiation with 5.10 eV incident photon energy under different local environment. (a) under air. (b) under nitrogen [99].

Figure 5.8 and Figure 5.9 depicts absorption spectra of PMPS in the VUV after subjected to 3.68 eV and 5.10 eV photon under dry air and nitrogen respectively. The photoinduced effect on the VUV spectra, shown in Figure 5.8 and 5.9 exhibited a trend in absorption modification observed with incident photon energy consistent with that found in the near-UV region. Just as exhibited in the near-UV spectra (Figure 5.7), higher photon energy exposures (i.e. at $h\upsilon$ = 5.10 eV) also induce more significant spectral changes after fluence levels of 3.3 J/cm^2 in the VUV spectral region. Under these exposure conditions a larger decrease in absorption strength and modification in spectral structure is observed. In contrast, 3.68 eV photon energy exposures produce less pronounced changes in the spectra collected (e.g. Figure 5.8). For example, 5.10 eV irradiation under an air atmosphere produces an overall change in absorption strength across the spectrum (as defined by the total peak area change derived from peak fitting, shown in Figure 5.10) of 39%. This is compared to a 13% change in absorption peak area for optical exposure at 3.68 eV with the same fluence level in air (Figure 5.8). In addition, the higher energy photon exposure produced a notable redistribution of absorption strength to higher energy in the spectral range 5 – 8 eV, including a marked narrowing of the absorption band centered at approximately 6.5 eV and the evolution of a shoulder near 5.5 eV (Figure 5.9). While some narrowing of the absorption band at approximately 6.4 eV is observed after exposure at 3.68 eV, the development of a shoulder in this spectral range is not observed (Figure 5.8).

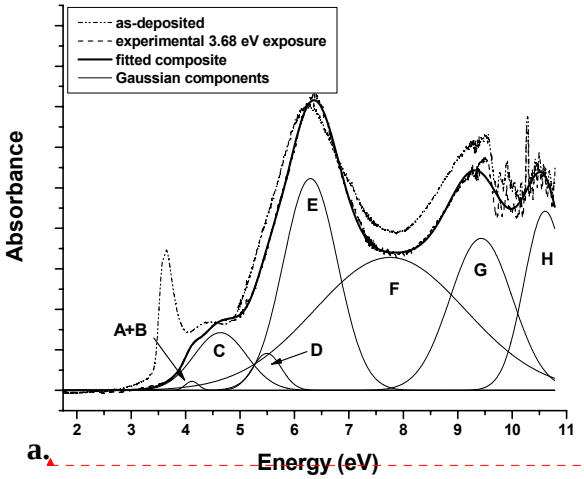

a.

Formatted: Font: 14 pt, Bold

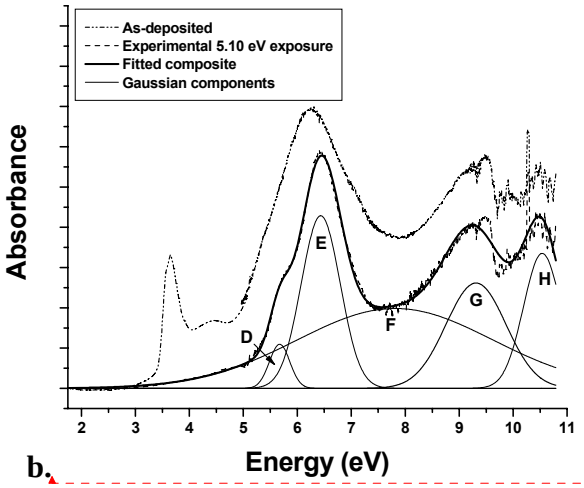

b.

Formatted: Font: 14 pt, Bold

Figure 5.10. Representative peak fitting results for PMPS absorption spectra. Dotted lines denote the experimental spectrum while bolded curves are the fitted peaks. The associated experimental spectrum and fitting curves for PMPS subjected to 3.68 eV (a) and 5.10 eV (b) irradiation in air are provided [99].

The effect of local atmospheric composition on the UV-visible absorption spectra modification during photo exposure is not as dramatic as those exhibited under varied excitation energy. In this case, different local environments during UV exposure appear to only influence the rate of absorption spectra change with fluence while producing only a limited impact on the final, saturated spectral structure measured in the UV-visible region [26,106].

Figure 5.11 depicts representative of the photoinduced change in fitted $\sigma - \sigma^*$ area that was observed as a function of cumulative fluence for PMPS films exposed under difference atmospheric composition after UV exposure. The behavior of σ-σ^* peaks area, which are associated with the length of Si-Si backbone chains, with cumulative fluence under different atmospheric composition is consistent regardless of the incident photon energy. It is clearly observed that the ambient atmospheric composition can affect efficiency with which photostructural changes are produced in the PMPS thin films, as illustrated by the differences in the photoinduced absorbance changes.

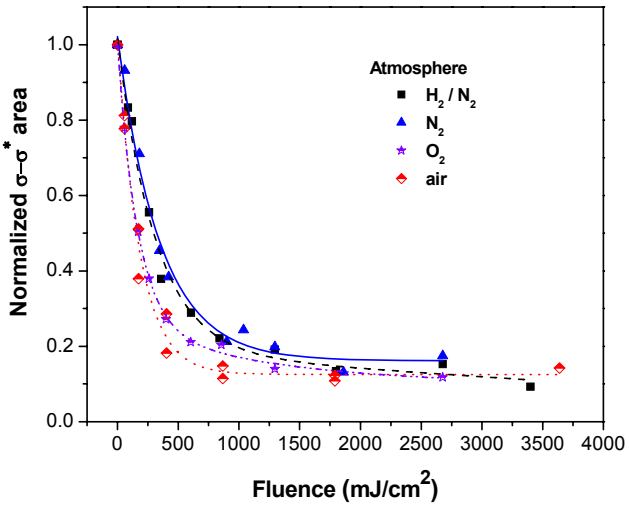

Figure 5.11. UV-induced modification on σ-σ* backbone peaks under different atmospheres. The connecting lines served as guide for easier comparison. [26,106].

Two general behaviors, observed in Figure 5.11 [26,106] are related to the presence of oxygen in local environment of the PMPS. First, similar fluence dependence is observed for the lowest energy peak area in air or oxygen when compared to that found in nitrogen or the N_2 / H_2 mixture. In addition, when oxygen is present, the rate of change in the $\sigma - \sigma^*$ peak area with increasing ultraviolet fluence is initially greater than found under anaerobic conditions. For example, the peak area of PMPS exposed without oxygen is found to be approximately 40% greater at 500 mJ/cm^2 than that corresponding sample exposed under oxygen environment. At greater fluences (up to 3.5 J/cm^2), all samples exhibited a general saturation of the low energy absorption band ultraviolet

bleaching response with final peak areas, obtained from fitting, falling between 15-20% of their initial value.

The effect of incident photon energy and atmospheric composition on refractive index change measured with the ellipsometer at 632.8 nm in PMPS samples can be observed in Figure 5.12 [26,106] for 3.68 eV irradiation and Figure 5.13 for 5.10 eV irradiation [106]. In both cases, the effect of the various atmospheric compositions studied is included. The maximum saturated refractive index change after irradiation at 3.68 eV was found to be -0.07 (at 632.8 nm) and -0.12 after irradiation at 5.10 eV, almost two times more than that observed after low photon energy exposure. The effect of irradiation environment can again be categorized into aerobic (N_2 and H_2 / N_2) and anaerobic (dry air and O_2), which is consistent with the trends observed in bleaching rate in the near-UV study in Figure 5.13. The aerobic atmospheric condition resulted in the largest refractive index changes under both excitation photon energy exposure. For example, irradiation with 3.68 eV UV under a nitrogen environment resulted in a refractive index change of -0.042, which is 37% lower than the Δn obtained under aerobic conditions. In contrast, the saturated refractive index change in response to 5.10 eV exposure produced a decrease in the refractive index change of 11% less than that that found under aerobic conditions. This difference indicates that the environmental effect is more pronounced under lower incident energy (3.68 eV) compared to 5.10 eV. Moreover, the pulse energy used in 5.10 eV does not have a measurable influence on the refractive index change observed which suggests that the mechanisms contributing to the refractive index changes are most likely associated with a linear absorption process (dependent

upon total cumulative fluence rather than the intensity of incident light) [99]. Irradiation with pulse energy at 8 mJ/cm^2/pulse at $h\nu = 5.10$ eV caused the PMPS films to become highly scattering in the visible, preventing refractive index measurement by ellipsometer.

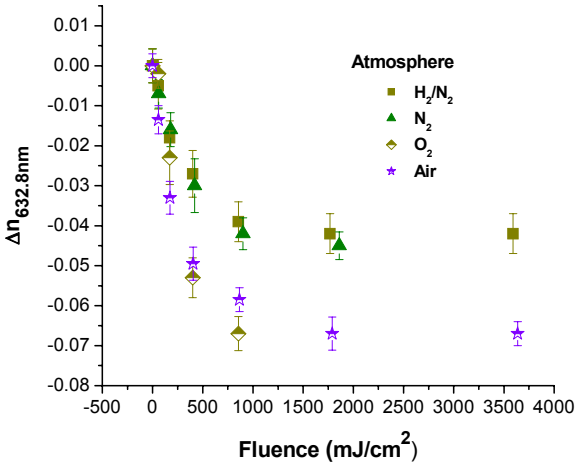

Figure 5.12. Photoinduced refractive index changes observed under varied atmospheres in PMPS thin films exposed to 3.68 eV incident light [26,106].

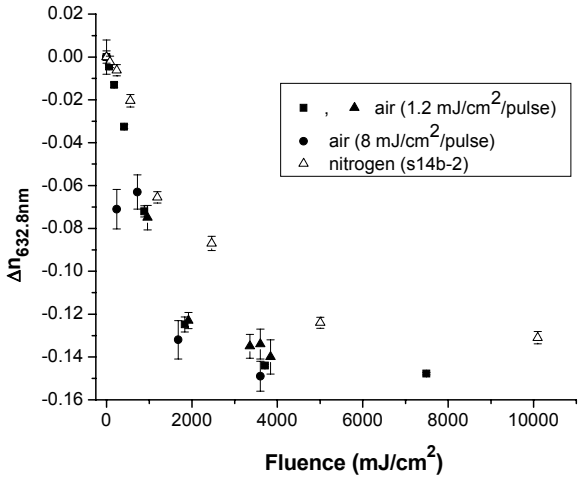

Figure 5.13. Photoinduced refractive index changes observed under varied atmospheres in PMPS thin films exposed to 5.10 eV incident light [106].

The corresponding thickness measurement of UV-irradiated PMPS films is provided in Figure 5.14. Different irradiation photon energies (3.68 eV and 5.10 eV) had a relatively small effect on the magnitude of the thickness changes observed compared to the impact of atmospheric composition. The thickness changes, which indicated a volume expansion, showed behavior consistent with that of the σ-σ^* peak evolution with UV fluence. In this case, the largest change occurred with UV irradiation of PMPS materials. Irradiation under air produced a 27% greater change in thickness (16 nm compare to 13 nm) compared to irradiation under nitrogen.

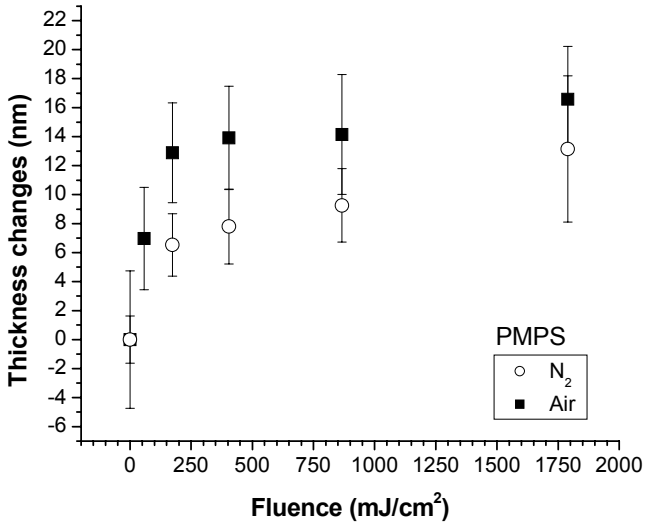

Figure 5.14. Photoinduced thickness modification of PMPS materials UV-irradiated under different local atmospheric compositions. The data were compiled from PMPS irradiation with 5.10 eV incident energy.

It can be seen in the Table 3 that the $\Delta n_{632.8}$ calculated using the Kramers-Kronig relationships (regardless of the spectral range used) is lower by an order of magnitude than those observed experimentally [99]. As described previously, the calculation error recorded in Table 3, is based on uncertainty in film thickness measurements (via stylus profilometry) and sample-to-sample variation. The calculation does show, however, that a higher energy exposure, 5.10 eV, produces a greater $\Delta n_{632.8}$ than exposure using 3.68 eV. This general result is consistent with trends observed in both the experimentally obtained Δn and in the overall photoinduced absorption changes observed in the near- and vacuum-UV spectra [26,101,106]. An examination of the data in Table 3 reveals that

the calculation does show that a simple absorption coefficient changes calculation to predict refractive index changes (Δn) is not sufficient to account for the Δn observed experimentally. Clearly this validates the effect of volume changes as well as other structural modifications, which are not observable to absorption spectral changes, on the photoinduced Δn.

Table 3. Kramers-Kronig calculations of $\Delta n_{632.8}$ using only absorption change in the near-UV and using absorption changes computed using both near-UV and VUV photoinduced spectral modifications after total fluence of 3.3 J/cm^2. Experimentally determined (ellipsometry) refractive index changes are also provided

$\Delta n_{632.8}$	Near-UV only	+/-	Near-UV + VUV	+/-	Experimental
3.68eV – air	-0.0070	0.0004	-0.0083	0.0005	-0.07
3.68eV – nit	-0.0056	0.0002	-0.0072	0.0003	-0.04
5.10eV – air	-0.0115	0.0005	-0.0166	0.0007	-0.13
5.10eV – nit	-0.012	0.001	-0.015	0.002	-0.11

5.3.2. Poly[bis-(ethylphenyl)silane] (PBEPS) and Ge-Si copolymer

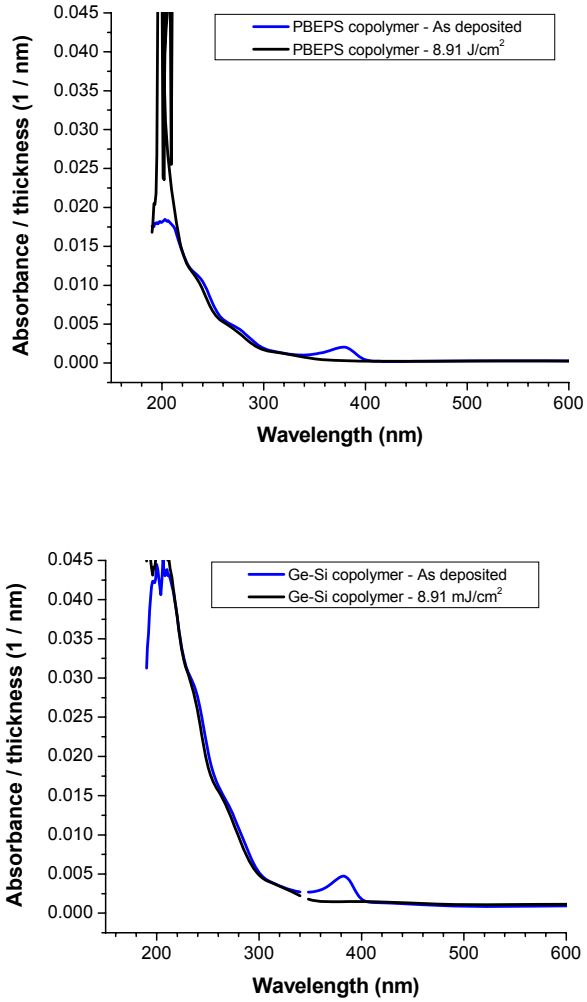

Figure 5.15. UV-induced modification of absorption spectra of (top) PBEPS and (bottom) Ge-Si copolymer in the UV-visible region using 3.35 eV (370 nm) incident energy.

Figure 5.15 illustrates the UV absorption spectral changes after UV irradiation (3.35 eV, 370 nm) of both PBEPS and Ge-Si copolymer respectively. The irradiation energy of 3.35 eV (370 nm) is resonant with the σ-σ^* transition, the lowest energy (longest wavelength) absorption peak at 372 nm. UV irradiation reduces the absorption peak associated with σ-σ^*; this is consistent with the scissioning of the backbone. However, the spectral photoinduced modification is isolated to σ-σ^* peak while higher energy transitions, which are associated with side groups, are not affected with UV exposure in the UV-visible range.

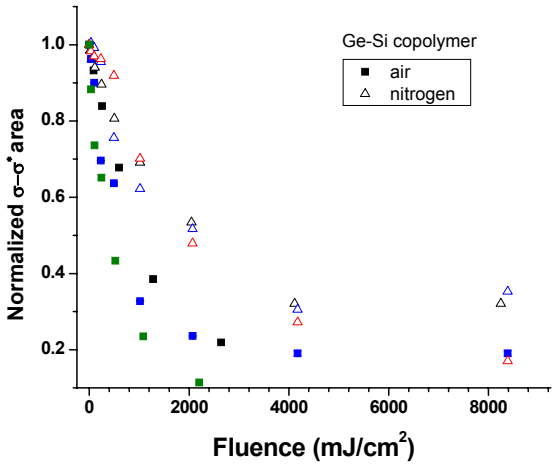

Figure 5.16. Photoinduced modification of the σ-σ^* absorption peak area observed in the UV-vis absorption spectra of Ge-Si copolymer irradiated under different atmospheric environments.

Figure 5.16 depicts the effect of UV fluence on the σ-σ^* absorption band area of Ge-Si copolymer under air and nitrogen environments. The results of the Gaussian peak fitting approach are also included. The general trend of observed peak area involves a fast bleaching rate in the beginning of irradiation process (low fluence) with a saturation of the peak area at higher fluences. The fluence needed to saturate the photomodification process in Ge-Si copolymer is significantly higher than in PMPS. (8.9 J/cm^2 compare to 3.3 J/cm^2). The aerobic environment, again, produces more efficient bleaching of the σ-σ* band when compared to an anaerobic atmosphere.

Representative absorption spectral behavior from the near-UV to the vacuum UV range in the Ge-Si co-polymer after UV irradiation is illustrated in Figure 5.17. In contrast with behavior in the UV-visible region, the absorption spectra increased in magnitude in the vacuum-UV region, between 5 eV to 7 eV range. The area of absorbance peaks corresponding to the phenyl group transition (B, C and D) increased by 6-7% after 8.91 J/cm^2 exposure of UV light with 3.35 eV (λ = 370 nm) incident energy. The local environment, both anaerobic and aerobic, showed insignificant differences between the area increases observed in these phenyl absorption bands upon irradiation.

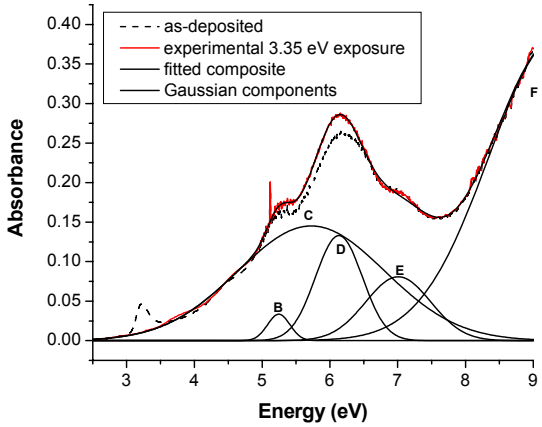

Figure 5.17. Representative peak fitting results for Ge-Si copolymer absorption spectra. Dotted lines denote the experimental spectrum while bolded curves are the fitted peaks after irradiated using 3.35 eV incident energy for the total fluence of 8.91 J/cm^2.

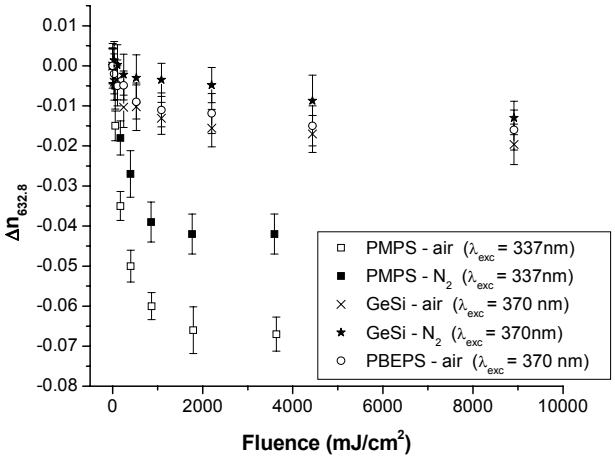

Figure 5.18. UV-induced refractive index changes at 632.8 nm of Ge-Si copolymer and PBEPS compared with PMPS under varied atmospheres. All samples were irradiated with UV-photon energies resonant with the lowest energy peaks observed in their respective UV-vis absorption spectra.

Ge-Si and PBEPS show photoinduced changes in refractive index with UV irradiation resonant with their respective σ-σ^* transitions as shown in Figure 5.18. A comparison of these responses with those of the PMPS material shows a consistent trend, in that the Δn saturated with increased UV fluence. In all cases, an aerobic local environment also served to enhance the maximum refractive index change produced. The Δn values obtained for the PBEPS and Ge-Si copolymer materials are generally lower than those observed in PMPS. Moreover, a larger UV fluence (resonant with the σ-σ^* transition) is necessary to saturate the photoinduced Δn in the PBEPS and Ge-Si copolymer. The saturated refractive index changes of Ge-Si copolymer measured at 632.8 nm are -0.020 and -0.012 for air and nitrogen respectively while the PBEPS refractive index change was -0.016 when irradiated under an aerobic environment after 8.91 J/cm^2 UV fluence. The refractive index changes for PMPS materials under the same conditions became saturated at -0.04 and -0.07 for air and nitrogen respectively after a UV-fluence of only 3.3 J/cm^2.

UV-induced volume expansion, represented by the thickness changes observed via ellipsometry, of both Ge-Si copolymer and PBEPS is shown in Figure 5.19. The variation in thickness of Ge-Si copolymer most likely resulted from poor film quality in the samples examined. Based on PBEPS results, the thickness exhibited no measurable change after UV-irradiation (0.6 nm ± 2.6 nm increase).

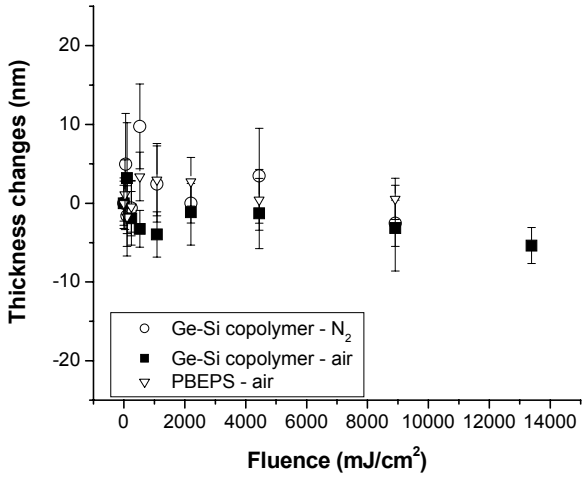

Figure 5.19. UV-induced thickness modification of PBEPS and Ge-Si copolymer after irradiation with 3.35 eV (370 nm) incident energy

5.4 UV INDUCED RESPONSES: Structural modifications: Vibrational spectroscopy

The corresponding FTIR results of UV irradiated samples are presented only for air and nitrogen atmosphere as representative of the aerobic and anaerobic conditions that constitute the extreme behavior observed in UV-visible study. The figures contain frequency windows that highlight infrared signature associated with backbone and side-group related vibrational modes. In general, the largest changes in FTIR spectra were observed under a combination of high incident photon energy and air environment. Conversely, anaerobic atmosphere and lower photon energy exposure produced the smallest changes in the infrared absorption spectra. This general trend agrees with that

observed in the previous section in which the largest changes in refractive index and UV absorption spectra occurred under an aerobic environment with high incident photon energy.

5.4.1. Poly[(methyl)(phenyl)silane] (PMPS)

Figure 5.20 shows a representative example of the vibrational structure change in the region of the 450 – 500 cm^{-1} in PMPS irradiated at the high photon energy (5.10 eV) and under an air environment. As discussed in the previous chapter, resonances in this frequency range have been associated with the structural continuity of the Si-Si backbone [57,100,102-103,108]. It is clear that the original peak at 460 cm^{-1} decrease, where as the intensity of another peak at 480 cm^{-1} increases simultaneously with UV fluence which is consistent with the formation of a silyne-type (branched) moiety [reference needed]. These observations are consistent with the initial photoscissioning of Si backbone.

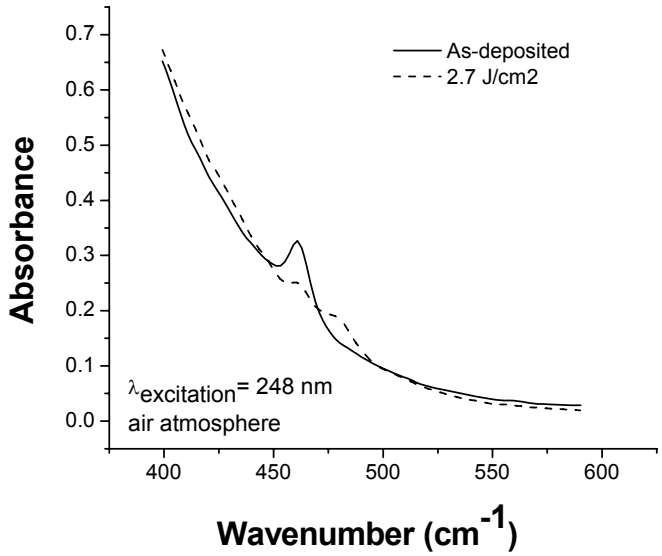

Figure 5.20. Infrared absorption near 500 cm^{-1} exhibited by PMPS film before and after exposure to 5.10 eV photons under an air atmosphere [101].

Figure 5.21 shows the IR spectra in the region of 950-1200 cm^{-1} subjected to different combinations of incident photon (3.68 eV and 5.10 eV) and local atmosphere (air and nitrogen) used in the studies. The high intensity peaks at 997 cm^{-1} and 1068 cm^{-1} are related to different phenyl in-plane vibrations while the absorption peak at 1100 cm^{-1} is due to Si-C phenyl vibration. A consistent trend in these figures is a broad absorption peak increase in the region of 1000-1100 cm^{-1} with increasing fluence. The presence of siloxane vibration modes (Si-O-Si) in this frequency range, was also confirmed using DFT calculations of (methyl)(phenyl)pentasiloxane. The broad increases in Si-O-Si

peaks centered at around 1050 cm^{-1} suggested linear siloxane structure formation. This observation supports an interpretation of UV-induced photomodification of PMPS structure as the production of siloxane bridge structures following the initial Si-energy (5.10 eV) irradiation in an aerobic environment which indicates the most effective photoscissioning of the Si backbone. These UV-irradiated vibrational spectra also contain a strong resonance at 1130 cm^{-1} that grew with UV irradiation, which was not observed in the as-deposited spectra. The strength of this band is highest under exposure conditions using a 5.10 eV excitation energy under an air atmosphere. Toman *et al.*, used quantum cluster calculation to identify this resonance as associated with cationic radical structures [74-75].

Figure 5.22 depicts IR spectra obtained with different combinations of both excitation photon energy (3.68 eV and 5.10 eV) and atmospheric composition (air and nitrogen) in the frequency range of 2000-2250 cm^{-1} where vibrational modes of the Si-H structure are anticipated [100]. Exposure with 3.68 eV under anaerobic condition produced the largest increase in absorption strength of the broad resonance peak at 2095 cm^{-1}. Simultaneous absorption increase and peak shift was observed with 5.1 eV exposure with the maximum peak shift to 2135 cm^{-1} observed under an air environment. A consistent trend occurs in the region near 870 cm^{-1}, where the Si-H related vibrational mode (wagging mode) is centered at 875 cm^{-1} [100]. These Si-H peaks were also confirmed with DFT calculation of normal modes of siloxane and silane oligomers structure which were terminated with hydride groups.

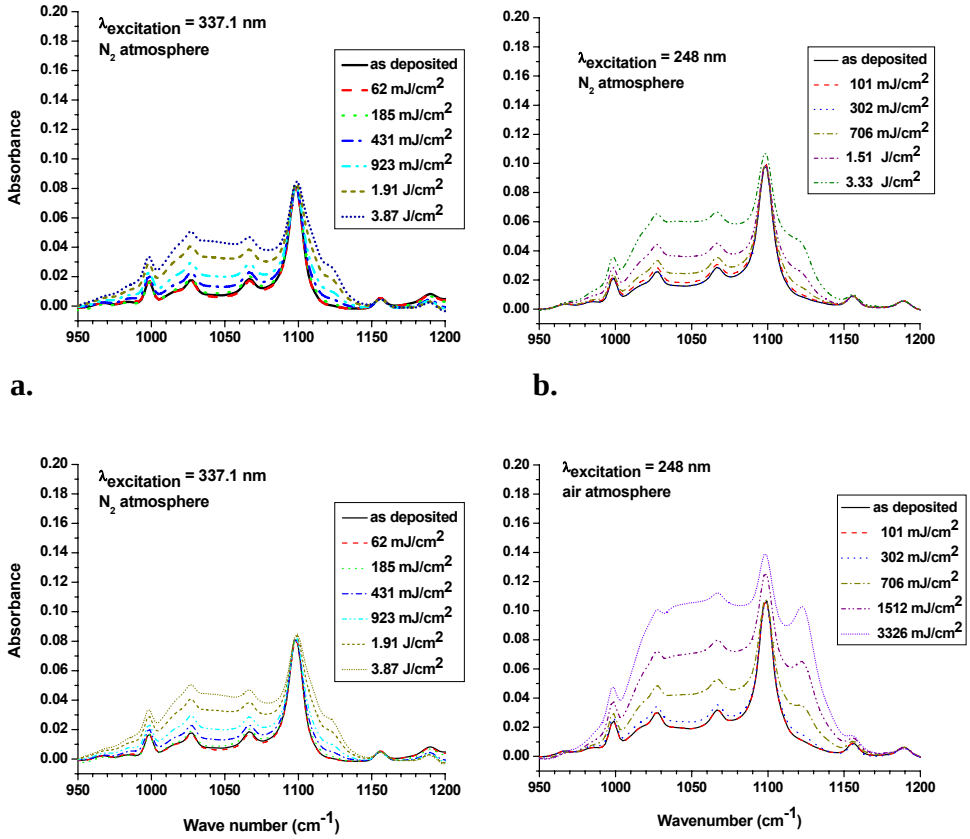

Figure 5.21. Infrared absorption 950-1200 cm^{-1} of PMPS under (a,b) nitrogen, (c,d) air as a function of cumulative UV fluence using (a,c) 3.68 eV and (b,d) 5.10 eV [101].

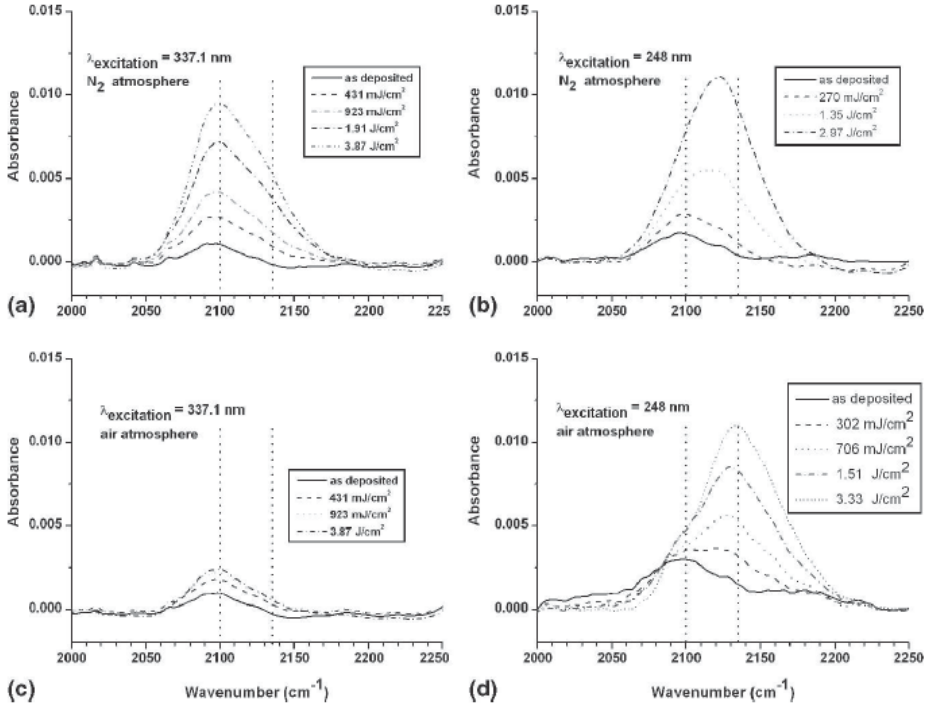

Figure 5.22. Infrared absorption in the region of 2000-2250 cm^{-1} of PMPS thin films upon UV irradiation under (a,b) nitrogen and (c,d) air as a function of cumulative UV fluence using (a,c) 3.68 eV and (c,d) 5.10 eV. Vertical lines, coincident with the peak position extremes observed over the range of the exposure conditions used are provided as a guide to the eye [101].

As described in a previous chapter, some resonance peaks were associated with methyl and phenyl attached on PMPS structure. Figure 5.23 and 5.24 present IR spectra in the regions near 1250 cm^{-1} and 3000 cm^{-1} respectively which represent some UV-induced changes to the organic side-groups. The figures exhibit maximum changes in absorption after irradiation with 5.10 eV under aerobic environment. In Figure 5.23, a

shift in absorption intensity to higher vibrational energy is observed with UV irradiation between two peaks associated with Si-CH_3 symmetric deformation mode in the 1250-1260 cm^{-1} range [100]. Figure 5.24 shows a reduction in intensity of vibrational modes corresponding to different C-H vibration modes in the 2990-3300 cm^{-1} range. These absorption peaks, however, are insensitive to low energy (3.68 eV) exposure regardless of environment used.

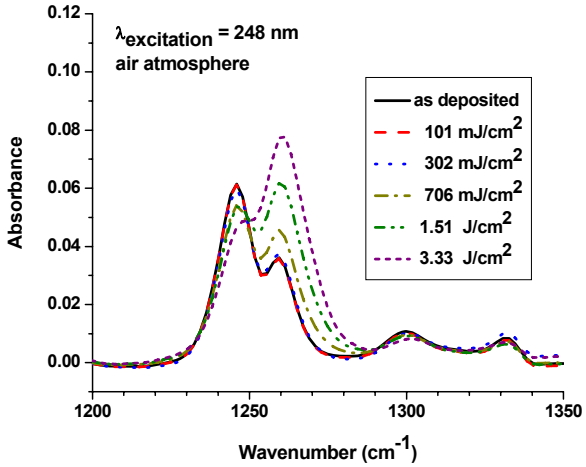

Figure 5.23. Infrared absorption near 1250 cm^{-1} of a PMPS film before and after exposure to 5.10 eV under an aerobic environment [101].

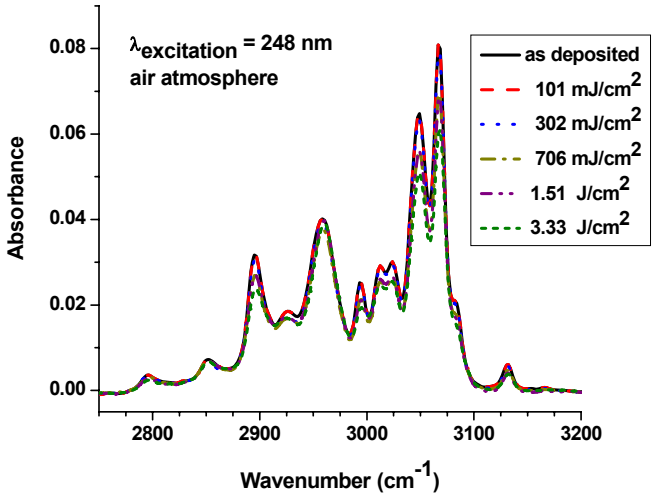

Figure 5.24. Infrared absorption near 3000 cm^{-1} of a PMPS film before and after exposure to 5.10 eV under an aerobic environment [101].

5.4.2. Poly[bis-(ethylphenyl)silane] (PBEPS) and Ge-Si copolymer

As discussed previously, that Ge-Si infrared spectra were dominated by vibrational modes associated with the bis(ethylphenyl)silane substituent rather than the germane structures. Photoinduced structural modification Ge-Si copolymer is expected to be similar to PBEPS. In this case, only Ge-Si copolymer is presented as there was insufficient PBEPS polymer for a complete study.

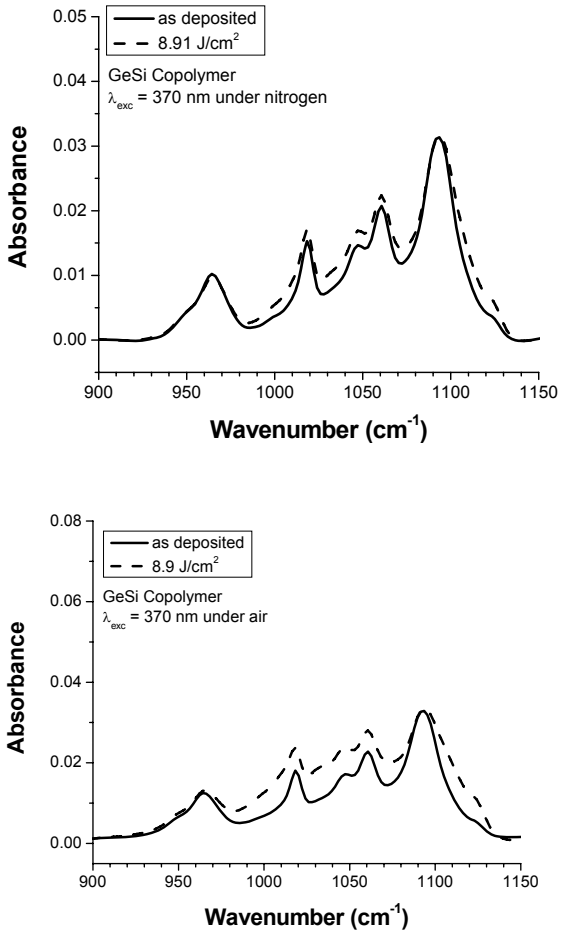

Figure 5.25. Infrared spectra of Ge-Si copolymer in the near 900 cm^{-1} before and after exposure at 3.35 eV (370 nm) incident photon under (top) nitrogen, (bottom) air.

Figure 5.25 depicts the IR spectra of the Ge-Si copolymer, irradiated under both anaerobic and aerobic environments, in the frequency range of 900-1150 cm^{-1}. Consistent with the PMPS spectra, the high intensity absorption peaks at 1020 cm^{-1} and

1070 cm^{-1} correspond to phenyl breathing modes while another peak centered at 1080 cm^{-1} is associated with the Si-phenyl vibration [100]. There is an overall increase in absorption magnitude in the range of 1000-1100 cm^{-1}, where the vibrational mode of Si-O-Si is anticipated.

It is clear that photoinduced modification of the Ge-Si copolymer involved the formation of siloxane bridges upon UV irradiation regardless of local environmental. As expected, the siloxane structure formation is more effective after UV-irradiation under aerobic conditions. The DFT calculation of germano-oxide structure normal modes and confirmed by literature [100,104,109], indicated Ge-O resonances peak at around 800-900 cm^{-1}. In the experimental results of UV-irradiated Ge-Si copolymer, no measurable changes in the germano-oxide structure formation were observed. This most likely resulted from the small number of participating germane substituents (5%) in the material structure.

Figure 5.26 contains representative infrared absorption spectra near 2100 cm^{-1} collected from the Ge-Si copolymer after irradiation under both air and nitrogen atmospheres. The Si-H stretching mode is anticipated to be centered at 2105 cm^{-1}, and is again confirmed by DFT calculation and literature [100]. Few Si-H structures existed in the starting Ge-Si films consistent with the weak absorption strength observed at 2105 cm^{-1} before UV irradiation. The increase in magnitude of this peak intensity after UV irradiation under nitrogen environment suggested more Si-H structures were formed under these slightly reducing atmospheric conditions. In contrast, UV irradiation in air has no effect in the magnitude of Si-H peak intensity.

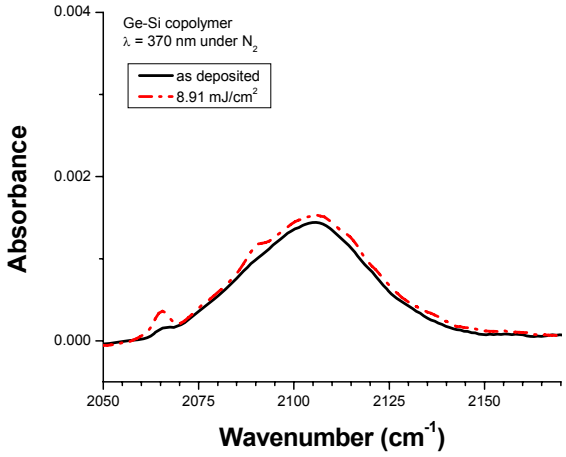

a.

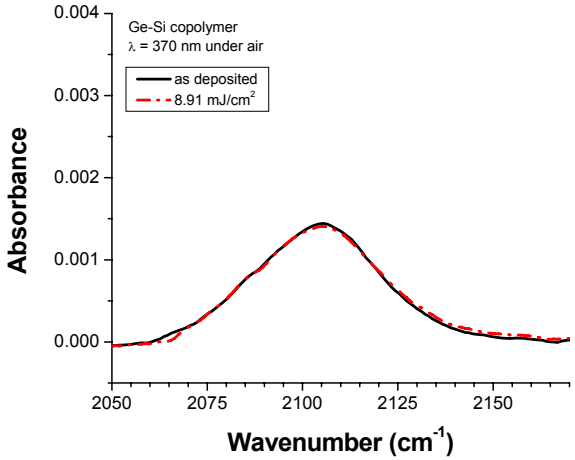

b.

Figure 5.26. Infrared spectra of Ge-Si copolymer in the near 2100 cm^{-1} before and after exposure of 3.35 eV (370 nm) incident photon under (a) nitrogen, (b) air

This trend is consistent with the PMPS photoinduced structural modification behavior previously discussed. In this case, passivating Si-H structures are more likely to form upon irradiation under anaerobic environments while low energy irradiation under aerobic condition produces the least amount of hydride structure.

There are no measurable changes in the magnitude of IR absorption peaks after UV irradiation in the frequency ranges for the organic side-group at 2900-3300 cm^{-1} regardless of atmosphere. This trend indicates that the photoinduced modification in the Ge-Si copolymer that is produced by UV irradiation involves only the backbone structure and has very limited impact on the organic side-groups.

5.5. APPLICATIONS OF UV-INDUCED PHOTOSENSITIVE MATERIALS: Bragg Grating

The ability to modify PMPS thickness and refractive index using 3.68 eV and 5.10 eV UV-irradiation provides the basis for the photoinduced formation of photonic device structures. In the current study, Bragg gratings were produced by UV-exposure of the material through a suitably designed zeroth-order phase mask element. The maximum efficiency of the PMPS gratings obtained by exposure using 5.10 eV irradiation was found to be 1.1% at an operational wavelength of 632.8 nm Although overall uniformity of the produced PMPS grating is relatively poor, profilometer measurement at perpendicular orientation to grating period showed some evidence of physical grating formation (Figure 5.27). The poor uniformity is probably caused by photon leakage

through zeroth-order of the phase mask. Long exposure time (high total fluence) coupled with zeroth-order photon leakage tends to "wash away" the grating formed on PMPS films as the contrast in both refractive index and thickness is lost.

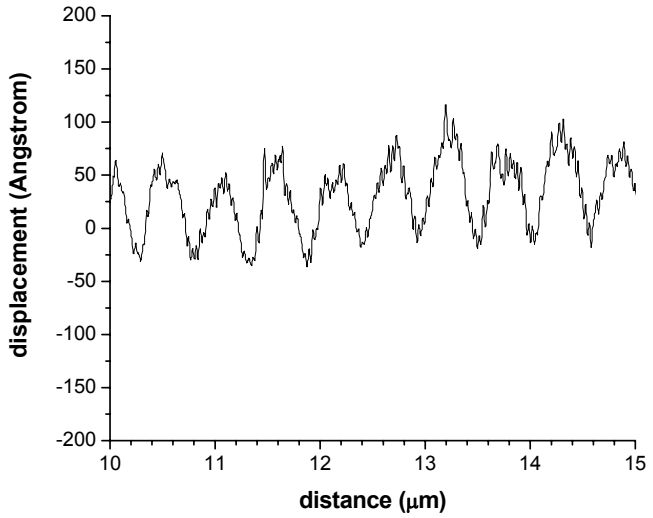

Figure 5.27. Topography of PMPS Bragg grating irradiated using 5.10 eV incident energy for 8 J/cm^2 total incident fluence.

5.6. THERMAL INDUCED RESPONSE: Electronic structure and optical properties

5.6.1. As-deposited poly[(methyl)(phenyl)silane] (PMPS)

Representative UV-visible absorption spectra of a PMPS thin film (silica substrate) subjected to an iterative isochronal heat treatment from 25 C to 350 C under nitrogen are provided in Figure 5.28. The spectral modifications are insignificant for heat

treatments up to 175 C while higher temperatures produced measurable changes in the absorption spectra obtained.

At T = 199 C, an increase in the magnitude of the absorption peak at 3.7 eV, associated with σ-σ^* transition of Si backbone, is observed. This contrasts the absorption strength in the higher energy region of the same spectrum, corresponding to side-group related transitions, in which only limited impact with heat treatment below 199C was observed. Further heat treatment at higher temperatures, above 223 C, decreases the magnitude of the absorption spectra over the entire measured wavelength range.

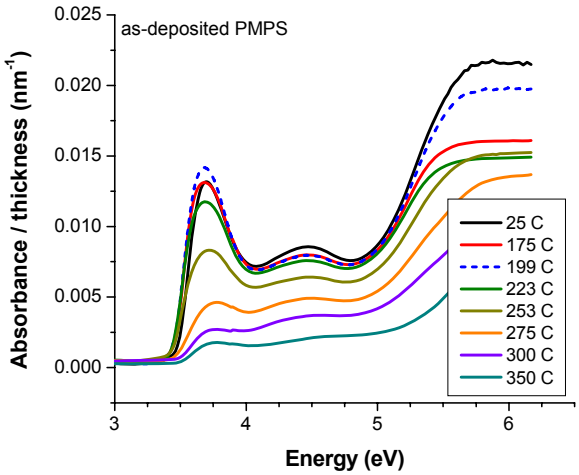

Figure 5.28. UV-visible absorption spectra of PMPS, normalized by film thickness, with isochronal heat treatment. More detail about dotted spectrum (199 C) is available in the text.

In addition to isochronal heat treatment of PMPS, which involved iterative heating PMPS films with increasing temperature, isothermal heat treatment of PMPS at different temperatures was used to further characterize the thermal effect on PMPS UV-visible absorption spectral behavior. The resulting absorption spectra of PMPS iteratively collected after 10 minute increments at temperature were fitted with Gaussian components to quantify thermally induced spectral modifications. The Gaussian fitting method used is analogous to the one used in characterizing the PMPS photoinduced modification. Figure 5.29 depicts normalized peak areas associated with σ-σ^* of PMPS UV-visible absorption spectra (at 3.7 eV) overall σ-σ^* area with full heat treatment schedule (up to 320 minutes) while Figure 5.30 provides closer look to σ-σ^* area evolution up to 50 minutes.

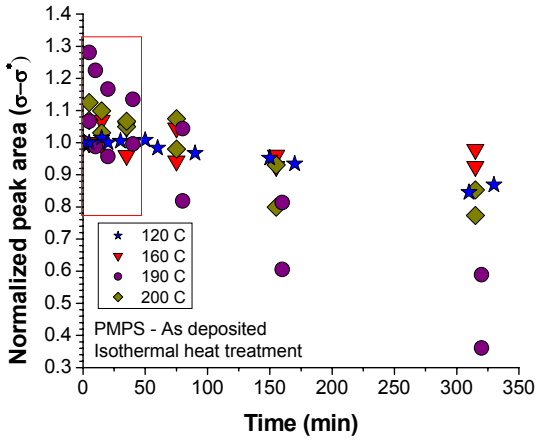

Figure 5.29. Thermally induced modification of σ-σ^* backbone peak area in PMPS with isothermal heat-treatment under nitrogen. The boxed area is provided in more detail in Figure 5.30.

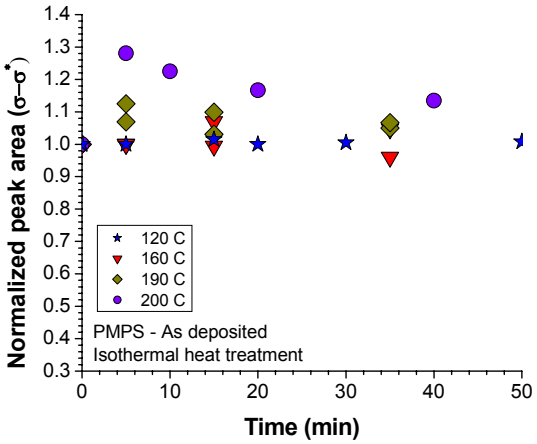

Figure 5.30. Thermally induced modification on σ-σ* backbone peaks area of PMPS in the early stages of isothermal heat-treatment under nitrogen.

The general trend of the σ-σ* absorption peak area during isothermal heat treatment is consistent with isochronal heat treatment. Heat treatment at 120 C provided relatively insignificant modifications on σ-σ* absorption bands topology. This behavior is anticipated as the PMPS thin films were heat treated at 120 C as part of the deposition process in order to remove any excess solvent. However, at higher temperature heat treatment, the σ-σ* absorption area increased in the first 5 minutes of heat treatment at 160 C and above (Figure 5.30). The magnitude of the σ-σ* area increase is dependent on heat treatment temperature. High temperature heat treatment, such as at 200 C, produced the most significant change in peak area, up to ~30% increase after 5 minutes of heat treatment, while, in contrast, heat treatment at 160 C caused only ~10% of increase in peak area with relatively longer heat-heat treatment (~15 minute).

Prolonged heat treatment (more than five minutes) decreased the area of the σ-σ^* absorption band, as shown in Figure 5.29. The heat treatment temperature determined the amount of total σ-σ^* area left as well as the rate of σ-σ^* area decrease. For example, heat treatment at 120 C and 160 C produced only a limited impact on peak area (to 90% of original peak area) while heat treatment at 200C produced the largest relative change in peak area with time both in total area as well as rate of area decrease.

5.6.2. Poly[(methyl)(phenyl)silane] (PMPS) pre-irradiated with UV (3.68 eV)

Absorption spectral behavior of PMPS thin films, pre-irradiated with 3.68 eV incident photon in the UV-visible region, shows a consistent trend with thermal treatment to that observed in as-deposited material under both isothermal and isochronal conditions. In the isochronal heat treatment of pre-irradiated PMPS from 25 C to 350 C, the absorption band associated with the σ-σ^* transition of the Si backbone chains was stable up to 150 C and showed an increase in magnitude after heat treatment at ~170 C while the peak decreasing in magnitude above 170 C. Heat treatment at higher temperature reduced the overall magnitude of the absorption spectra in the observed spectral range.

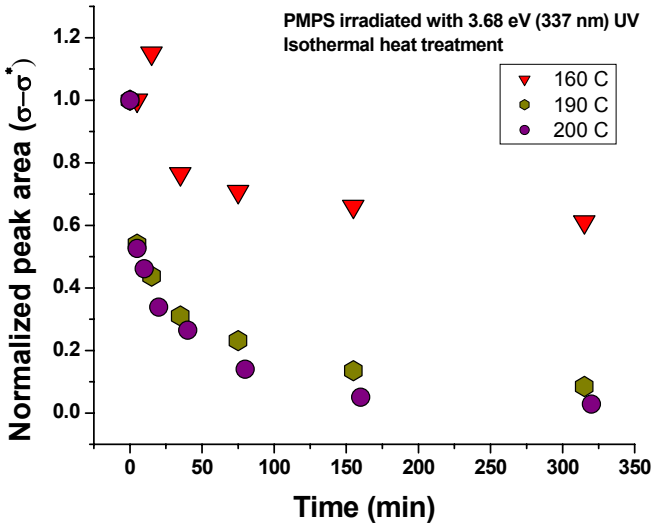

Figure 5.31. Thermally induced modification on σ-σ* backbone peaks of PMPS pre-irradiated with 3.68 eV incident energy, with isothermal heat-treatment under nitrogen.

Figure 5.31 depicts the normalized area of the σ-σ* absorption band of PMPS, pre-irradiated with 3.68 eV incident energy, with isothermal heat treatment as a function of heating time. The area of the σ-σ* absorption band, in general, decreases with heat treatment. The σ-σ* peak area, however, shows a 20% increase in peak area after heat treatment at 160 C for 15 minutes before it decreases and saturates at 60% of initial peak area. The peak area increase was not observed in heat treatment at higher temperature (190 C and 200 C). In contrast, the peak area decreased in magnitude only <10% of initial peak area with heat treatment above 160C. A thermal study of PMPS pre-

irradiated with higher UV energy (5.10 eV) is not available as the observed σ-σ^* peak (at 3.7 eV) in the absorption spectra was completely removed with 5.10 eV irradiation.

5.7. THERMAL INDUCED RESPONSE: Vibrational structure of PMPS

5.7.1. As-deposited poly[(methyl)(phenyl)silane] (PMPS)

Figure 5.32 illustrates the effect of heat-treatment on the overall IR spectra of PMPS before and after iterative isochronal heat-treatment up to 325 C.

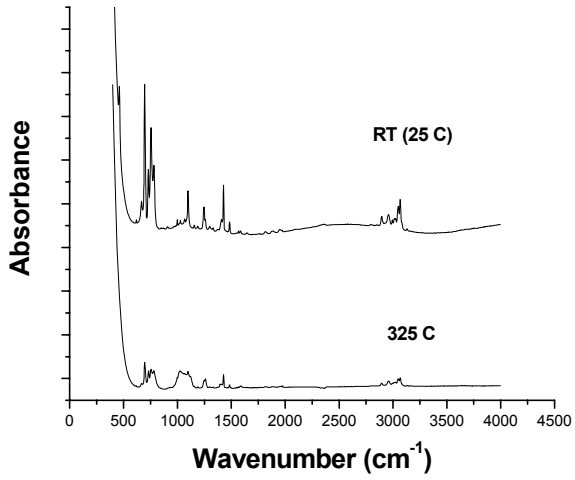

Figure 5.32. IR spectra of PMPS before and after sequential isochronal heat-treatment up to 325 C heat treatment in the 400-4000 cm^{-1} region.

The heat treatment up to 325 C produced significant modification on the overall spectrum. In general, absorption spectra decreased across the measured frequency range

with the exception of the 1000-1100 cm^{-1} region which has been associated with Si-O-Si absorption bands.

One of the fundamental structural modifications anticipated with thermal energy is Si backbone scissioning. An absorption band centered at 450 cm^{-1} associated with Si backbone decreased in magnitude after heat treated at 160 C, which is consistent with the temperature needed to modify the σ-σ^* transition peak observed in the UV-visible region. The Si-Si absorption band is barely measurable after heat treatment of 325 C, which suggests that the Si-Si backbone moiety is significantly disrupted by the heat treatment. The absorption band near 2100 cm^{-1} associated with Si-H stretch, which has relatively low initial absorbance, shifted 30 cm^{-1} to lower energy (Figure 5.33). The Si-H shift to lower energy is associated with shorter Si chains [110].

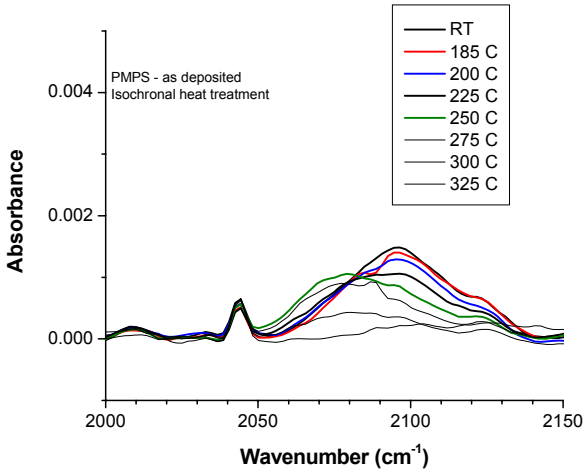

Figure 5.33. IR spectra of as-deposited PMPS heat treated with sequential isochronal temperature in the frequency range near 2100 cm^{-1}

Figure 5.34 shows evolution of PMPS IR spectra during isochronal heat-treatment near the 1000 cm^{-1} frequency range. Heat treatment below 145 C typically did not produce measurable changes in the absorption magnitude over the frequency range examined; however, the exact temperature to produce modifications in absorption strength was specific to the bands and their associated vibrational modes. Absorption bands in the 1000-1100 cm^{-1} region, which are associated with bridging Si-O-Si [100], increased in magnitude after the ~200 C heat treatment. After a full round of heat treatment (i.e. to 325 C), the Si-O-Si absorption band growth is slightly skewed to 1030 cm^{-1} which is associated with short cyclic Si-O-Si chain [100]. The cyclic siloxane formation after heat treatment was also observed by Jambe *et al.*,using NMR analysis [89]. A peak centered at 1130 cm^{-1} developed on the shoulder of the Si-O-Si band after heat treatment at 275 C which is consistent with Si radical structure formation. [74,91-92]. A Si-phenyl band centered at 1100 cm^{-1} decreased in magnitude after heat-treatment at 200 C suggesting Si-phenyl bond disruption [100]. Smaller sharp bands associated with different =C-H vibration (at 1000 cm^{-1}, 1030 cm^{-1} and 1070 cm^{-1}) are anticipated to decrease in magnitude, however, these peaks were superimposed with Si-O-Si bands which hindered measurable changes in absorption strength with heat treatment.

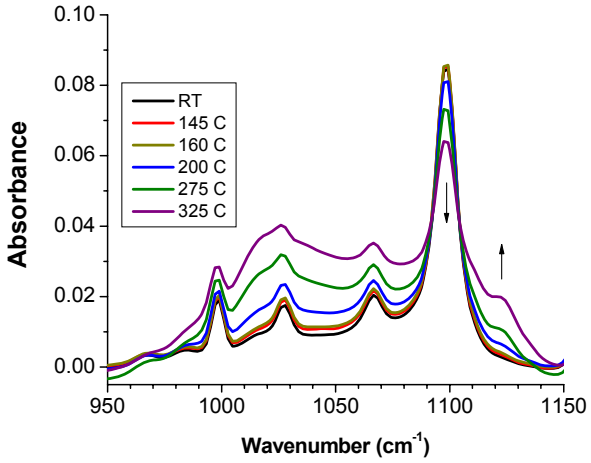

Figure 5.34. IR spectra of as-deposited PMPS heat treated with sequential isochronal annealing (10 minutes) in the frequency range near 1000 cm^{-1}.

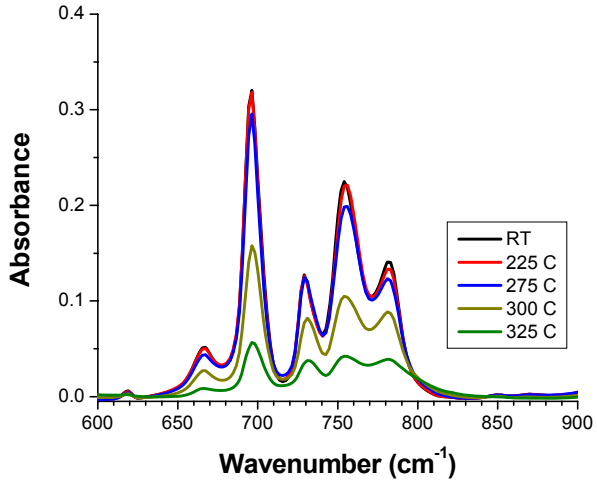

Figure 5.35. IR spectra of as-deposited PMPS heat treated with sequential isochronal annealing (10 minutes) in the frequency range of 600-900 cm^{-1}.

Figure 5.35 exhibits the thermally induced spectral modification of vibrational bands associated with different side-groups in the wavenumber region of 600-900 cm^{-1}. Absorption bands associated with side-groups, in general, decreased in magnitude after heat treatment above 275 C. A similar trend is also observed in the higher energy region (2750 – 3300 cm^{-1}) which contains different C-H vibration modes of the side groups, (see Figure 5.36).

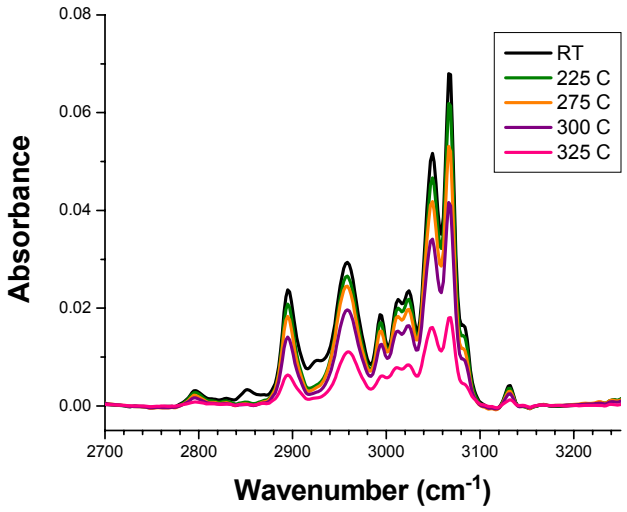

Figure 5.36. IR spectra of as-deposited PMPS heat treated sequentially under isochronal (10 minutes) conditions.

5.7.2 Poly[(methyl)(phenyl)silane] pre-irradiated with UV (3.68 eV)

Heat treatment of PMPS films that were pre-irradiated under 3.68 eV UV energy, exhibited additional structural modifications, beyond those produced by UV irradiation under both nitrogen and air atmospheres. For example, the IR absorption band at 450 cm^{-1}, corresponding to the Si-Si stretching vibration, decreased further in magnitude after heat treatment of PMPS thin films pre-irradiated under nitrogen (anaerobic PMPS) or air environments (aerobic PMPS). Atmospheric effects were observed, however, in terms of the temperature at which the peak decreases occurred in the PMPS pre-irradiated materials. In this case, the Si-Si stretching mode did not decrease significantly until higher temperatures under aerobic conditions when compared to an identically irradiated film thermally treated under an anaerobic atmosphere, i.e. 225 C vs. 200 C for the aerobic and anaerobic conditions, respectively.

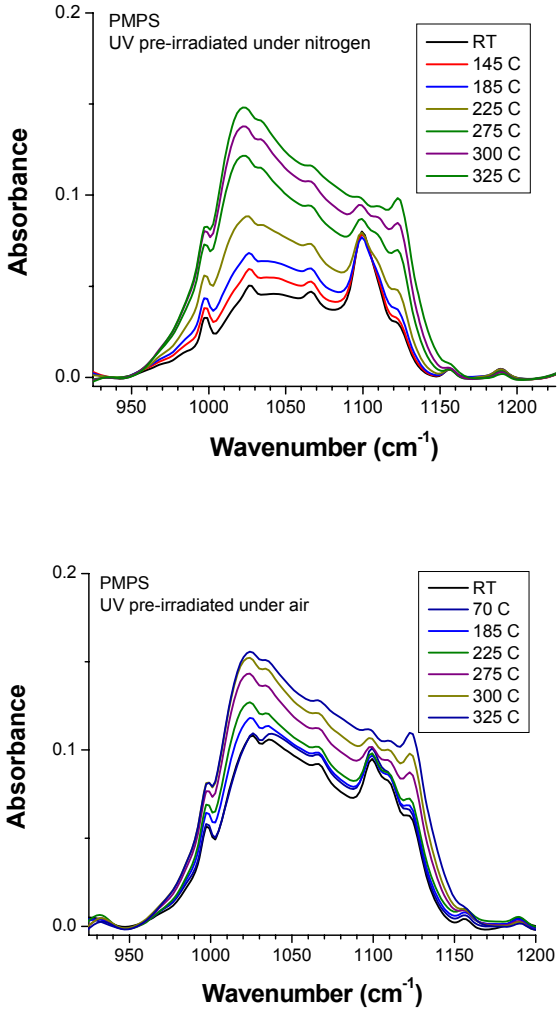

Figure 5.37. IR absorption spectra in the frequency range of 950-1200 cm^{-1} of PMPS pre-irradiated using UV (3.68 eV) under (top) nitrogen and (bottom) air, after sequential isochronal heat treatment.

Figure 5.37 illustrates the thermally induced evolution of IR absorption of pre-irradiated PMPS films treated under both anaerobic (top) and aerobic (bottom) atmospheres in the frequency region near 1100 cm^{-1} where the Si-O-Si vibrational band is anticipated. Siloxane structures existed in the initial pre-irradiated PMPS materials before heat treatment, therefore, the absorption band at this region does exist at room temperature. Photoirradiation under aerobic environment is more effective than under anaerobic environment which resulting in more Si-O-Si linkages formed under aerobic irradiation conditions, as observed in higher absorption observed in this frequency range. Regardless the amount of starting Si-O-Si structure in both PMPS irradiated under aerobic and under anaerobic condition, the final shape and maximum absorbance value closely resemble to each other which suggests similar final products occurred after heat treatment under both irradiation conditions.

Si-O-Si band growth in pre-irradiated PMPS regardless local environment (in Figure 5.37) is skewed to lower energy (faster at 1020 cm^{-1} compared to that observed at 1050 cm^{-1}). This suggests the formation of short-chain, cyclic Si-O-Si structure [100]. The Si-O-Si formed in isochronal heat-treatment of pre-irradiated PMPS is shorter and has a more ring-like structure than in as-deposited PMPS which has a more linear chain Si-O-Si conformation. This is supported by the FTIR data which exhibits a less skewed (at ~1050 cm^{-1}) Si-O-Si vibrational band growth (Figure 5.34).

The formation of Si-O-Si in photoirradiated PMPS, regardless of local atmospheric environment during optical exposure, occurred at lower temperatures than as-deposited PMPS (at 145 C to 200 C). The Si-O-Si formation is accompanied by a

decrease in the intensity of absorption bands corresponding to the Si-phenyl and Si-H groups. The frequency bands correspond to Si-phenyl group are located at 695 cm^{-1}, 730 cm^{-1}, 755 cm^{-1} (Figure 5.38) and 3000 – 3070 cm^{-1} (Figure 5.39). However, this temperature range is still lower than that corresponding to phenyl group cleavage from the main Si chains (>200C). Therefore, the decrease in these Si-phenyl bands is likely caused by the indirect effect of backbone scissioning.

Figure 5.39 contains representative IR spectra in the frequency range of 2900 – 3250 cm^{-1} which not only contain phenyl-related vibrational bands (3000-3070 cm^{-1}) but also methyl vibrational bands at 2900 cm^{-1} and 2960 cm^{-1} [100]. Although phenyl-related bands start to decrease at 145 C, significant band bleaching occurred after annealing above 200 C. The methyl bands exhibit decreasing strength at relatively higher temperature than the phenyl vibrational bands (~250 C to 200 C). The higher decomposition temperature is consistent with the stronger methyl bonds (Si-C) than phenyl ring bonds (C-C), 90 kcal/mol compare to 85 kcal/mol. At lower temperatures (70-115 C) before degradation, all vibrational bands, corresponding to phenyl and methyl groups, show an increase in magnitude, which is consistent with structural relaxation observed in UV-visible absorption spectra. Both phenomena are observed consistently regardless of the environment used during photoirradiation of PMPS.

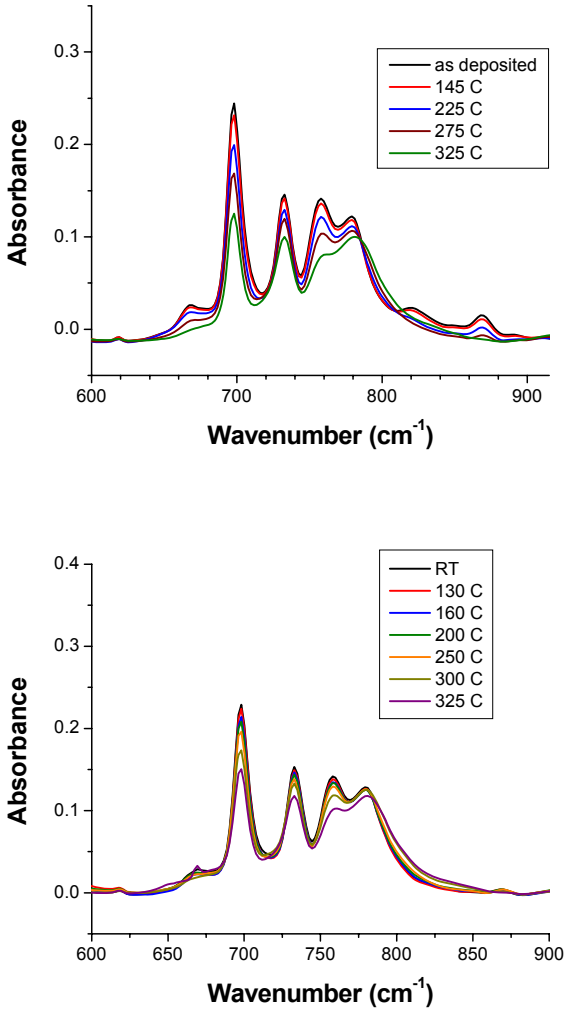

Figure 5.38. IR absorption spectra in the frequency range of 600-900 cm^{-1} of PMPS pre-irradiated using UV (3.68 eV) under (top) nitrogen and (bottom) air, after sequential isochronal heat treatment.

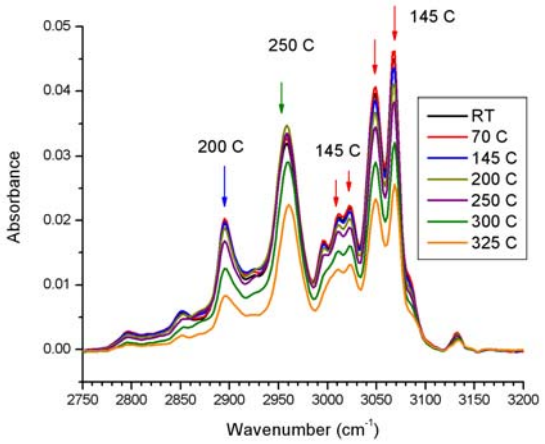

Figure 5.39. Representative of IR absorption spectra of PMPS pre-irradiated using UV (3.68 eV) under nitrogen after sequential isochronal heat treatment in the frequency range of 2750-3200 cm^{-1}. The arrows indicate temperature at which vibrational bands started to decrease.

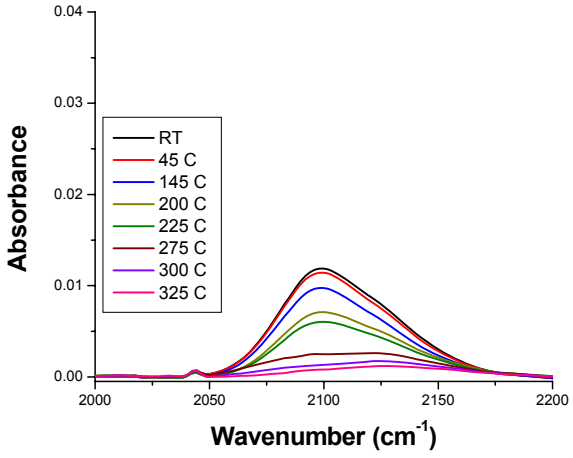

Figure 5.40. IR absorption spectra near 2100 cm^{-1} of PMPS pre-irradiated using UV (3.68 eV) under nitrogen after sequential isochronal heat treatment.

Vibrational bands associated with Si-H are only observed in PMPS pre-irradiated under anaerobic environment as photoirradiation under anaerobic environment encourages Si-H structure growth [101]. The Si-H vibrational bands located at 870 cm^{-1} (Figure 5.38) and near 2100 cm^{-1} (Figure 5.40) decreases in magnitude after heating above 145 C which is consistent with Si-H bond degradation.

6. DISCUSSION

6.1 AS-DEPOSITED MATERIALS PROPERTIES

6.1.1. Electronic excitation: UV-visible and Vacuum UV (VUV) absorption spectroscopy

As-deposited poly[(methyl)(phenyl)silane] (PMPS)

As mentioned, Reference [59] provides a structural interpretation of the spectral features observed that has served as the basis for the selection of component Gaussian peaks used to fit the experimental data shown in Figure 5.2. In terms of structural moieties, the component contributions to the VUV absorption spectrum can be divided into those arising from states associated predominately with the Si-Si backbone (and its conformations) and those involving transitions linked to the side-groups (methyl, phenyl).

The absorption peaks associated with the Si-backbone are centered at 3.60 eV and 3.72 eV, 7.65 eV (see Figure 5.2). These absorption bands have also been observed in different alkyl silanes structures [111]. The lowest energy absorption peaks at 3.63 eV (labeled: A in Figure 5.2) and 3.78 eV (labeled: B) are assigned to the lowest energy σ-σ* transition of the conjugated Si backbone chains with *trans* and *gauche* conformations, respectively [62]. The absorption band centered at 7.65 eV (labeled: F) is associated with a higher order transition of σ-σ^* of Si backbone which occurs from the bottom of the valence band to the top of the conduction band [59,112].

Continuing to refer to Figure 5.2, absorptions bands at 9.44 eV (labeled: G) and 10.5 eV (labeled: H) are attributed to transitions associated with backbone-alkyl group interaction. These resonances are consistent with computational and experimental

investigations of trimethylphenylsilane that exhibit similar methyl resonances at 9-10 eV associated predominately with the Si-C covalent bond [113-114]. These resonance bands could be assigned to an isolated methyl transition as suggested in Reference 59 and 111. However, these bands decreased in magnitude after UV-irradiation of 3.68 eV and 5.10 which are relatively too low in energy to dissociate methyl components. In this case, it is reasonable to assume that the transitions are related to backbone structures [99].

Phenyl rings produce absorption peaks located at 4.29 eV (labeled: C in Figure 5.2), 5.31 eV (labeled: D) and 6.17 eV (labeled: E). The absorption peak centered at 4.29 eV corresponds to a transition between a delocalized Si backbone electron and an unoccupied π^* orbital of the phenyl rings [59,62]. The analogous absorption bands, at 5.31 eV and 6.17 eV, have also been observed in phenylsilane [115] and polystyrene [103] which attributed to S_2 and S_3 type of transition. The 5.31 eV and 6.17 eV peaks are reminiscent of S_2 and S_3 type transitions observed in benzene [102] and are tentatively associated with analogous transitions in this case.

<u>As-deposited poly[bis-(ethylphenyl)silane] (PBEPS) and Ge-Si copolymer</u>

Figure 5.1 shows the UV-visible absorption of Ge-Si and PBEPS. The lowest energy absorption maxima due to the σ-σ^* transition of backbone chains is located at ~3.28 eV (380 nm). This transition is ~0.40 eV lower in energy (~40 nm) and in absorption magnitude compared to the analogous transition in PMPS. As discussed in previous section, lower σ-σ^* energy observed in PBEPS and Ge-Si copolymer than in PMPS can be attributed to different factors.

The addition of aryl components in polysilane is known to reduce the σ-σ^* transition energy [69-70], however, the addition of an extra aryl substituent to an existing aryl-silane compound (i.e. PMPS) results in only a minimal change of the σ-σ^* transition energy [68,71]. Both PBEPS and Ge-Si copolymer contain the bis-(ethylphenyl) group which enforces an all-*trans* backbone conformation . Such conformations have been found to exhibit a lower energy electronic transition than the *gauche* and *trans* mixed conformations in PMPS [55,66-67]. The lower molecular weight of the PBEPS and Ge-Si copolymers, as confirmed by GPC results, is anticipated to also contribute to a lower σ-σ^*oscillator strength compared to PMPS materials [55], consistent with the lower magnitude in absorption observed (Figure 5.1).

The absorption spectra of the Ge-Si copolymer film exhibit very similar spectral characteristics in the UV-visible region when compared to the PBEPS absorption spectra (Figure 5.1). This is expected as a major component in both PBEPS and the Ge-Si copolymer is bis(ethyl-phenyl)silane (100% in PBEPS and 95% in Ge-Si copolymer). In this case, absorption bands assignments are therefore derived from insight obtained from the PMPS materials. Figure 5.1 shows that the lowest energy absorption of Ge-Si absorption, which is associated with σ-σ^* of the backbone, is shifted to lower energy from 3.28 eV to 3.24 eV (378 nm to 382 nm). The 0.04 eV shift of the σ-σ^* transition to lower energy is attributed to the 5% germane substituent in the Ge-Si copolymer backbone [52]. Other possible contributions to the lower energy σ-σ^* transition in the Ge-Si copolymer are associated with the bonding of long hexyl chains the germane substituents. The long alkyl chains are known to crystallize and enforce a *trans* backbone conformation [66-67].

The Ge-Si thin films are heated to 120 C for 30 minutes as part of the deposition process. This temperature is probably close to glass transition temperature of the materials considering T_g of long chain MW is ~122C [116]. As a result, Ge-Si copolymer is free to move and long hexyl chains attached to Ge backbone allowing the formation of interchain close packing structures which resulting in more *trans* structure and an overall reduction in the σ-σ^* transition energy below that observed in PBEPS.

Higher energy transition bands corresponding to side-groups in the Ge-Si copolymer are presented in Figure 5.3. The absorption bands associated with the Si backbone (Figure 5.3) are centered at 3.3 eV (labeled: A in Figure 5.3), 7.2 eV (labeled: E) and 9.1 eV (labeled: F). The absorption band at 7.2 eV corresponds to a higher order transition of the backbone between the bottom of the valence band to the conduction band [59,112]. The absorption bands above 9 eV are typically associated with alkyl-related transitions which exist in methane [98,117] as well as in alkyl-containing polysilane such as poly(methylphenylsilane) [59], poly(di-n-butylsilane) [111] and poly(di-n-hexylsilane) [118]. However, the Si-alkyl structure does not exist in Ge-Si materials, therefore, the absorption band centered at 9.1 eV is assigned to combination of hexyl group on the germane substituent and ethyl group attached to phenyl side-group.

The phenyl-related absorption bands of the Ge-Si copolymer, shown in Figure 5.3, are centered at 5.2 eV (B), 5.8 eV (C) and 6.1 eV (D). As mentioned previously, Gaussian components were used to fit the experimental data. Analogous to the PMPS materials, an absorption band associated with the σ-π^* is expected to have energy slightly higher than the σ-σ^* transition of the backbone chain centered at 3.3 eV [59,62].

However, the experimental spectra of Ge-Si copolymer fit reasonably well without the addition of an extra Gaussian component in this region. An initial "guess" Gaussian absorption band in this region was transformed upon fitting into a larger peak centered at 5.2 eV (labeled: B in Figure 5.3). The absorption energy of the phenyl-related transitions i.e. S_2 and S_3, could vary between 0.5 eV to 1.0 eV depending upon the phenyl group derivative [112,115]. The Ge-Si copolymer contains a phenyl-ethyl group attached to the silane substituent as well as a phenyl attached to the germane substituent. In this case, the S_2 and S_3 transitions of these phenyl groups with different derivatives (depending upon their attachment to the silane or germane portion of the backbone) are expected to vary in energy. The absorption bands centered at 5.2 eV (labeled: B), 5.8 eV (labeled: C) and 6.1 eV (labeled: D) in Figure 5.3 represent these different phenyl transitions. Detailed assignments of phenyl related transitions in Ge-Si copolymer are not available due to lack of absorption data in vacuum-UV region for Si-phenyl-ethyl and Ge-phenyl in the literature.

6.1.2. Molecular structure: Vibrational spectroscopy and Density Functional Theory (DFT) calculation

The identification of vibrational bands observed in IR spectroscopy was achieved using both a comparison to past work and modeling of analogous oligomeric systems via Density Functional Theory (DFT) calculation. The normal-mode computation based on energy minimized structures provided reasonable agreement to experimental results and

could be used to provide additional insight into the origins of vibrational peaks in the experimental spectrum. Discrepancies between the computed and experimental spectra are expected as the model structure used in the DFT computation only involved relatively short chain (5 Si monomers) compare to the materials used in experiment which had a weight-average molecular weight of 42,000 (PMPS material) (i.e. an average chain length of 350). Thus, the computations will provide no information on long chain behavior which would include steric effects on backbone chain topology and an effective sampling of conformational variation along the chain length. In contrast, the computation will also provide additional information on the molecules/atom (i.e. hydrogen) used to terminate calculated system. Since the calculated system only involves a few repeat units, the contribution from structures located at the beginning and end of the molecular chain become more important, contributing additional bands (such as Si-H) which otherwise are not observable in the longer chain materials.

Similarly, Ge-Si copolymer is too large a system for a direct DFT calculation. In order to provide accurate representation Ge-Si copolymer used in the experiment, DFT calculations of more than a few hundred repeat units would be required to represent the 5% of germane substituent in the system. In this case, the effect of different side-groups and backbone on vibrational spectra was analyzed by replacing side-groups and backbone from (methyl)(phenyl)pentasilane systematically to gain insight into the vibrational behavior exhibited by the Ge-Si copolymer structure. Similarly, comparing the normal mode calculation of (methyl)(phenyl)pentasilane and (methyl)(phenyl)pentagermane, shown in Figure 40, provides insight into the origin of vibrational bands specific to the

germane backbone. Both (butyl)(phenyl)butagermane and (bisphenyl)butasilane resemble the Ge-Si copolymer structure in order to identify side-groups related vibrational bands. However, the Ge-Si copolymer consisted of more complicated side-groups than these structures. For example, the copolymer contains bis-(ethylphenyl) on the silane substituent and (phenyl)(hexyl) on germane components. This contrasts the focus of the normal mode calculation based on bis(phenyl) on silane and butyl on germane. These simplified normal mode calculated structures thus represent a compromise between model fidelity and available computing resources.

6.2 UV-INDUCED MODIFICATIONS OF MATERIALS PROPERTIES

6.2.1. Photoinduced electronic excitation modification: UV-visible and Vacuum UV (VUV) absorption spectroscopy of poly[(methyl)(phenyl)silane] (PMPS)

Effect of irradiation energy

Absorption bands in the PMPS UV-visible spectra decreased in absorption magnitude upon UV irradiation. The UV irradiation with 3.68 eV, which is resonant with the lowest energy absorption peak, reduced the absorption intensity of the peak centered at 3.7 eV associated with σ-σ^* transition of Si backbone. The absorption peak also shifted to higher energy with UV irradiation, shown in Figure 5.7. The decrease in absorption intensity is consistent with the photoinduced scissioning of the Si-Si backbone. As Si-Si bonds are broken into smaller chains, the strength of the optical absorption associated with the presence of the conjugated structure is reduced [77-81].

The blue shift in the associated transition energy with exposure can be qualitatively interpreted in terms of 1-D confinement of carriers along the conjugation length of the chains. As the length of chains is decreased with ultraviolet irradiation, the energy of allowed states in the remaining polymer chain will tend to increase, exhibiting increased optical transition energy as the conjugation length is reduced [119].

In the vacuum-UV region, however, the higher order transition associated with the Si-backbone (located at approximately 7.65 eV) does not appear to be significantly affected by irradiation at 3.68 eV (Figure 5.8) [79]. This peak is tentatively assigned to a transition from sub-band edge states within the valence band to states within the conduction band. This transition has been previously found to be insensitive to Si chain length [59,99,112]. Finally, absorption bands at 9.44 eV and 10.5 eV were found to decrease in area more than 10% under 3.68 eV illuminations. In calculation and experimental investigations of trimethylphenylsilane, methyl resonances in the range 9-10 eV have been associated predominately with the Si-C covalent bond at the methyl group [113-114], prompting a similar assignment in the present study. The decrease in absorption strength observed in this energy range, however, appears to reflect a contribution from the conjugated Si-Si bonding states to alkyl-based transitions in the polymerized system.

Exposure with 5.10 eV is resonant with the phenyl side-group transitions, and it is thus, anticipated to primarily disrupt the phenyl groups present in PMPS. The concurrent decrease in the $\sigma - \sigma^*$ band (associated with the polysilane backbone) as well as the π- π^* band (aryl moiety) is consistent with the presence of an energy transfer process to the

backbone. This is not unlikely given the established tendency for molecular orbital admixing in this system [62]. Interestingly, irradiation with 5.10 eV produced a much smaller blue shift of the remaining $\sigma - \sigma^*$ transition band energy (Figure 5.7b) than that observed under 3.38 eV illumination (0.4 eV for 3.38 eV exposure vs. 0.2 eV shift for 5.10 eV illumination). In a previous section the influence of molecular structure on the lowest energy ($\sigma - \sigma^*$) transition energy was discussed. Based on the photoinduced change in absorption intensity observed across the near-UV spectral range, photoexposure at 5.10 eV is anticipated to both disrupt Si chains as well as the phenyl side-groups. Photodisruption of the phenyl group is expected to have a two-fold influence on the lowest absorption transition energetics, by affecting steric contributions to the backbone chain conformation attained and by altering the extent of orbital admixing between the phenyl side-groups and the backbone. Both of these effects, will tend to shift the $\sigma - \sigma^*$ transition band to higher energy. The fact that the 5.10 eV exposure was less effective at producing a blue shift in the lowest transition energy absorption band in PMPS indicates that the photostructural modification on the allowed energy states of the molecular system is more complex than described above, involving photostructural responses that are not directly linked to backbone conformation, for example, but that could produce a red-shift in the $\sigma - \sigma^*$ transition energy.

One possible effect which could contribute to a lower $\sigma - \sigma^*$ transition energy is a reduction in Si-Si distance after photomodification. While only a qualitative argument, a tight-binding model for molecular orbital formation would indicate that a reduced Si-Si bond distance would promote increased overlap of adjacent atomic bonds to form

molecular orbital states. This would result in increased energy broadening of the bonding and anti-bonding orbital bands as the number of Si-orbitals participating in the structure increases, thus reducing the HOMO-LUMO transition energy. Again, such a simplified model completely neglects the influence of side group sterics and state admixing. Proceeding with this argument, however, photodisruption of phenyl components within PMPS would reduce steric constraints on the structure and, in addition to any backbone chain conformation effects, might also result favor the reduction in Si-Si bond distance within the chain.

However, our DFT calculation of free standing oligomers (see below) reveals that the nature of the side-group has only a limited effect in Si-Si distance. The Si-Si distances in bis(phenylethyl)silane (higher steric constraints) and methylphenylsilane, for example, are nearly the same (2.34 A to 2.36 A, respectively). Note also that the trend in Si-Si bond distance between the side-group having high steric bulk and that anticipated to have only limited steric effects is in the opposite sense to that needed to promote a red-shift in the HOMO-LUMO energy with side-group disruption. Clearly, however, a more in-depth computational analysis of these trends is required to connect nuclear position changes with the electronic energetics of the molecular. Moreover, a full computational investigation of the energetics of these systems will require the use of models consistent with the long-chain (polymeric) nature of the material as this will also significantly influence the energetics of extended states in these structures.

The difference in the blue-shift of the lowest energy transition band observed between 3.68 eV and 5.10 eV exposure may also be discussed in terms of variation in the

distribution of chain lengths produced during photoexposure. Given the anticipated variation in HOMO-LUMO energy with chain length, the 3.68 eV photons should be selectively absorbed by chain lengths providing a HOMO-LUMO energy near resonant with the incident photon energy. Similarly, longer chain lengths (with lower HOMO-LUMO energies) should also absorb the incoming photons. Thus, the chain-length-selected absorption the 3.68 eV excitation, and the ensuing disruption of the longer chain lengths in the molecular weight distribution in the polymer, preferentially leaves shorter chains behind and produces a shift in the overall shape of the molecular weight distribution toward a shorter average chain length, resulting in the observed blue shift. In contrast, if the primary excitation of the Si-Si backbone under 5.1 eV photon irradiation is via indirect paths (see discussion above), i.e. subsequent to resonant excitation of the phenyl moiety, there should be no preferential excitation of the Si-Si chains according to their length. Thus, while the overall average chain length (and average molecular weight) will decrease with irradiation, the selective disruption of longer chains is not expected and the chain length (or molecular weight) distribution will exhibit only a rigid shift with little modification in the shape of the distribution. The additional effect of preferential disruption of longer chains upon near-resonant excitation at 3.68 eV may, therefore, be a contributor to the larger blue shifts observed in the $\sigma - \sigma^*$ absorption band observed. Clearly, a more involved analysis is necessary to fully establish this factor as a contributor to the observed effects of excitation energy on near-UV absorption.

As mentioned earlier, exposure with 5.10 eV photons (Figure 5.9) reduces the overall absorption band area by ~20% more than that observed under 3.68 eV (Figure

5.8) exposure (under either air or nitrogen). Exposure with UV energy of 5.10 eV completely removed absorption bands associated with σ-σ^* transition at 3.60 eV and 3.72 eV with significant reduction in peak height observed for the 7.65 eV higher order backbone resonance. Referring to Figure 5.10a (vs. Figure 5.10b) in the Results chapter, Si-alkyl absorption bands at 9.55 eV and 10.72 eV, in general, decrease more rapidly with fluence at 5.10 eV compared to 3.68 eV exposure. These spectral changes support the photoinduced scissioning process to form silyl radical known to be a primary photostructural modification mechanism in these polysilylene systems [32,53,82-84]. Moreover, these results are consistent with FTIR data which indicate a more effective disruption of Si-Si bridging structures under higher energy photon exposure [85-86,101]. A primary result of the photoscissioning process elucidated by these FTIR studies was the formation of siloxane bridging units within the PMPS structure as a means to stabilize the disruption in Si-Si bond conjugation [101].

All peaks associated with phenyl transitions at 4.29 eV, 5.31 eV and 6.17 eV also decreased in height (and fitted peak area) more abruptly with 5.10 eV illumination. In fact, the fitting procedure produced reasonable agreement with the experimental spectra when the band centered at 4.29 eV was removed, indicating a complete bleaching of this resonance (see Figure 5.10b). This behavior is consistent with the assignment of these peaks to transitions linked to the aromatic side-group. Three similar resonances, associated with benzene electronic states, have been examined previously and their oscillator strengths computed [115]. In this case, the lowest energy transition (the first singlet transition, S_1) was found to have the lowest oscillator strength. With the

association of the 4.29 eV peak to an analogous transition in the phenyl moiety of the PMPS it is reasonable to expect that this absorption peak will be the first to be lost as photoinduced disruption of these structures proceeds with UV-exposure and the signal level falls below the measurement detection limit. The remaining phenyl-related transitions shift to higher energy, in agreement with that observed for monomeric phenylsilane [112,115] which is analogous to effects observed in the present study under 3.68 eV photon exposures. The higher energy shift observed under lower photon energy illumination, however, were less pronounced, serving to further confirm that the higher energy photons are more effective in producing backbone scissioning than the lower energy optical radiation, consistent with prior vibrational spectroscopy results from these materials [101]. The magnitude of absorption bands associated with phenyl transitions (5.31 eV and 6.17 eV) decays exponentially with increasing fluence. This is consistent with both ring-opening reactions photooxidation to form dialdehydes, which have been observed for photo-oxidation in polystyrene [85] than complete phenyl ring removal [86].

The smaller absorption bleaching (in both magnitude and spectral breadth) observed in 3.68 eV irradiation is consistent with the reduced refractive index change recorded under this condition (Figure 5.12, 5.13). For example, 3.68 eV irradiation under air produced a maximum $\Delta n = -0.07$ while 5.10 eV irradiation under the same conditions reached a maximum $\Delta n = -0.14$. The decrease in material refractive index after UV-irradiation is linked to siloxane formation after oxygen insertion into the scissioned Si backbone chain; more siloxane formed translates into a greater magnitude of refractive change [101]. Photomodification under current excitation conditions is most

likely a one-photon process as demonstrated in Figure 5.13. In this case, the refractive index change after irradiation with 5.10 eV, is strictly related to the amount of fluence but is independent of intensity (i.e. pulse energy for a given pulse length). A two photon (nonlinear) process would exhibit intensity dependence in refractive index changes.

The volume of PMPS was found to expand upon UV irradiation as observed in ellipsometric measurements of thickness (Figure 5.14). Again, most of the expansion is likely due to incorporation of oxygen into backbone structure to form siloxane linkages. Moreover, DFT energy minimization of a 5 and 10 repeat unit siloxane-based methylphenyl-containing molecules, shows that to the structure tends to assume a puckered ring conformation, further supporting an increase in volume associated with siloxane structures upon irradiation (Figure 6.1).

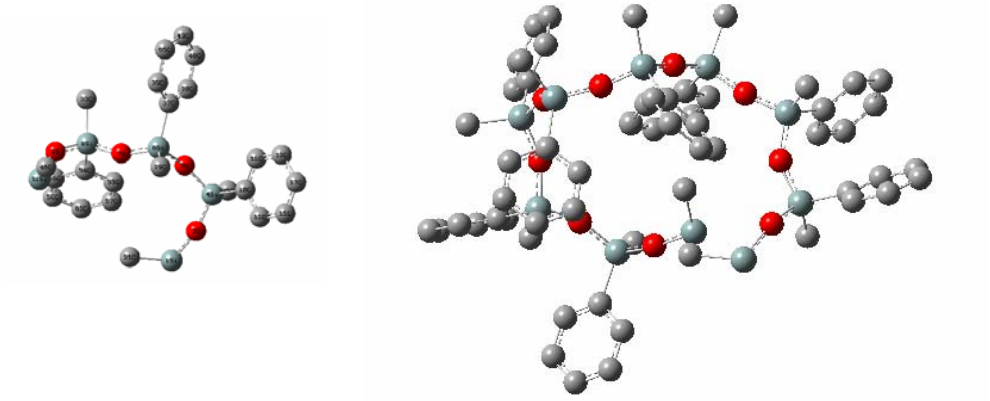

a. pentasiloxane **b. decasiloxane**

Figure 6.1. DFT energy-minimized structures (methyl)(phenyl)siloxane oligomers. All atoms are stabilized with hydrogen. Grey ball = C, red = O, green = Si. (a) pentasiloxane (b) decasiloxane

Kramers-Kronig analysis of the absorption change (Table 3) shows lower calculated refractive index changes than those observed via experimental measurements. However, even calculations including the VUV region were still lower than experimental values by at least an order of magnitude. Moreover, the effect of local environment on the computed $\Delta n_{632.8}$ was not as pronounced as that observed experimentally. Clearly the influence of even significant absorption strength changes in the VUV, far removed from 632.8 nm, were not sufficient to fully explain the large refractive index modifications observed at this wavelength. The limited effect of the VUV spectral modifications on optical constant changes in the visible, however, is not unexpected given the spectral behavior of the Kramers-Kronig relationships. It is clear that other mechanisms (e.g. density changes associated with bond disruption, reformation, and siloxane formation) must be contributing to the observed refractive index changes in these materials [99].

Effect of local environment

The availability of oxygen in the local environment during photoexposure influence the bleaching rate of the σ-σ^* absorption bands as illustrated in Figure 5.11. The behavior is consistent with the disruption of the Si-Si conjugated bond structure in PMPS. UV-exposure under aerobic environment thus provides a more dramatic photostructural change when compared to anaerobic environments under the same irradiation conditions [13,26,99,101,106].

The absorption spectra modification in both UV-visible and vacuum-UV (VUV) regions confirmed that UV-exposure under aerobic environments is more effective in disrupting the Si-Si conjugated bond structure present in PMPS than identical exposures under anaerobic conditions. For example, the Si-alkyl absorption bands at 9.55 eV and 10.72 eV exhibit larger reductions in peak heights (and areas) under an air atmosphere with similar fluences at either 3.68 eV (Figure 5.8) or 5.10 eV (Figure 5.9). This general trend is observed in the spectral modifications exhibited across the VUV region for transitions either directly associated with the Si-Si backbone or indirectly influenced by the condition of the Si-Si backbone (e.g. conjugation length, extent of state delocalization) through contributions to the character of electronic states involved in side-group transitions [99].

Higher refractive index changes attained in the aerobic environment is associated with more effective siloxane formation in the presence of oxygen. High energy irradiation 5.10 eV shows a less pronounced influence of local environment as photooxidation influences both the Si backbone and phenyl moieties. FTIR results have shown that the presence of oxygen during exposure tends to stabilize the Si-Si bond photoscissioning through the formation of siloxane bridging structures while exposure under anaerobic conditions suppresses this effect [26,106]. The FTIR results will be discussed in more detail in latter section.

The effect of energy and local environment is important from the technological point of view. In the write-as-needed application, high irradiation energy (5.10 eV) and

an aerobic writing environment will be important maximize the refractive index change obtained.

6.2.2. Photoinduced structural modification: Vibrational spectroscopy of poly[(methyl)(phenyl)silane] (PMPS)

The vibrational absorption data provides an opportunity to correlate the final structure of the material with the optical exposure conditions used. This additional insight supports a better understanding of the nature of photoinduced structure modification that accompanies the photodisruption of Si conjugated bonds evidenced in electronic absorption studies.

The vibrational spectra of PMPS after UV exposure is consistent with a disruption of the Si backbone, as evidenced by a reduction in the absorption strength of the symmetric stretching vibrational mode of Si-Si (460 cm^{-1}), shown in Figure 5.20 in the Results section. Moreover, excitation with 5.10 eV also produces peak height reduction on the absorption bands associated with C-H vibration on the phenyl group (Figure 5.24). The height reduction of these bands is limited compared to the phenyl-associated electronic structure bleaching. This can be interpreted in terms of photo-induced electron density redistribution of shorter backbone chains and surrounding environment. Excitation with 5.10 eV disrupted aromatic ring in longer chain scale while retaining shorter chain characteristic of the original atomic configuration and its associated vibrational behavior [101].

Figure 5.21 shows a general increase in siloxane linkage absorption with fluence. This effect is more pronounced under aerobic photowriting environment regardless of irradiation energy. In addition, irradiation with 5.10 eV produces more siloxane than that observed under 3.68 eV as evidenced by a larger absorption strength increase in the 1000-1100 cm^{-1} range. The siloxane structure formation in the anaerobic (nitrogen) environment is most likely caused by residual oxygen present in the chamber after purging. As described previously, the atmospheric composition was attained by displacement of ambient air inside the chamber in atmospheric pressure without previous evacuation of the chamber. However, there is a clear correlation between the absorption strength of the vibrational resonances associated with oxygen incorporation and intentional oxygen addition to the local atmosphere during UV irradiation (Figure 5.21).

Absorption peaks associated with Si-H increased more in magnitude under an air environment compared to nitrogen with 3.68 eV UV irradiation shown in Figure 5.22(a) and 5.22(c). These observations appear to support the view that 3.68 eV irradiation under oxidizing conditions favors retention of backbone continuity through oxygen insertion to form siloxane bridging structures. In contrast, in the nitrogen environment, the photostructural modification is dominated by the formation of chain-terminating hydrides that compete with siloxane linkage formation. Therefore, modification of final structure connectivity is anticipated as a function of local atmosphere with the lower energy exposure.

With irradiation at 5.10 eV, the Si-H absorption peaks shift to higher energy (Figure 5.22(b) and 5.22(d)). Si-H resonances are known to exhibit energy shifts,

consistent with those observed in the current study, as the number of Si-H bonds increases [100]. Therefore, this observation, coupled with the larger reduction of the Si-Si symmetric stretch vibration (Figure 5.20) and increased backbone modification under anaerobic condition exhibited under 5.10 eV irradiation suggest a more substantial disruption in the backbone structure and Si local environment. The local atmospheric effect influences the magnitude of an absorption frequency shift and an increase in hydride vibrational absorption is observed regardless of atmospheric composition under 5.10 eV exposures.

The general trends observed in the vibrational results for 5.10 eV vs. 3.68 eV, exposure, e.g. an increased photostructural changes in backbone related structures and a limited impact of atmospheric identity, are correlated with the refractive index changes of PMPS shown in Figure 5.14. In this case, larger refractive index changes observed were only moderately influenced by the availability of oxygen in the local atmosphere during optical exposure.

Further examination of the spectra in Figure 5.21 reveals the strong development of a resonance at 1130 cm^{-1} with UV exposure (what wavelength) that was not observed in the as-deposited materials. The strength of this band is highest under exposure with 5.10 eV under an air atmosphere. Recent quantum cluster calculation and experimental results of Toman *et al.*, [74-75] also confirms the development of this resonance in PMPS, consistent with cationic radical structures generated upon chemical oxidation. The formation of cationic radical structures is also accompanied by vibrational band development at 480 cm^{-1} (Figure 5.20) and the shift in the absorption strength of Si-

methyl in the 1240-1260 cm^{-1} range toward higher energy (Figure 5.23). Toman *et al.*, has produced this structural modification via chemical oxidation using iodine rather than photoinduced means [75]. We observed similar structural modification via thermal oxidation which will be discussed in a later section.

6.2.3. Photoinduced electronic excitation modification: UV-visible and Vacuum UV (VUV) absorption spectroscopy of poly[bis-(ethylphenyl)silane] (PBEPS) and Ge-Si copolymer

As discussed earlier, the electronic structures of poly(bis-phenylethyl)silane (PBEPS) and Ge-Si copolymer are similar, with the exception of slightly lower Ge-Si σ-σ^* backbone transition energy in the UV-visible region. This similarity in electronic structure is most likely caused by 5% of Ge in Ge-Si copolymer while the balance of the material structure is the same as PBEPS. The photoinduced responses under the same exposure conditions, for both PBEPS and Ge-Si copolymer, are anticipated to be similar, as illustrated in Figure 5.15 in the Results section.

Only the 3.35 eV (370 nm) photon source was used in this study, due to lack of an available compact solid source in the higher energy range at the time of experiment. The photoinduced absorption spectral modification in the UV-visible with 3.35 eV is consistent with PMPS irradiated with analogous photon energy (3.68 eV). The decrease in the absorption band intensity at 3.30 eV and its shift to higher energy is consistent with Si backbone scissioning. Interestingly, the absorption bands due to phenyl group in the

region between 5 – 6.5 eV (Labeled B, C and D; Figure 5.17) increase with UV-irradiation independent of local environment. Since the excitation energy is relatively low (3.3 eV) to access phenyl related resonances, this can be interpreted in term of photoinduced electron density redistribution to form more stable shorter chains structure. Higher order σ-σ^* absorption bands, centered at 7.2 eV (Labeled E), are anticipated to reduce in intensity with UV irradiation as observed in PMPS irradiated with 3.68 eV. However, this phenomenon is most likely below the equipment detection limit as it was not observed in the experimental results.

Photoinduced changes in the σ-σ^* absorption band area observed in Ge-Si copolymer material was associated with Si-Si backbone scissioning (Figure 5.16). As anticipated, oxygen availability in local environment during UV irradiation influences the rate of photoinduced modification of electronic structure which is consistent with the trends observed in PMPS. The aerobic environment provides for a more effective photoinduced effect compared to the anaerobic environment under the same irradiation conditions and total fluence. However, the photoinduced modification in Ge-Si copolymer is less pronounced than that of the PMPS, as evidenced by the longer exposure time (more total fluence) required to saturate σ-σ^* absorption band area reduction in the Ge-Si copolymer (Figure 5.16) compared with that of the PMPS material (Figure 5.11). The less effective photoinduced modification can be linked to lower absorbance in Ge-Si copolymer than in PMPS thin films (0.005 to 0.011) as shown in Figure 5.1. As discussed before, the lower absorbance in Ge-Si copolymer is caused by shorter backbone chains present in the polymer samples examined.

Refractive index changes in Ge-Si copolymer show behavioral trends consistent with those of PMPS. The aerobic environment, again, produces higher refractive index changes than the anaerobic environment after the same total UV-fluence. The aerobic environment provides oxygen which is incorporated into backbone structure to form oxide linkages as observed in vibrational spectroscopy. Consistent with UV-visible absorption spectral behavior, saturation of refractive index changes attained in Ge-Si copolymer and PBEPS require more fluence compared to PMPS under identical exposure conditions (photon energy and local atmospheric composition) (Figure 5.20). This is again attributed to less effective photon absorption in Ge-Si copolymer and PBEPS than in PMPS.

6.2.4. Photoinduced structural modification: Vibrational spectroscopy of poly[bis-(ethylphenyl]silane (PBEPS) and Ge-Si copolymer

As discussed previously, the vibrational absorption of Ge-Si copolymer is dominated by silane substituents. Therefore, Ge-Si copolymer photoinduced modifications are expected to be similar to the photoinduced behavior of PMPS. The photon energy used in Ge-Si copolymer, 3.35 eV (370 nm), is resonant with the backbone transition (σ-σ^*). This caused structural modification limited to only the backbone structure. Consistent with photomodification in PMPS, photoinduced structural modification in Ge-Si copolymer depends on local environment during photowriting. Photoirradiation under aerobic environment encourages Si-O-Si growth while

photoirradiation under anaerobic promotes terminating hydride formation as illustrated in Figure 5.25 and Figure 5.26, respectively. We expected germane components to scission and participate in photomodification before silane substituents as Ge-Si components have lower vibrational energy than Si-Si (351 cm^{-1} to 450 cm^{-1}). This is indicative of the lower bond strength of Ge-Ge compared to Si-Si [109]. Although the germano-related oxide structure formation is anticipated, there is no evidence of Ge-O-Ge likely due to the limited germane concentration in the Ge-Si copolymer as well as Si-O-Ge which is also anticipated to form with photomodification. The anticipated IR absorption band associated with this mixed bridge structure (Si-O-Ge) is located at 650 cm^{-1} as observed with Raman spectroscopy in germanosilicate glass [120-122]. This absorption band was inconsistent with FTIR observation as it overlaps with a CO_2 stretch vibration from the ambient air atmosphere present in the optical path of the spectrometer [100]. The photomodification of the Ge-Si copolymer (Figure 5.25 and 5.26) is relatively small compare to PMPS (Figure 5.21 and Figure 5.22) for siloxane and Si-H formation in PMPS). These results are again consistent with the electronic absorption study in that the σ-σ^* absorption band area decrease and refractive index modification also scale in a similar manner. The Ge-Si copolymer generally required more UV fluence than PMPS to obtain a similar modification in FTIR peak area again attributed to less efficient photon absorption at the resonance energy in the copolymer system (lower absorption strength at the excitation photon energy).

6.3. THERMAL-INDUCED MODIFICATIONS OF MATERIALS PROPERTIES

6.3.1. OPTICAL PROPERTIES: UV-visible absorption spectroscopy and refractive index: As-deposited poly[(methyl)(phenyl)silane] (PMPS)

Thermally induced structural modifications of PMPS were consistent with those caused by photon irradiation. Initial structural modifications of as-deposited PMPS at lower temperature occurred in the Si-Si backbone structure which have lower interatomic bond energy than the side-group (Si-C, C-C) structure. The bond strength for Si-Si and Si-H are ~80 kcal/mol and ~79 kcal/mol while for Si-C, C-H and C-C are ~90 kcal/mol, ~100 kcal/mol and ~85 kcal/mol) consequently [88].

Iterative isochronal heat treatment (from 25 C to 350 C) does not induce any changes up to 175 C as observed with UV-visible spectroscopy (see Figure 5.28). However, the next heat treatment on the same PMPS thin films at 199 C increased the lowest energy absorption band corresponding to σ-σ^* transition which is most likely due to backbone relaxation. It is important to note that no effort is made to obtain a minimum energy structure in the polymer after spinning. The 120 C hot plate treatment was primarily used to drive off residual solvent. It is likely that some volume of the as-deposited film material is characterized by bond topologies that are in a higher energy configuration than that expected based on the side-groups involved and the backbone conformation anticipated. The isochronal anneal at temperatures above the glass transition (112 C – 122 C [116]) will allow the rearrangement (relaxation) of larger structural elements in the polymer, i.e. the backbone, into more energetically favorable configurations. Thus, a greater percentage of the chain structure present in the film

attains a lower energy conformation, increasing the contribution to the absorption peak associated with this Si-Si chain conformation. While the apparent structural relaxation occurred at temperatures greater than Tg the heat-treatment time used in the study may have been too short to allow sufficient structural rearrangement to produce a change in the absorption spectrum. Above 223 C, all absorption bands of PMPS reduced in magnitude which suggests dissociation of both backbone and phenyl groups in PMPS.

Isothermal heat treatment at 160C – 200C (Figure 5.29) produces an increase of PMPS σ-σ^* absorption peak area in the first 5 minutes of heat treatment before decreasing with longer time at temperature. Again, this is consistent with structural rearrangement at glass transition temperature (112 C – 122 C) [116]. Clearly, more in-depth study of the temperature-time dependence of these interesting relaxation phenomena could provide additional insight into the fundamental kinetics of these structural processes (see Future Work). Prolonged heat treatment at temperatures well above this glass transition temperature, however, dissociates the backbone chains resulting in a decrease of the σ-σ^* absorption band area. Heat treatment at 120C produces a much smaller change in backbone absorption band area because the PMPS thin films were heated at this temperature as part of deposition process to eliminate any excess solvent and any modification in structure has already occurred.

The rearrangement of backbone topology observed in absorption spectroscopy is also consistent with the refractive index changes (Δn) of PMPS (Figure 5.30) observed. Heat treatment at temperatures above 120C (at 190C and 200C) increased the Δn of PMPS. Although the maximum thermal induced refractive index change was relatively

small compare to those produced by UV exposure (-0.03 compare to -0.14), the thermal treated of PMPS thin films produced significant large scale film cracks which made the films almost opaque due to increased scattering. This behavior also prevents the collection of reliable refractive index measurements.

6.3.2. OPTICAL PROPERTIES: UV-visible absorption spectroscopy and refractive index: Poly[(methyl)(phenyl)silane] (PMPS) pre-irradiated with 3.68 eV

Thermally induced modification of PMPS which had previously been irradiated with 3.68 eV photon energy exhibited a consistent trend to that observed in as-deposited (un-irradiated) PMPS. Isochronal heat treatment caused the σ-σ^* absorption band to increase at 170 C, lower than that observed in the as-deposited PMPS (199 C). In isothermal heat treatment, only heat treatment at 160 C produces an increase in area of backbone related absorption bands. The lower relaxation temperature in the pre-irradiated PMPS compare to the as-deposited one is most likely due to shorter chain length and a corresponding reduction in the activation energy for rearrangement associated with these structural elements. The as-deposited PMPS contains a greater percentage of long-chain Si backbone units compared to pre-irradiated PMPS which should have a reduced average molecular weight after UV irradiation at 3.68 eV breaks the Si backbone and forms both hydride and siloxane structures [101]. Therefore, shorter Si chains in pre-irradiated PMPS are easier to rearrange compare to long Si chains in as-deposited PMPS.

From a technological standpoint, an understanding of thermally induced modification in structure and optical behavior is important for device performance. Typical photosensitive photonic systems use photopatterned refractive index structures, in which the active region is the photoirradiated section. The working temperature of such devices is typically below 120 C. Based on the current findings, prolonged time at elevated temperature can significantly affect both the absorption and refractive index of the material, both in as-deposited and irradiated material. Such phenomena can then deteriorate system performance severely. The as-deposited region exhibits a reduction in refractive index, which reduces the refractive index gradient between active and blank region, before turning opaque at elevated temperatures.

6.3.3. MATERIALS STRUCTURE: Vibrational spectroscopy: as-deposited poly[(methyl)(phenyl)silane] (PMPS)

One of the fundamental structural modifications anticipated with increased thermal energy (elevated temperature) is Si backbone scissioning. An absorption band, centered at 450 cm^{-1}, has been associated with Si backbone and exhibits a decrease in magnitude after heat treatment at 160 C. This temperature is consistent with that needed to modify the σ-σ^* transition peak observed in the UV-visible region. It is also consistent with Si-Si backbone scissioning in PMPS at 150 C as observed using Gel Permeation Chromatography (GPC) and Differential Scanning Calorimetry (DSC) [89-90]. The Si-Si vibrational absorption band is barely measurable after heat treatment at 325 C, which

suggests that a very limited amount of Si-Si is left after heat treatment. The silane monomer from PMPS started to form at heat treatment at 270 C as observed during pyrolysis of PMPS using mass spectrometer [91-92]. The absorption band near 2100 cm^{-1}, associated with Si-H stretch, has a relatively low absorbance initially and shifts to lower energy by approximately 30 cm^{-1} upon thermal treatment above 185 C (Figure 5.33). The Si-H band shift to lower energy is associated with the development of shorter Si chains with thermal treatment [110].

Thermal treatment of PMPS also produced siloxane structures, as anticipated. However, after a full round of heat treatment (until 325 C), the Si-O-Si absorption band growth is slightly skewed to 1030 cm^{-1} which is associated with short cyclic Si-O-Si chain (Figure 5.34) [100]. The cyclic siloxane formation after heat treatment was also observed by Jambe *et al.* ,using NMR analysis [89]. Additional siloxane-related bands were anticipated to form at 758 cm^{-1} and 1258 cm^{-1} but were not observed. The absorption magnitude increases of these bands might be too small and buried underneath the competing bands of the side group. A peak centered at 1130 cm^{-1} developed on the shoulder of the Si-O-Si band after heat treatment at 275 C which is associated with Si radical structures (Figure 5.34) [75]. The radical formation, observed in thermal oxidation, photoirradiation [101], and chemical oxidation using iodine [75], is most likely to be a primary intermediate process in oxidation of polysilane.

Phenyl disruption occurred for heat-treatment above 200 C as indicated by the decrease in vibrational absorption peak area in the corresponding phenyl resonance. The disruption is likely associated both with a ring opening mechanism and complete

detachment of the group from the backbone given the similarity in bond energy between C-C and Si-C (85 kcal/mol and 90 kcal/mol, respectively). A similar trend is observed in the UV-visible absorption as π-π^* absorption bands at 4.5 eV (Figure 5.28) in which a decrease in peak area is observed above 199 C. Methyl groups begin to dissociate at higher temperatures compared to the phenyl group (275 C for the methyl group vs. 200 C for the phenyl group). This is indicated by a reduction in the absorption strength of vibrational bands related to methyl side groups. The dissociation temperature for both methyl and phenyl group are consistent with observation by Pan *et al.* [91-92]. They observed C_6H_6 and CH_3 formation from thermal decomposition of PMPS using mass spectrometry. The C_6H_6 product started to form at ~280 C from PMPS films while CH_3 began to form at ~270 C.

6.3.4. **MATERIALS STRUCTURE: Vibrational spectroscopy: Poly[(methyl)(phenyl)silane] (PMPS) pre-irradiated with 3.68 eV**

Heat treatment of PMPS films that were pre-irradiated under 3.68 eV UV energy, produced further modifications of the molecular structure of PMPS regardless of local atmospheric composition (air or nitrogen) used during photowriting. The decrease in absorption band strength associated with of the Si-Si stretch of pre-irradiated PMPS occurs at higher temperatures, i.e. 225 C vs. 200 C for the aerobic and anaerobic conditions respectively, compared to as-deposited PMPS (160 C). The backbone scissioning of Si-Si bonds in PMPS starts at 150 C, observed using DSC and GPC [89-

90]. This result suggests that the higher Si-Si degradation temperature in material pre-irradiated at 3.68 eV is due to a limited equipment sensitivity to detect changes early in the process at 160 C.

Oxidation of PMPS irradiated under anaerobic conditions began at 145 C (Figure 5.37). This was accompanied by a reduction in Si-H related band area at the same temperature. This suggests that the siloxane structures were produced by replacing hydrogen in Si-H with oxygen. Bond strength of Si-H is close to Si-Si (~79 kcal to ~80 kcal) which results in similar degradation temperature [88]. The Si-O-Si vibrational band in PMPS pre-irradiated under anaerobic conditions begins to grow faster at 145 C compare to that in PMPS pre-irradiated under aerobic conditions. This is likely due to more readily available potential oxidation sites (Si-H) in the PMPS pre-irradiated under anaerobic atmospheres as compared to only limited Si-H structures in the PMPS pre-irradiated under aerobic conditions. The siloxane structures produced in any pre-irradiated PMPS generally exist in short chain rings as indicated by an imbalance in the growth of siloxane bands (faster at 1020 cm^{-1} compared to 1050 cm^{-1}) shown in Figure 5.37 [100].

At lower temperature (70 C -115 C), before degradation, all vibrational bands corresponding to phenyl and methyl group show an increase in magnitude, which is consistent with structural relaxation observed in UV-visible absorption spectra. The photowriting process occurs below the glass transition temperature which prevents photomodified structural segments (including those resulting from oxidation and chain scissioning) from forming their lowest energy conformations by the surrounding material volume. For example, the photoinduced siloxane formation appears to result in a linear

siloxane conformation as monitored by vibrational spectroscopy. Upon thermal annealing, a shift in the IR absorption strength toward resonance energies consistent with a ring conformation is observed (Figure 5.37). Remembering that the DFT analysis predicts that the lowest energy conformation of the oligomeric siloxane structure is ring-like in nature, the temperature-dependent IR data can be interpreted in terms of the relaxation of the photoinduced siloxane structures toward more energetically favorable conformations when the temperature moves beyond Tg for the surrounding, unmodified material. Previous discussion concerning the near-UV, lowest energy transition, has detailed the likely presence of silane chain relaxation at these temperatures. Thus, at elevated temperatures, the unreacted material surrounding the siloxane moieties begins to accommodate local structural rearrangements, allowing the formation of siloxane ring-like conformations that were previously prevented by mechanical constraints from the surrounding material at T<Tg used during photoirradiation.

Conversely, siloxane moieties formed through thermal oxidation occur with the matrix material above Tg . Here, the low energy siloxane ring conformations are obtained directly upon oxidation as structural rearrangements accompanying oxidation can be readily accommodated by the surrounding structure.

The phenyl vibration bands between 3000 cm^{-1} and 3100 cm^{-1} begin to decrease at 145 C, although major absorption bands decrease occur at T>200C (Figure 5.39). While photoinduced modification caused by 3.68 eV irradiation mainly affect the Si backbone, it has only a limited impact on the phenyl side-groups as discussed earlier. Therefore, the phenyl-related bonds of pre-irradiated PMPS thin films should exhibit

similar behavior to that observed in as-deposited PMPS. An initial slight decrease in phenyl vibrational bands after 145 C annealing is most likely an indirect effect of Si backbone scissioning. This behavior, i.e. a slight decrease in phenyl-band absorption strength, is also observed after photoirradiation under 3.68 eV

7. CONCLUSION

Polysilane based materials exhibit promising photosensitive properties for write as-needed applications. In the present work, we demonstrated the ability to tune the photoexcitation to different UV energies by manipulating the molecular structure of the polymer, through the addition of different organic side-groups and through the secondary modification of backbone catenates as mediated by the side-group sterics. Poly[(methyl)(phenyl)silane] (PMPS) exhibited an absorption peak at 337 nm (3.68 eV) associated with the $\sigma - \sigma^*$ transition of the silicon backbone and another at approximately 248 nm (5.10 eV) that was resonant with the $\pi - \pi^*$ transition associated with the phenyl side-groups. By introducing bis-phenylethyl side groups in poly[bis-(phenylethyl)]silane (PBEPS), the backbone conformation changed from mixed *gauche* and *trans* to all-*trans* conformation. As the result, poly(bis-phenylethyl)silane (PBEPS) exhibited a $\sigma - \sigma^*$ transition shifted to 378 nm (3.28 eV). Replacing 5% of silane component in PBEPS to (ethylphenyl)germane further shifts the backbone $\sigma - \sigma^*$ transition to 382 nm (3.24 eV).

Photoirradiation of these polysilane and Ge-Si copolymer materials produced refractive index changes accompanied by an increase in film thickness. PMPS irradiated with 248 nm (5.10 eV) and 337 nm (3.68 eV) produced a maximum refractive index change of -0.14 and -0.07, respectively, after a total fluence < 5 J/cm^2 under the same irradiation environment. In comparison, PBEPS and the Ge-Si copolymer irradiated with a 370 nm (3.35 eV) LED photon source only attained a maximum refractive index change

of -0.020 with total fluence, 8 J/cm^2. Higher total fluences were needed to saturate refractive index changes in the Ge-Si copolymer when compared to those required for saturation of the response in PMPS (8 J/cm^2 compare to 5 J/cm^2). The effect is likely due to the lower absorption strength at incident energy that can be associated with the lower Ge-Si copolymer molecular weight.

Based on these results, the ability to manipulate polysilane electronic structure (and optical absorption) through molecular modifications associated with both the backbone and side-group structures, offers an ability to tune the material excitation energy to those compatible with commercially available solid-state sources to be used in the targeted "write-as-needed" application. Moreover, the large refractive index changes attained under relatively low total UV fluence (short writing time) also enhance the compatibility of these materials with the limited writing times typically available and the lower output fluence characteristic of many integrable solid-state sources.

The local environment during UV-irradiation plays an important role in the characteristics of photoinduced structural modification, and the associated changes in optical constants. Photowriting under an aerobic atmospheric environment produced higher refractive index changes than that produced under an anaerobic environment. The high refractive index changes attained resulted from contributions arising from such factors as a reduced film density, increased contributions from oxide linkage photoproducts, and absorption spectral changes produced (via Kramers-Kronig). Both integrated spectroscopic investigations and modeling indicated that the aerobic local environment during photowriting encourages the formation of a siloxane bridge

structures. DFT modeling of siloxane structures in an oligomeric system shows that these oxide linkages tend to form a puckered ring conformation which is consistent with a reduction of film density and an increase film thickness. However, the oxide linkage growth is suppressed with irradiation under anaerobic environment when terminating hydride structure growth is favored.

Temperatures below the glass transition temperature (Tg = 120 C) tend not to degrade film optical properties or propensity for photosensitivity. At increasing treatment temperatures (in nitrogen atmosphere) above the glass transition, a rearrangement of polymer chains is observed, supported by an enhancement in backbone-related absorption features for T< 120 C. Beyond this point, disruption of the polymer structure is observed. Thermally induced structural decomposition with increasing temperature begins at both Si-H and Si-Si bonds, as they have relatively similar binding energy. Disruption of phenyl rings in PMPS materials occurs at higher temperature than backbone scissioning (T= 200 C). Finally, methyl and phenyl group cleavage from backbone chains is finally observed at the highest temperatures (T = 280 C). Spectroscopic investigation indicates that final product of thermally induced structural modification was short-chain, siloxane ring structures.

The results arising from the thermal treatment of previously irradiated material provide some early insight into the cooperative nature of the structural transformations occurring within the polymers and the inherent differences between the two methods of material “excitation”. In this case, optically induced structural changes, i.e. siloxane bridge formation, occur below the glass transition. Based on the isochronal FTIR studies

described earlier, the reduced structural accommodation (relaxation) afforded by the unreacted surrounding material appears to limit the ability of the photomodified structural segment (i.e. that associated with the chain scission and oxidation) to assume the low energy conformation associated with the newly transformed siloxane chain moeity. This contrasts the effect of energy addition to the structure through thermal treatment. In this case, the entire structure is affected by the thermal energy addition such that local bond scissioning and siloxane formation is concurrent with an overall increase in compliance of the surrounding materials (for temperatures above Tg). Thus, newly formed siloxane chains are more likely to assume conformations consistent with lower energy configurations predicted by the DFT modeling of the current study: puckered, nonlinear-shaped moieties.

From a technological standpoint, photomodification in an aerobic environment with high UV energy is preferable as it produces a maximum refractive index change with the least amount of total fluence. This translates into less writing time, a favorable characteristic for the targeted application. Environmental temperatures below the glass transition temperature (below 120C for PMPS) typically will not affect device performance. However, at higher temperatures (above 160C), the as-deposited “blank” region begins to degrade, producing a reduction in the material refractive index and an overall propensity for UV-photosensitivity. In a device structure, the refractive index contrasts between “blank” and “active” region can thus be reduced upon exposure to temperature excursions beyond the glass transition. At extreme temperatures (above 200C for PMPS) widespread cracking of the film is evident, causing enhanced light

scattering and optical loss. These thermal issues must be taken into consideration when designing write-as-needed optical systems using polysilane-based materials.

8. FUTURE WORK

The present work compared the effect of different side-groups and backbone catenates of polysilane-based materials on materials photosensitivity and electronic structures using three different types of polysilane-based materials: Poly[(methyl)(phenyl)silane] (PMPS), poly[bis-(ethylphenyl)silane] (PBEPS) and poly(bis-ethylphenyl)silane-co-(hexylmethyl)germane (Ge-Si copolymer). However, there are too many structural variables represented by these materials; not only did they have very different side-groups, but the molecular weights are very different as well. As discussed previously, the backbone transition ($\sigma - \sigma^*$) energy, which is major factor in determining the excitation energy for the material, arises from contribution from side-group constituents, backbone conformation, and molecular chain length. A more controlled suite of polymer systems and samples is needed, to obtain a more complete picture of how different backbone catenates and side-group constituents affect optical properties and photosensitive response. For example, ideal systems would consist of PMPS, PBEPS, poly[(methyl)(phenyl)]germane and poly[bis-(phenylethyl)]silane-co-[(methyl)(phenyl)]germane with similar chain length. An investigation of the proposed systems will enable a more systematic investigation of the effect of different side-groups and backbone catenates on material electronic structure and photosensitivity.

On a fundamental level, further study regarding the nature of photoexcitation paths in these systems is needed. Clearly, the present work has elucidated the presence of significant variation in photomediated changes of both the electronic and vibrational structures of the polysilane materials examined with changes in excitation photon energy.

The mechanisms and potential effects of direct vs. indirect excitation on the evolution of polymer chain length and conformation must be understood to more fully evaluate both the origins of optical constant and thermal stability changes observed in these materials. Certainly more detailed excitation energy studies would help to provide such insight.

Isochronal heat treatment with increasing temperature provides interesting insight on materials relaxation behavior and thermal stability. However, the iterative, isochronal heat treatment study pursued necessarily integrates material modifications over the entire thermal history of the sample, making a direct examination of characteristic relaxation or structural modification time scales impossible. Isothermal heat treatment at specific temperatures identified through examination of the isochronal studies will be crucial in subsequent analysis of the dynamics of structural changes at elevated temperatures. DSC measurement on the polysilane polymer system will also provide additional insight on relaxation temperature of different components (backbone or side-groups).

Another interesting study is to compare photoinduced and thermally induced refractive index and thickness changes in PMPS materials. In the current study, heat treatment at high temperature induced defects and cracks in the films which prevented useful ellipsometer measurements as well as reproducible profilometer measurements. Kramers-Kronig calculation of refractive index changes using absorption coefficient changes would provide some insight into such thermally induced refractive index changes.

The present study is also not complete for all the polysilane systems examined. For example no thermal study on PBEPS and Ge-Si copolymer systems has been

pursued, due to a lack of materials. In order to completely characterize both PBEPS and Ge-Si copolymer as potential candidates for write-as-needed applications, understanding their thermal stability will be crucial.

9. REFERENCES

1. A. Inoue, M. Shigehara, M. Ito, M. Inai, Y. Hattori, T. Mizunami, *Optoelectronic Device and Technology* **10**, 119-130 (1995).

2. B.G. Potter, M.B. Sinclair, *Journal of Electroceramics* **2:4**, 295-308 (1995).

3. G.D. Maxwell, B.J. Ainslie, *Electronics Letters* **31**, 95-96 (1995).

4. V. Mizrahi, P.J. Lemaire, T. Erdogan, W.A. Reed, D.J. DiGiovanni, R.M. Atkins, *Journal of Applied Physics* **63**, 1727 (1993).

5. M. Takahashi, A. Sakoh, K. Ichii, Y. Tokuda, T. Yoko, J. Nishii, *Applied Optics* **42**, 4594-4598 (2003).

6. E. Hecht, in *Optics*, 4th edition, Addison-Wesley, p. 199, San Francisco CA (2002).

7. P. Niay, M. Douay, P. Bernage, W.X. Xie, B. Leconte, D. Ramecourt, E. Delevaque, J.F. Bayon, H. Poignant, B. Poumellec, *Optical Materials* **11**, 115 (1999).

8. P.J. Lemaire, A.M. Vengasakar, W.A. Reed, D.J. Giovanni, *Applied Physics Letter* **66**, 2034 (1995).

9. T.A. Strasser, *O.F.C. 96 Technical Digest OSA*, 81 (1996).

10. R.M. Bryce, H.T. Nguyen, P. Nakeeran, R.G. DeCorby, P.K. Dwivedi, C.J. Haugen, J.N. McMullin, S.O. Kasap, *Journal of Vacuum Technology A.* **22**, 1044-1047 (2004).

11. A.B. Seddon, *Journal of Non-crystalline Solids* **184**, 44 (1995).

12. S.R. Elliott, *Physics of Amorphous Materials*, 2nd edition, Longman, Harlow UK (1990).

13. B.G. Potter Jr., K. Simmons-Potter, H. Chandra, G.M. Jamison, W.J. Thomes Jr., *Journal of Non-crystalline Solids* **352**, 2618 (2006).

14. T. Sato, N.M. Yokoyama, *Journal of Photopolymer Science and Technology* **5**, 679 (2003).

15. S. Miura, A. Kobayashi, H. Naito, Y. Matsuura, K. Matsukawa, H. Inoue, *Synthetic Metals* **137**, 1405 (2003).

16. F.S. Kipping, J.E. Sands, *Journal of Chemical Society* **119**, 837-847 (1921).

17. S. Yajima, J. Hayashi, M. Omori, K. Okamura, *Nature* **261**, 683-685 (1976).

18. J.P. Wesson, T.C. Williams, *Journal of Polymer Science Part A. Polymer Chemistry* **17**, 2833 (1979).

19. P. Wesson, T.C. Williams, *Journal of Polymer Science Part A. Polymer Chemistry* **19**, 65 (1981).

20. R. West, L.D. David, P.I. Djurovich, K.L. Stearley, K.S.V. Srinivasan, H. Yu, *Journal of American Chemical Society* **103**, 7352 (1981).

21. R.E. Trujillo *Journal of Organometallic Chemistry* **198**, C-27 (1980).

22. A. Wolff, R. West, *Applied. Organometallic Chemistry* **1**, 7 (1987).

23. R.G. Kepler, J.M. Zeigler, L.A. Harrah, S.R. Kurtz, *Physical Review B.* **35**, 2818 (1987).

24. J.R. Koe, M. Fujiki, M. Motonaga, H. Nakashima, *Macromolecules* **34**, 1082 (2001).

25. K. Simmons-Potter, G.M. Jamison, B.G. Potter Jr., W.J. Thomes Jr., and C.C. Phifer, *Materials Research Society Symposium Proceedings* **726** (2002) 401.

26. B.G. Potter Jr., G.M. Jamison, H. Chandra, K. Simmons-Potter, and W.J. Thomes Jr., *Materials Letters* **59** (2005) 326.

27. Y. Sakurai, S. Okuda, N. Nagayama, M. Yokoyama, *Journal of Materials Chemistry* **11**, 1077 (2001).

28. C.G. Pitt, in *Homoatomic Rings, Chains and Macromolecules of Main Group Elements,* A.C. Rheingold, Ed., Elsevier, Amsterdam, 203-234 (1977).

29. P. Trefonas III, R. West, *Journal of Polymer Science* **23**, 2099-2107 (1985).

30. T. Imori, V. Lu, H. Cai, T.D. Tilley, *Journal of the American Society* **117**, 9931-9940 (1995).

31. K. Mochida, S. Nagano, *Inorganic Chemistry Communications* **1**, 289 (1998).

32. R. Miller, J. Michl, *Chemical Review* **89**, 1359-1410 (1989).

33. R. West, *Comprehensive Organometallic Chemistry*, Editor E. Abel, Pergamon Press, Oxford, England (1982).

34. R. West, *Pure and Applied Chemistry* **54**, 1041 (1982).

35. P. Trefonas III, P.I. Djurovich, X.H. Zhang, R. West, R.D. Miller, D. Hofer, *Journal of Polymer Science Part C – Polymer Letters* **21**, 819 (1983).

36. C.T. Aitken, J.F. Harrod, E. Samuel, *Journal of Organometallic Chemistry* **279**, C11 (1986).

37. C.T. Aitken, J.F. Harrod, E. Samuel, *Journal of American Chemical Society* **108**, 4059 (1986).

38. T.D. Tilley *Accounts of Chemical Research* **26**, 22 (1993).

39. K. Dioumaev, J.F. Harrod, *Organometallics* **13**, 1548 (1994).

40. T. Shono, S. Kashimura, M. Ishifune, R. Nishida, *Journal of Chemical Society – Chemical Communication* **1161** (1990).

41. R.D. Miller, R. Sooriyakumaran, *Journal of Polymer Science Part A. – Polymer Chemistry* **25**, 111 (1987).

42. T. Shono, S. Kashimura, H. Murase, *Journal of Chemical Society – Chemical Communication* **896** (1992).

43. H. Gilman, W.H. Atwell, G.L. Schwebke, *Journal of Organometallic Chemistry* **2**, 369 (1964).

44. H. Gilman, D.R. Chapman, *Journal of Organometallic Chemistry* **5**, 392 (1966).

45. E.A. Halevi, G. Winkelhofer, M. Meisl, R. Janoschek, *Journal of Organometallic Chemistry* **294**, 151 (1985).

46. J.T. Nelson, W.J. Pietro, *Journal of Physical Chemistry* **57**, 1365 (1988).

47. V. Balaji, M. Michl, *Polyhedron* **10**, 1265 (1995). and reference therein.

48. C. Sandorfy, *Canadian Journal of Chemistry* **33**, 1337 (1955).

49. H. Bock, W. Ensslin, *Angewandte Chemie International Edition* **10**, 404 (1971).

50. P. Trefonas III, R.West, R.D. Miller, *Journal of American Chemical Society* **107**, 2737 (1985).

51. S. Kozima, K. Kobayashi, M. Kawanisi, *Bulletin of the Chemical Society of Japan* **49**, 2837 (1976).

52. K. Takeda, K. Shiraishi, N. Matsumoto, *Journal of American Chemical Society* **112**, 5043 (1990).

53. P. Trefonas, R. West, R.D. Miller, *Journal of the American Chemical Society* **107**, 2737 (1985).

54. M.B. Robin, in *Higher Excited States of Polyatomic Materials*, Academic Press; New York 1974, Vol 1, 305.

55. P. Trefonas, R. West, R.D. Miller, D. Hofer, *Journal of Polymer Science Part C – Polymer Letter* **21**, 823 (1983).

56. J.F. Rabolt, D. Hofer, R.D. Miller, G.N. Fickes, *Macromolecules* **19**, 611 (1986).

57. Y.A. Skryshevskii, A.Y. Vakhnin, *Physics of the Solid State* **43**, 589 (2001).

58. K.A. Klingensmith, J.W. Downing, R.D. Miller, J. Michl, *Journal of American Society* **108**, 7438 (1986).

59. C.C. Phifer, W.J. Thomes Jr., K. Simmons-Potter, B.G. Potter Jr., *Journal of Chemical Physics* **120**, (1613).

60. K. Navrátil, J. Šik, J. Humliček, and S. Nešpůrek, *Optical Materials* **12**, 105 (1999).

61. S. Toyoda, M. Fujiki, *Macromolecules* **34**, 2630 (2001).

62. L.A. Harrah, J.M. Zeigler, *Macromolecules* **20**, 601 (1987).

63. J.M. Zeigler, L.A. Harrah, A.W. Johnson, *SPIE Proceedings* **539**, 166 (1985).

64. R. Miller, R. Sooriyakumaran, *Journal of Polymer Science Part C. Polymer Letter* **25**, 321 (1987).

65. R. Miller, R. Sooriyakumaran, *Macromolecules* **21**, 3120 (1987).

66. J.R. Damewood Jr. and R. West, *Macromolecules* **18(2)**, 159 (1985)

67. J.R. Damewood Jr. *Macromolecules* **18,** 1795 (1985).

68. H. Ishii, A. Yuyarna, S. Narioka, K. Seki, S. Hasegawa, M. Fujino, H. Isaka, M. Fujiki, N. Matsumoto, *Synthetic Metals* **69** (1995).

69. C.G. Pitt, R.N. Carey, E.C. Loren Jr., *Journal of American Chemical Society* **94**, 3806 (1972)

70. H. Sakurai, *Journal of Organometallic Chemistry*. **200**, 261 (1980)

71. R.D. Miller and R. Sooriyakumaran, *Macromolecules* **21**, 3120 (1987)

72. M. Ishikawa, M. Kumada, *Advanced Organometallic Chemistry* **19**, 51 (1986).

73. M. Ishikawa, M. Kumada, *Review Silicon, Germanium, Tin, Lead, Compound* **4**, 7 (1979).

74. P. Toman, S. Nespurek, J.W. Jang, and C.E. Lee, *International Journal of Quantum Chemistry* **101**, 746 (2005).

75. P. Toman, S. Nespurek, J.W. Jang, C.E. Lee, *Current Applied Physics* **2**, 327 (2002).

76. Y. Nakayama, H. Inagi, M. Zhang, *Journal of Applied Physics* **86**, 768 (1999).

77. H. Ban, K. Sukegawa, *Journal of Polymer Science Part A. Polymer Chemistry* **26**, 521 (1988).

78. T. Sato, N. Nagayama, M. Yokoyama, *Journal of Photopolymer Sciences and Technology* **16**, 674 (2003).

79. T.A. Iarina, E.E. Said-Galiev, I.I. Tverdokhlebova, V.V. Men`shov, *Polymer Science A.* **37**, 589 (1995).

80. H. Ban, K. Sukegawa, *Journal of Applied Physics* **26**, 521 (1988).

81. J.A. Villegas, R. Olayo, J. Cervantes, *Journal of Inorganic Organometallic Polymers* **7**, 51 (1997).

82. Y. Nakayama, S. Noyoyama, T. Dohmaru, L. Han, *Solid State Communication* **92**, 591 (1994).

83. L.A. Hornak, T.W. Weidman, E.W. Kwock, *Journal of Applied Physics* **67**, 2235 (1990).

84. Y. Matsuura, K. Matsukawa, H. Inoue, *Chemistry Letter*, 244 (2001).

85. W.J. Thomes Jr., K. Simmons-Potter, C.C. Phifer, B.G. Potter Jr., G.M. Jamison, J.E. Jones, D.J. Casadonte Jr., *Journal of Applied Physics* **96**, 6313 (2004).

86. K. Ohta, I. Hatsuo, *Appl. Spectrosc.* **42**, 952 (1988).

87. A. Watanabe, T. Komatsubara, O. Ito, *Journal of Applied Physics* **77**, 2796 (1995).

88. R. Walsh, *Account Chemical Research* **14**, 246 (1981).

89. B. Jambe, J. Marchand-Brynaert, J. Devaux, *Journal of Polymer Sciences Part A. Polymer Chemistry* **33**, 1283 (1995).

90. H.K. Kim, K. Matyjaszewski, *Journal of Polymer Sciences Part A. Polymer Chemistry* **31**, 299 (1993).

91. L. Pan, M. Zhang, Y. Nakayama, *Japanese Journal of Applied Physics* **39**, 1378 (2000).

92. L. Pan, M. Zhang, Y. Nakayama, *Chemistry of Materials* **11**, 1326 (1999).

93. I. Kuritka, P. Horvath, F. Schauer, J. Zemek, *Polymer Degradation and Stability* **91**, 2901 (2006).

94. G.M. Jamison, unpublished results.

95. K. Ohta, I.Hatsuo, *Applied Spectroscopy* **42**, 952 (1988).

96. M. J.; Trucks Frisch, G. W.; Schlegel, H. B.; Scuseria, G. E.; Robb, M. A.; Cheeseman, J. R.; Montgomery, Jr., J. A.; Vreven, T.; Kudin, K. N.; Burant, J. C.; Millam, J. M.; Iyengar, S. S.; Tomasi, J.; Barone, V.; Mennucci, B.; Cossi, M.; Scalmani, G.; Rega, N.; Petersson, G. A.; Nakatsuji, H.; Hada, M.; Ehara, M.; Toyota, K.; Fukuda, R.; Hasegawa, J.; Ishida, M.; Nakajima, T.; Honda, Y.; Kitao, O.; Nakai, H.; Klene, M.; Li, X.; Knox, J. E.; Hratchian, H. P.; Cross, J. B.; Bakken, V.; Adamo, C.; Jaramillo, J.; Gomperts, R.; Stratmann,

R. E.; Yazyev, O.; Austin, A. J.; Cammi, R.; Pomelli, C.; Ochterski, J. W.; Ayala, P. Y.; Morokuma, K.; Voth, G. A.; Salvador, P.; Dannenberg, J. J.; Zakrzewski, V. G.; Dapprich, S.; Daniels, A. D.; Strain, M. C.; Farkas, O.; Malick, D. K.; Rabuck, A. D.; Raghavachari, K.; Foresman, J. B.; Ortiz, J. V.; Cui, Q.; Baboul, A. G.; Clifford, S.; Cioslowski, J.; Stefanov, B. B.; Liu, G.; Liashenko, A.; Piskorz, P.; Komaromi, I.; Martin, R. L.; Fox, D. J.; Keith, T.; Al-Laham, M. A.; Peng, C. Y.; Nanayakkara, A.; Challacombe, M.; Gill, P. M. W.; Johnson, B.; Chen, W.; Wong, M. W.; Gonzalez, C.; and Pople, J. A., Gaussian 03, Revision C.02 (Gaussian Inc. , Wallingford, CT, 2004).

97. R.G. Messerschmidt, M.A. Harthcock (eds), *Infrared Microscopy*, Marcel Dekker, New York (1988).

98. Y. Kanemitsu, M. Kondo, K. Takeda, *Light Emission from Novel Materials*, 1 (1994).

99. H. Chandra, B.G. Potter Jr., G.M. Jamison, W.J. Thomes Jr., *Journal of Applied Physics* **102**, 033110 (2007).

100. G. Socrates, *Infrared and Raman Characteristic Group Frequencies: Table and Charts*, 3rd ed. (John Wiley & Son, Chichester NY, 2001).

101. B.G Potter Jr., H. Chandra, K. Simmons-Potter, G.M. Jamison and W.J. Thomes Jr., *Journal of Materials Research* **21,** 2393-2400 (2006).

102. A.M. Botelho do Rego, O. Pellegrino, M.R. Vilar, *Macromolecules* **34**, 3987 (2001).

103. A.M. Botelho do Rego, M. Rei Vilar, J. Lopes da Silva, "Mechanisms of vibrational and electronic excitation of polystyrene films in high resolution electron energy loss spectroscopy," *Journal of Electron Spectroscopy and Related Phenomena* **85**, 81 (1997).

104. K. Ulbricht, V. Chvalovsky, *Journal of Organometallic Chemistry* **12**, 105 (1968).

105. M.P. Brown, R. Okawara, E.G. Rochow, *Spectrochimica Acta* **16**, 595 (1960).

106. B.G Potter Jr., H. Chandra, K. Simmons-Potter, G.M. Jamison and W.J. Thomes Jr., *Physics and Chemistry of Glasses: European Journal of Glass Science and Technology Part B* **47**, 105-109 (2006).

107. M. Fujiki, *Chemical Physics Letter* **198**, 177 (1992).

108. K.H. Pannell, J.M. Rozell, J.M. Zeigler, *Macromolecules* **21**, 276 (1988).

109. R.J. Cross, F. Glockling, "Infrared spectra of organogermanes," *Journal of Organometallic Chemistry* **3**, 146 (1965).

110. G. Lukovsky, *Solid State Communication* **29**, 571 (1979).

111. R.H. French, J.S. Meth, J.R.G. Thorne, R.M. Hochstrasser, R.D. Miller, *Synthetic Materials* **49-50**, 499 (1992).

112. H. Tachibana, Y. Kawabata, S.-y. Koshihara, T. Arima, Y. Morimoto, and Y. Tokura, *Phys. Rev. B* **44**, 5487 (1991).

113. T. Veszprèmi, Y. Harada, K. Ohno, H. Mutoh, *J. Organomet. Chem.* **244**, 115 (1983).

114. T. Veszprèmi, Y. Harada, K. Ohno, H. Mutoh, *J. Organomet. Chem.* **252**, 121 (1983).

115. A. Ioannidou-Philis, J. G. Philis, A. A. Christdoulides, *Journal of Molecular Spectroscopy* **121**, 50 (1987).

116. J.L.C. Fonseca, C.P. Barker, J.P.S Badyal, *Macromolecules* **28**, 6112 (1995)

117. L.C. Lee, C.C. Chiang, *Journal of Chemical Physics* **78**, 688 (1983)

118. J.H. Wang, K. Liu, Z. Min, H. Su, R. Bersohn, J. Preses, J.Z. Larese, *Journal of Chemical Physics* **113**, 4346 (2000).

119. T. Ari, H. Güven, N. Ecefit, *Journal of Electron Spectroscopy and Related Phenomena* **73**, 13-23 (1995).

120. S.K. Sharma, D.W. Watson, J.A. Philpotts, T.L Rough, "Raman study of the structure of glasses along the join SiO_2-GeO_2", *Journal of Non-Crystalline Solids* **42**, 326 (1988).

121. N. Shibata, M. Horigudhi, T. Edahiro, *Journal of Non-Crystalline Solids* **45**, 115 (1981).

122. D.G. Chen, B.G. Potter, J.H. Simmons, *Journal of Non-Crystalline Solids* **178**, 135 (1994).